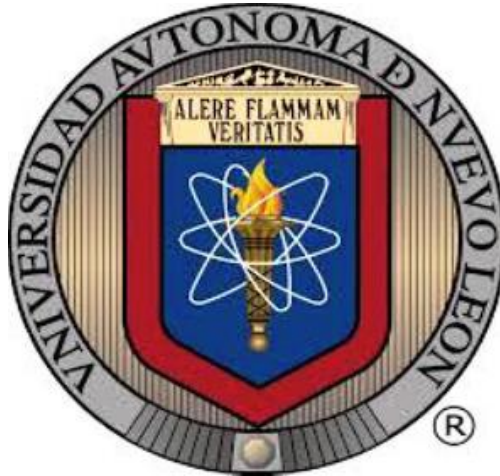


**UNIVERSIDAD AUTÓNOMA DE NUEVO LEÓN
FACULTAD DE CIENCIAS QUÍMICAS**



Control óptico de la expresión génica en sistemas biológicos mediante nanopartículas de oro: Expresión génica fototérmica en *Escherichia coli* y silenciamiento génico en *Chlamydomonas reinhardtii*

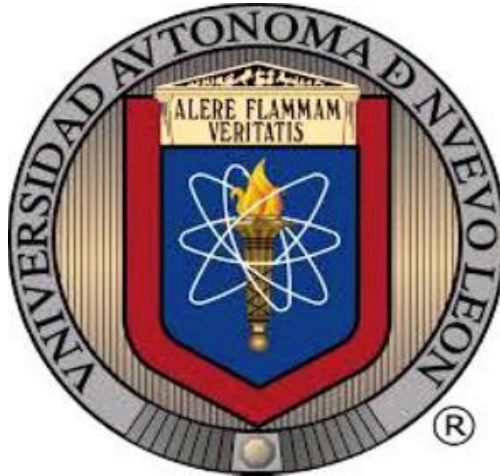
POR

HOSSEIN ALISHAH ARATBONI

**COMO REQUISITO PARCIAL PARA OBTENER EL GRADO DE
DOCTOR EN CIENCIAS CON ORIENTACIÓN EN MICROBIOLOGÍA
APLICADA**

ABRIL, 2020

**UNIVERSIDAD AUTÓNOMA DE NUEVO LEÓN
FACULTY OF CHEMICAL SCIENCES**



Optical Control of Gene Expression in Biological Systems Using Gold Nanoparticles: Photothermal Gene Expression in Escherichia coli and Gene Silencing in Chlamydomonas reinhardtii

By

M.C. Hossein Alishah Aratboni

**As a partial requirement to obtain the Degree of
Doctor in sciences with Orientation in Applied Microbiology**

April, 2020

Optical Control of Gene Expression in Biological Systems Using Gold
Nanoparticles: Photothermal Gene Expression in *Escherichia coli* and Gene
Silencing in *Chlamydomonas reinhardtii*

Thesis approval:

Dr. José Rubén Morones Ramírez

President

Dr.

Secretary

Dr.

Vocal

Dr.

Vocal

Dr.

Vocal

Dra. María Elena Cantú Cárdenas

Sub-Director of Postgraduate Studies

Optical Control of Gene Expression in Biological Systems Using Gold
Nanoparticles: Photothermal Gene Expression in *Escherichia coli* and Gene
Silencing in *Chlamydomonas reinhardtii*

Thesis Review:

Dr. José Rubén Morones Ramírez

Supervisor

Dr. Xristo Zárate Kalfópulos

Tutorial Committee

Dr. Juan Francisco Villarreal-Chiu

Tutorial Committee

Dr. Ulrico J Lopez-Chuken

Tutorial Committee

Dra. María Elena Cantú Cárdenas

Sub-Director of Postgraduate Studies

ACKNOWLEDGEMENTS

I would like to thank all the people and institutions that, directly and indirectly, were present during my professional life. To CONACyT and the Faculty of chemical sciences for their financial supports, as well as for the facilities and necessary equipment for the development of the experiments performed.

First and foremost, I would like to express my sincere thanks to my supervisor, Dr. José Rubén Morones Ramírez for giving me the opportunity to carry out this research in his lab. I thank him for his guidance, advice, encouragement and patience throughout my studies at UANL. I would like to thank my tutorial committee, Dr. Xristo Zárate Kalfópulos, Dr. Juan Francisco Villarreal-Chiu and Dr. Ulrico J Lopez-Chuken for their support, helpful suggestions, sharing their knowledge to advise me, and apply the necessary corrections in my research. I also really appreciate all the hard work Dr. Rahim Foroughbakch Pournavab have done to help me in during this time. I thank Dr. S. Yousef Ebrahimipour, Dr. Azael Martínez de la Cruz, Dra. María Elena Cantú Cárdenas and Dra. María Aracely Hernández Ramírez for great help and guidance in different condition. I thank all the past and present members of the Dr. Ruben's Lab (Paco, Javier, Diego, Dago, Pepi, Alex, Pako, Angel, Albert, Enrique, Jordy etc.) for their help, friendship and making my stay at UANL.

I must thank my parents, for they have dedicated their lives to making sure the door was open for any opportunity I wanted to pursue, be it by raising me, teaching me, supporting me, praising me when I got it right. To my amazing sisters and brothers for their help and encouragement, thank for supporting me in every phase of life.

Last but definitely not least, I must thank the queen of my life, my lovely wife;

My dear wife, your love and support made me a better person and every day you make my day by your sweet smile. You are the biggest and sweetest blessing of my life .Thanks for being my happiness. Thank you for your love, care, support and sacrifice you are doing for me. I couldn't write the thesis if you were not here to help me and sacrifice for me.

DEDICATION

To my Love Nahid

Who supported me throughout these years and her unconditional love has changed my world.

Table of Contents

CHAPTER 1	22
Introduction	22
1.1 Biofuels	22
1.2 Microalgae biofuels	23
1.3 Microalgae cultivation	24
1.4 Nanotechnology	26
1.5 Nanoparticles	26
1.6 Gold nanoparticles	28
1.7 Synthesis of AuNPs	30
1.8 Localized surface plasmon resonance	30
1.9 Plasmonic heat	31
1.10 Nanoplasmonic Optical Switch	33
1.11 Usage of AuNPs for the photothermal protein production as a new application in engineered biological systems	35
1.12 RNA thermometer	38
1.13 Microalgae Lipid	38
1.13.1 Lipids in <i>Chlamydomonas reinhardtii</i> (<i>C. reinhardtii</i>)	40

1.13.2 <i>Carnitine-acylcarnitine translocase</i> gene.....	43
CHAPTER 2	45
Background	45
CHAPTER 3	52
Hypothesis and Objectives	52
3.1 Hypothesis	52
3.2 Objectives	52
3.2.1 General objective	52
3.2.2 Specific objectives.....	52
CHAPTER 4	54
Experimental Methodology	54
4.1 Materials and Reagents	54
4.2 Equipment.....	54
4.3 Synthesis of AuNPs	55
4.4 Characterization of the obtained nanoparticles.....	55
4.5 Laser and LED light source and their temperature profile statistical analysis	56
4.5.1 Set-up the Laser for temperature profile measurements	56

4.5.2 Statistical analysis for Laser temperature profile	57
4.5.3 Set-up and assessing the LED chip suitability and feasibility for large scale use.....	58
4.5.4 Experimental temperature profile for LED	59
4.5.5 Theory and simulation for LED	59
4.6 Strains of used bacteria	59
4.7 Growth Media of Bacteria	60
4.7.1 LB medium	60
4.8 Culture the bacteria strain.....	60
4.9 Design of genetic temperature sensor for <i>E. coli</i> DH5 α TM	60
4.10 Toxicity test of AuNPs on <i>E. coli</i> DH5 α	62
4.11 Photothermal protein production by LED in <i>E. coli</i> DH5 α	63
4.12 Strain of used microalgae	64
4.13 Growth Media of microalgae	64
4.13.1 TAP medium for culturing of <i>C. reinhardtii</i>	64
4.14 Microalgae Cultivation and Maintenance	68
4.14.1 Analysis of Samples	68
4.15 Preparation of oligonucleotide-conjugated AuNPs.....	69

4.15.1 Required oligonucleotide	69
4.15.2 Attachment of DNA to AuNPs.....	71
4.16 In-vitro test of antisense photothermal dehydridization	73
4.17 Switches delivery into the microalgae cells	74
4.18 Experimental setup for photothermal releasing of antisense oligonucleotide to gene silencing.....	75
4.19 RNA extraction and quantification.....	75
CHAPTER 5	78
Results	78
5.1 Microalgae Growth analysis	78
5.2 Characterization of the obtained nanoparticles	79
5.2.1 UV–Vis Spectra Analysis.....	79
5.2.2 Transmission Electron Microscopy Analysis	81
5.2.3 Selected-area electron diffraction pattern (SAED).....	81
5.2.4 Energy dispersive X-ray spectroscopy (EDS).....	82
5.2.5 Zeta-potential of synthesized AuNPs	82
5.3 Effect of different AuNPs concentration, Laser illumination time and Laser power amounts on temperature changes of colloidal AuNPs	85
5.4 LED and statistical analysis	90

5.5 Theory and simulation.....	96
5.6 Toxicity test of AuNPs on <i>E. coli</i> DH5 α	101
5.7 Photothermal protein production by LED in <i>E. coli</i> DH5 α	102
5.8 Conjugation of sense and antisense oligonucleotides to switches	104
5.9 In-vitro confirmation of antisense photothermal dehybridization .	106
5.10 Confirmation of switches delivery into the microalgae cells and RNA quantification	107
CHAPTER 6	112
Discussion	112
CHAPTER 7	119
Conclusions	119
CHAPTER 8	123
References	123

List of figures

Figure 1. 1 The Lycurgus Cup in reflected (a) and transmitted (b) light.	28
Figure 1. 2 Extinction spectra of AuNPs with diameters ranging from 10 to 100 nm at mass concentration 0.05 (mg/ml).....	29
Figure 1. 3 Extinction of particles plasmons through the polarization of metallic nanoparticles.....	31
Figure 1. 4 Decays of the localized surface plasmon.....	32
Figure 1. 5 Photothermal dehybridization of antisense DNA from AuNP using continuous-wave illumination.	35
Figure 1. 6 Structure of TAG and convert it to biodiesel	39
Figure 1. 7 The figure illustrates two possible pathways for TAG formation following the assumed route in the chloroplasts or over the ER membranes in the cytosol.....	42
Figure 1. 8 Activation and transition of fatty acids into matrix of mitochondria [164].	44
Figure 2. 1 World biodiesel production and trade.....	46
Figure 2. 2 Regional distributions of world biodiesel production and use in 2025 [175]......	47

Figure 4. 1 Experimental setup for measuring the temperature profile of gold nanoparticle solutions.	57
Figure 4. 2 Experimental setup for measuring the temperature profile of AuNPs solutions.....	58
Figure 4. 3 Genetic temperature sensor structure.....	61
Figure 4. 4 Example disulfide bond reduction of a 3'-Thiol-Modifier C6 S-S oligonucleotide.....	71
Figure 4. 5 Conjugation of sense oligonucleotide to AuNPs surfaces.....	72
Figure 4. 6 Conjugation of antisense oligonucleotide to sense strand.	73
Figure 5. 1 Cell growth profile of <i>C. reinhardtii</i> in TAP growth medium.....	79
Figure 5. 2 Surface plasmon resonance (SPR) excitation of the nanoparticles. 80	
Figure 5. 3 UV–vis absorption spectrum of AuNPs; 30 minutes and after 4 months later synthesis.	81
Figure 5. 4 (A), (B) TEM, (C) HRTEM and (D) SAED pattern of synthesized AuNPs.....	83
Figure 5. 5 Particle size distribution of the synthesized AuNPs.	84
Figure 5. 6 EDS spectrum of synthesized AuNPs.....	84
Figure 5. 7 Zeta potential of synthesized AuNPs.	85

Figure 5. 8 Pareto chart showing the main effects of the various factors and their interaction on the temperature change of the colloidal AuNPs.	86
Figure 5. 9 Response surface curve for interaction effect.....	94
Figure 5. 10 Extinction, absorption, and scattering cross sections for a 20.44 nm AuNP in water.	97
Figure 5. 11 Time dependent temperature calculations for two concentrations of 44 ppm and 88 ppm.....	99
Figure 5. 12 Calculated local collective heating of ensemble of AuNPs in the cuvette of 10mm×12.2mm×22.4mm	100
Figure 5. 13 (A) Temperature distribution along xz plane at y=11.2 mm at t=10 minutes	101
Figure 5. 14 OD of Bacteria samples.....	103
Figure 5. 15 The average RFU of the mCherry proteins of E. coli DH5α™	104
Figure 5. 16 Color change of AuNPs solution in the switches synthesis process	105
Figure 5. 17 Changes in the UV-vis absorption spectrum when an aqueous dispersion of 20.44 nm AuNPs is treated with thiolated sense oligonucleotides and then with the antisense oligonucleotides.....	106
Figure 5. 20 Confocal microscopy images	108
Figure 5. 21 comparative RT-PCR.....	110
Figure 5. 22 Fluorescence images of Nile red-stained C. reinhardtii cells, 2h after gene silencing.	111

Figure 6. 1 Krebs cycle; Necessity of Acetyl-CoA to start Krebs cycle..... 115

Figure 6. 2 Conversion of Oxaloacetate to PEP pathway. 116

Figure 6. 3 TAG synthesis pathway; synthesis of TAG from DHAP that is one of the intermediate compounds of Glycolysis..... 117

List of tables

Table 1. 1 Different growth modes of microalgae.....	25
Table 4. 1 Volume and concentration of TAP-Medium stock solutions.	66
Table 4. 2 Modified DNA oligonucleotides and their melting temperatures (T _m).	70
Table 4. 3 Thermocycler program (RT-PCR) used for the quantification of gene expression.....	76
Table 5. 1 ANOVA result for the experimental parameters which affecting temperature of AuNPs solution.	88
Table 5. 2 Predicted and actual values of ΔT for the confirmation the regression model.....	90
Table 5. 3 Four experimental variables screened by full factorial design at different levels.....	91
Table 5. 4 ANOVA for the experimental parameters of full factorial design.	91
Table 5. 5 Analysis of variance (ANOVA) for response surface quadratic model.	95

Abbreviations

LSPR	Localized Surface Plasmon Resonance
ONCOS	Oligonucleotides on a Nanoplasmonic Carrier-based Optical Switch
ROS	Reactive Oxygen Species
NPs	Nanoparticles
AuNPs	Gold Nanoparticles
SD	Shine–Dalgarno
ssDNA	Single-Stranded DNA
dsDNA	Double-Stranded DNA
5'-UTR	5'-untranslated region
TAG	Triacylglycerol
PUFAs	Polyunsaturated Fatty Acids
SFAs	Saturated Fatty Acids
EPA	Eicosapentaenoic Acid
DPA	Docosapentaenoic Acid
DHA	docosahexaenoic Acid
ER	Endoplasmic Reticulum

UV-Vis spectroscopy	Ultra Violet-Visible Spectroscopy
SPR	Surface Plasmon Resonance
TEM	Transmission Electron Microscopy
HRTEM	High-Resolution Transmission Electron Microscopy
SAED	Selected Area Electron Diffraction
fcc	Face-Centered Cubic
EDS	Energy dispersive X-ray spectroscopy
LED	Light Emitting Diode
CW	Continuous Wave
RMS	root mean square
RSE %	Residual Standard Error Percentage
n-6 LC-PUFA	Omega-6 Long-Chain Polyunsaturated Fatty Acids
MCs	Mitochondrial Carriers
CACT	<i>Carnitine/Acylcarnitine Translocase</i>
Tub	<i>Tubulin</i>
RNAi	RNA interference
miRNAs	microRNAs

siRNAs	small interfering RNAs
pNA–AuNPs	Polyvalent Nucleic Acid Gold Nanoparticles
TAP	Tris-Acetate-Phosphate
AON-GFP	GFP expression by antisense oligonucleotide
O ₂	Oxygen
H ₂	Hydrogen
C	Carbon
Cu	Copper
CO ₂	Carbon Dioxide
NH ₄ ⁺	Ammonium
NO ₃ ⁻	Nitrate Ion
HAuCl ₄	Tetrachloroauric(III) Acid
CH ₃ COOH	Acetic Acid
H ₂ NC(CH ₂ OH) ₃	Tris(hydroxymethyl)-Aminomethan
NH ₄ Cl	Ammonium Chloride
MgSO ₄ .7H ₂ O	Magnesium Sulfate Heptahydrate
CaCl ₂ .2H ₂ O	Calcium Chloride Dihydrate
K ₂ HPO ₄	Dipotassium Phosphate

KH_2PO_4	Monopotassium Phosphate
$\text{Na}_2\text{EDTA} \cdot 2\text{H}_2\text{O}$	Disodium Dihydrate
$\text{ZnSO}_4 \cdot 7\text{H}_2\text{O}$	Zinc Sulfate Heptahydrate
H_3BO_3	Boric Acid
$\text{MnCl}_2 \cdot 4\text{H}_2\text{O}$	Manganese(II) Chloride Tetrahydrate
$\text{FeSO}_4 \cdot 7\text{H}_2\text{O}$	Iron(II) Sulfate Heptahydrate
$\text{CoCl}_2 \cdot 6\text{H}_2\text{O}$	Cobalt(II) Chloride Hexahydrate
$\text{CuSO}_4 \cdot 5\text{H}_2\text{O}$	Copper(II) Sulfate Pentahydrate
$(\text{NH}_4)_6\text{MoO}_3$	Ammonium Molybdate Tetrahydrate
CH_3COOH	Acetic Acid
HAuCl_4	Tetrachloroauric(III) acid
AuCl_3	Gold trichloride
Na_2HPO_4	Disodium Phosphate
NaH_2PO_4	Monosodium Phosphate
DDT	Dithiothreitol
(-SH)	Thiol
PBS	Phosphate-Buffered Saline
MŪ	Deionized Water

Conc.	Concentration
mM	Milimolar
nM	Nanomolar
ml	Milliliter
μ l	Microliter
g	Gram
h	Hour
nm	Nanometer
cm	Centimeter
W	Watt
mW	Milliwatt
V	volt
kV	KiloVolt
KeV	Kilo Electron Volt
mV	Millivolts
Ω	Ohm
P_{LED}	power of LED
μ g/ml	Microgram Per Milliliter

g/L	Gram Per Liter
w/w	Weight By Weight
CFU/mL	Colony-Forming Unit per Milliliter
Cell/ml	Cell per Milliliter
Tm	Temperature
pH	Potential Hydrogen
n	Number
%	Percentage
°	Degree
°C	Degree Celsius
Adj	Adjusted
R ²	R-squared (coefficient of determination)
ANOVA	Analysis of Variance
df	Degrees of Freedom
SS	Sum of Squares
MS	Mean Squares
F-Value	Fisher's test value
P-Value	Probability Value

CCD	Central Composite Design
RSM	Response Surface Methodology
LB	Luria–Bertani
rpm	revolutions per minute
OD	Optical Density
ppm	Parts Per Million
BMD	Broth Micro-Dilution
CLSI	Clinical and Laboratory Standards Institute
MIC	Minimum Inhibitory Concentration
SAR	Specific Absorption Rate
RFU	Relative Fluorescence Units
dd-H ₂ O	Double-Distilled Water
$\mu\text{mol}/\text{m}^2/\text{s}$	Micromole Per Square Meter Per Second
W_s	Sample Weight
W_0	Primary Weight
ω	Omega
ϵ_0	Local Dielectric Constant
bp	Base Pair

F Primer	Forward Primer
R Primer	Reverse Primer
6-FAM	6-Carboxyfluorescein
RNP	Radius of AuNPs
I	Intensity
d	Distance
ΔT	Temperature Change
<i>et al.</i>	<i>et alia</i>
etc	et cetera
Eq.	Equation
min	Minute

RESUMEN

MC Hossein Alishah Aratboni

Fecha de graduación: Abril, 2020

Universidad Autónoma de Nuevo León

Facultad de Ciencias Químicas

Título de Estudio: Control óptico de la expresión génica en sistemas biológicos mediante nanopartículas de oro: Expresión génica fototérmica en *Escherichia coli* y silenciamiento génico en *Chlamydomonas reinhardtii*

Número de páginas: 144

Candidato para el grado de Doctorado en Ciencias con orientación en Microbiología Aplicada

Área de estudio: Desarrollo de Aplicaciones de Nanobiotecnología

Las nanopartículas de oro pueden ser encontrados de diferentes formas, tamaños y que determinan sus características químicas y físicas. Las propiedades físicas y químicas de las nanopartículas metálicas pueden ser moduladas al cambiar su forma, tamaño y la química de su superficie. Por lo tanto, esto ha permitido su uso en una gran variedad de aplicaciones en los sectores industriales y académicos. Una de las características de las nanopartículas metálicas es su habilidad para actuar como convertidos de energía optotérmicos. Esta característica ha sido utilizada en muchas aplicaciones donde las nanopartículas son acopladas con sistemas de respuesta térmica para generar una respuesta óptica. En este estudio, nosotros sintetizamos nanopartículas metálicas que son mayormente esféricas en su forma con un promedio de diámetro de 20.07 nm. En este estudio, nosotros

utilizamos dos fuentes de luz: LED y láser. Diferentes enfoques estadísticos fueron utilizados para medir la potencia y capacidad funcional de la luz láser y LED así como identificar a la variable más necesaria para incrementar la temperatura en una solución de nanopartículas de oro. En este trabajo se realizaron simultáneamente técnicas teóricas y experimentales para evaluar los diferentes factores que afectan la generación de calor en la superficie de nanopartículas cuando son expuestas a una longitud de onda específica por la luz láser y LED. Respecto al láser, los resultados mostraron que los factores que más contribuyeron al cambio de temperatura exhibido en la solución de nanopartículas resultaron ser el poder del láser, la concentración de las nanopartículas de oro, la interacción tiempo \times láser y el tiempo de iluminación. Nosotros reportamos un modelo de regresión que permite predecir la generación de calor y cambios de temperatura con errores estándares residuales en menos de 4%. Los resultados son altamente relevantes para diseños futuros y en el desarrollo de aplicaciones donde las aplicaciones de nanopartículas sean incorporadas en los sistemas para inducir un cambio en la temperatura a partir de la exposición de con luz. Respecto al LED, nosotros analizamos estadísticamente la temperatura producida en la superficie de las nanopartículas de oro cuando utilizando LED como fuente de luz. Los resultados mostrados que los efectores principales y las interacciones de todos los factores fueron significativos. Finalmente, basados en el modelo de regresión presentado, los coeficientes de regresión y los resultados de ANOVA nos permiten presentar un poderoso modelo de regresión que muestra las relaciones entre la temperatura de cambio y sus variables. Nosotros simulamos el cambio de generación de nuestras nanopartículas de oro cuando la solución con nanopartículas de oro era iluminada con una fuente de luz LED. Nosotros demostramos que el máximo incremento de temperatura en la solución de nanopartículas (resultados de simulación) cotejaron excelentemente con nuestras observaciones (resultados prácticos).

Para evaluar nuestra aplicación fototérmica obtenida a partir de nanopartículas de oro en un sistema biológico en células, evaluamos su factibilidad en la producción de proteína con enfoque fototérmico por primera vez. Para lograr este objetivo, utilizamos luz LED en vez de un dispositivo láser al considerarse como un método nuevo, barato, inofensivo y conmutable para sistemas biológicos vivos. Después de sintetizar las nanopartículas de oro y obtener su perfil de temperatura, nosotros diseñamos un gen sintético, donde el sitio de unión a ribosoma pudiera ser activo y trabajar eficientemente a 37°C. Basado en el modelo de regresión lineal y en análisis de respuesta de superficie de curva, nosotros encontramos el cómo proveer la temperatura necesaria. De esta manera, nosotros mostramos el uso de nanopartículas metálicas y LED como fuente de luz pueden trabajar eficientemente en una estructura tipo *stem-loop* que contiene un sitio a unión a ribosoma y consecuentemente una alta producción de mCherry es logrado. Además, para mostrar su factibilidad en la desbridamiento de dsDNA unido a nanopartículas metálicas a partir de LED como fuente de luz, nosotros elaboramos conmutadores (nanopartículas de oro acoplados con dsDNA) y finalmente fueron caracterizados. Entonces, nosotros mostramos la factibilidad del desbridamiento del dsDNA unido a nanopartículas de oro (prueba *in vitro*) utilizando LED como fuente de luz bajo diferentes longitudes de onda. La prueba demostró ser exitosa y se mostró la probabilidad de que el calor generado fototérmica pueda ser utilizado para el silenciamiento de genes por antisentido en células de microalgas vivas.

CHAPTER 1

Introduction

1.1 Biofuels

More than 80% of global energy demand today is met from fossil fuel [1]. It has become obvious that continued reliance on fossil fuel energy resources is unsustainable, owing to higher energy prices, finite fossil fuel reserves, and rising atmospheric carbon dioxide (CO₂) levels. As a result, researchers and policy-makers are exploring alternative energy feedstock in the hope of averting some of the most unfortunate scenarios. This includes the production of biofuel, which is biodegradable, renewable, and non-toxic. Biofuel also contributes no net CO₂ or sulfur to the air and emits less atmospheric pollutants than fossil fuel [2].

In recent years, the demand for liquid biofuels in the transport sector has shown rapid global growth. There are three types of biofuels: first, second and third generation biofuels. They are characterized by their sources of biomass, their limitations as a renewable source of energy, and their technological progress [3]. First generation biofuels, also known as conventional biofuels, are those which are made from feedstocks that can also be consumed as human food. The feedstocks for first-generation fuels include food crops like corn, sugarcane, sugar beet, wheat and sorghum. They have contributed to increases in world prices for food and animal feeds. They also have the potential to have a negative impact on biodiversity and competition for water in some regions. Additionally, biomass for first generation biofuels requires lots of land to grow [4].

Second generation biofuels use biomass, meaning any plant-derived material, as a feedstock - much like first generation biofuels. But unlike first generation biofuels this biomass can be derived from non-edible sources and/or waste matter [4]. Second generation biofuels generate higher energy yields per acre than 1st generation fuels. They allow for use of poorer quality land where food crops may not be able to grow. The goal of second generation biofuel processes is to extend the amount of biofuel that can be produced sustainably by using biomass consisting of the residual non-food parts of current crops, such as stems, leaves and husks [5].

The third generation biofuel feedstock is algae (especially microalgae) which could give a viable alternative to fossil fuels [6]. Algae is the oldest plant living in the freshwater, saline and even sewage. There are around 2100 genera, 27,000 species of algae living in the world [7].

1.2 Microalgae biofuels

Many advantages exist for using microalgae-derived biofuels: (1) microalgae cells have much higher solar energy conversion efficiencies in photosynthesis [8]. The maximum conversion efficiency of solar energy to biomass is 8-10% for microalgae, but only 4.6% for C3 plants and 6% for C4 plants; (2) microalgae are capable of all year round production in some areas, and some microalgae are capable of accumulating large amounts of lipids (up to 70% w/w) [9], (3) The cultivation of microalgae for biofuel production can potentially be carried out on non-arable land, and thus do not directly compete with food production [10]; (4) considering minimal evaporation of closed photobioreactor systems and the capability of some marine and halophilic algal strains, microalgal cultivation can save large amounts of fresh water compared with traditional biofuel crops; in addition, some microalgae can

recycle water and nutrients from effluent streams, therefore, it is beneficial for treatment of waste water [11]; (5) Some microalgae can also synthesize desirable compounds with different biological activities, like β -carotenoids, docosahexaenoic 3 acid (DHA), polysaccharides, vitamins, with commercial or pharmaceutical applications [12-14].

Microalgae have shown great potential to produce a wide spectrum of fuel products in pilot studies: (1) hydrogen (H_2) via direct and indirect biophotolysis, (2) biodiesel through transesterification (converting the lipid), (3) biomethane via anaerobic digestion (Fermentation of Algal Biomass), (4) bioethanol by converting the starch (the storage component) and Cellulose (the cell wall component), (5) bio-oil via thermochemical conversion, and (6) green diesel and gasoline through direct catalytic hydrothermal liquefaction[15-17].

1.3 Microalgae cultivation

In general, microalgae growth occurs in four modes, including photoautotrophy, photo-heterotrophy, heterotrophy, and mixotrophy (table 1.1) [18]. As photosynthetic microorganisms, microalgae depend on sunlight and CO_2 as the energy and carbon source for growth. In photoautotrophic species, the microalgae cells use solar energy and CO_2 as a carbon source [19]. While in photo-heterotrophy, cells use light for energy, fixation of nitrogen and organic matter as a carbon source without CO_2 [20]. Under heterotrophic growth conditions, instead of harvesting light and assimilating CO_2 from air, microalgae use organic carbon substrates such as glucose, acetate, and glycerol as their energy and carbon source [21]. Mixotrophic growth is a combination of phototrophic and heterotrophic conditions, where some microalgae strains have the capability to combine autotrophic photosynthesis and the heterotrophic assimilation of organic compounds, either simultaneously or sequentially [21].

Table 1. 1 Different growth modes of microalgae.

Growth mode	Energy source	Carbon source	Light availability requirements
Photo-autotrophic	Light	Inorganic	Obligatory
Heterotrophic	Organic	Organic	No requirements
Photoheterotrophic	Light	Organic	Obligatory
Mixotrophic	Light and organic	Inorganic and organic	No obligatory

Microalgae cultures with organic carbon sources increase the biomass production and lipid/carbohydrate contents in cells [22].

The advantages of heterotrophic cultivation of microalgae, in comparison with photo-autotrophic cultivation are the following: (1) Higher growth rate and biomass density (2) Higher lipid content per dry weight of cells; (3) Higher biomass productivity per area of culture; (4) Cheaper and simpler bio-reactor design; (5) Easier scaling-up process; (6) The possibility to manipulate biomass composition by changing the culture medium's organic substrate that stimulates specific metabolic and biosynthetic pathways; and (7) Potential to remove organic carbon and several types of nitrogen and phosphorus compounds from wastewater [21-24].

Mixotrophic growth offers several advantages: (1) Higher growth rates than either heterotrophic or photo-autotrophic regimes by shortening growth cycles and producing higher biomass; (2) Prolonged exponential growth phase; (3) Reduction of lost biomass from respiration during dark hours; (4) Reduction or

stopping of photo-inhibitory effect; (5) Flexibility to switch the cultivation regime to heterotrophic or photo-autotrophic regimens at will; and (6) Protection from photo-oxidative damage stimulated by accumulating oxygen in enclosed photo-bioreactors [21, 22, 25].

1.4 Nanotechnology

The word "Nano" originates from a Latin word which means "dwarf " [26]. In recent years, nanotechnology has attracted more attention in science due to its different applications [27]. Nanotechnology is an emerging multidisciplinary scientific field which involves the understanding and control of matter on the nanometer (a nanometer is one billionth of a meter, about ten times the width of a hydrogen atom) scale. In another word, Nanotechnology is the construction and use of functional structures designed from atomic or molecular scale with at least one characteristic dimension measured in nanometers. When characteristic structural features are intermediate between isolated atoms and bulk materials in the range of approximately 1–100 nm, the objects often display physical attributes substantially different from those displayed by either atoms or bulk materials. We should distinguish between nanoscience and nanotechnology. Nanoscience is a convergence of physics, chemistry, materials science, and biology, which deals with the manipulation and characterization of matter on length scales between the molecular and the micron size. Nanotechnology is an emerging engineering discipline that applies methods from nanoscience to create products [28].

1.5 Nanoparticles

Generally, NPs are constituted of several tens or hundreds of atoms or molecules and can have a variety of sizes and morphologies (amorphous, crystalline, spherical, needles, etc.). NPs are the most fundamental component in

the fabrication of a nanostructure, and is far smaller than the everyday objects we use. For example, roughly eight hundred 100 nm-sized NPs are required to match the width of a human hair. Owing to their small size effect, large surface effect, and quantum tunnel effect, the NPs demonstrate special physical properties and can be widely used in a variety of applications. A number of artificial or engineered NPs have been developed. Engineered NPs have unique properties compared to bulk materials and their commercial uses growing rapidly [29]. Some of these engineered NPs are being used in a wide variety of consumer products such as cosmetics. The most momentous and great invention of nanotechnology is the metallic NPs having preferable property to that of its bulk structure [30] and show promise in advancing the fields of medical and electronic future applications based on their unique optical characteristics. Compared with bulk metal, metallic NPs have lower melting points, higher surface areas, specific optical properties, higher mechanical strengths, and better magnetizations properties. Therefore, with wide range of applications available, NPs in many high-technology scientific work such as biosensors, diagnostic assays, anti-bacterial agents, drug and gene delivery vehicles, contrast agents and so on is in used [31, 32]. Among these important applications, the optical property is one of the attractive characteristic of a nanoparticle which is considered by researchers. For instance, AuNPs with different size have different color; red color (for particles less than 100 nm) or blue/purple (for larger particles). And silver nanoparticle is yellowish gray color. Several examples such as the famous Lycurgus Cup -manufactured by the Roman empire show that unique optical characteristics of NPs have been used even before the 4th century AD. Based on the analysis of the glass, it was found that the glass contains a very small quantity of metallic Nano-sized particles of silver (66.2%), gold (31.2%), and copper (2.6%). Due to these NPs, when a light source is placed inside the cup, its color changes from green to red (Figure 1.1).



Figure 1. 1 The Lycurgus Cup in reflected (a) and transmitted (b) light. (Image courtesy of © the Trustees of the British Museum.)

1.6 Gold nanoparticles

Among all types of NPs, AuNPs due to the size- and shape-dependent optical, electrical and thermal properties, easily tunable optical properties, known surface chemistry, and relatively easy synthesis are being developed as diagnostic reagents [33], drug carriers [34], contrast agents [35], photothermal agents [36] and radiosensitisers [33, 37]. Gold (Au) atomic number 79, electronic configuration [Xe] $4f^{14} 5d^{10} 6s^1$, is a yellow, malleable, shiny, and ductile metal. Colloidal gold, also known as a suspension consisting of sub-micron AuNPs [38]. While colloidal AuNPs have been known to have been used for centuries in stained glass, they didn't receive scientific evaluation until Michael Faraday began in 1852 [39]. With continues study, in 1857, Michael Faraday for the first time produced “colloidal gold” in solution and observed their unique optical properties [40]. The actual scientific study on AuNPs started in 1908 when Gustav Mie described a mathematical explanation by using Maxwell equations that described the extinction spectra of spherical and ellipsoidal nano-objects that demonstrated the optical properties of metallic colloids [41]. The dominating optical feature of

AuNPs with size of 2 to 100 nm is the localized surface plasmon resonance (SPR). Localized surface plasmon resonance (LSPR) is an optical phenomenon generated by light when it interacts with conductive NPs that are smaller than the incident wavelength [42]. Compared to any other chromophores, smaller AuNPs, sizes between 2 to 20 nm have higher absorbance with a possibility of reaching high light-to-heat conversion efficiency [43]. In contrast, particle sizes above 20 nm, have larger extinction cross-sections, high photo stability, and the ability to amplify the electromagnetic field near the metal surface [43]. The optical properties of spherical AuNPs are highly dependent on the nanoparticle diameter. Figure 2.2 shows a strong extinction, the sum of scattering and absorption, maximum between 510-580 nm in aqueous solution due to their LSPR. Smaller AuNPs absorb light and have peaks near 520 nm, while larger spheres exhibit increased scattering and have peaks that broaden significantly and shift towards longer wavelengths. Larger AuNPs scatter more light both because they have larger optical cross sections, and increase a ratio of scattering to total extinction [43]. With the development of nanoscience, the optical properties of AuNPs have shown tremendous interest in plasmon-based technologies. Localized surface plasmons can be excited by optical excitation, leading to the device development of small-scaled optical antenna with enhanced electric fields [44].

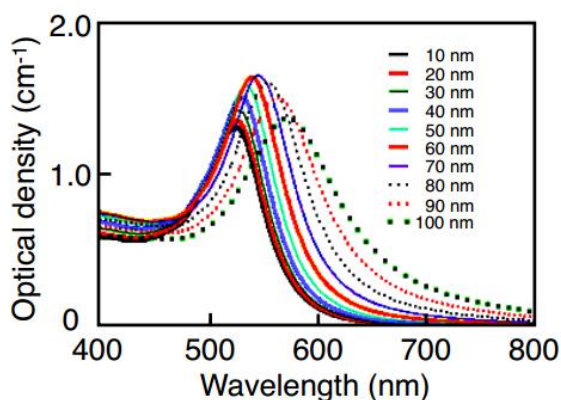


Figure 1. 2 Extinction spectra of AuNPs with diameters ranging from 10 to 100 nm at mass concentration 0.05 (mg/ml). (Image courtesy of © 2017 nanoCamposix, Inc.)

1.7 Synthesis of AuNPs

While Faraday first described the reduction of tetrachloroauric(III) acid (HAuCl_4) to form colloidal gold suspensions in 1857 [39], the most popular method used today was devised by Turkevich *et al.*, in 1951 [45]. To control the size and shape of AuNPs during synthesis, we must consider the balance between the two processes involved, which are the nucleation and grow of crystallites. Various combination of reducing and surface-stabilizing agent have been reported for the control of the nanoparticle formation. Citrate is the typical reducing agent used to obtain spherical gold nanoparticle in an aqueous solution [46-48]. In the Turkevich reaction citrate has important role in colloidal dispersion stabilizing. In this method, citrate being oxidised to form dicarboxy acetone, while in parallel Au^{3+} ions are reduced to Au^{1+} ions and subsequently to Au^0 atoms. During this process dicarboxy acetone acts as an “organiser” molecule and attaches to the NPs surfaces and stabilizes colloidal dispersion. The presence of citrate on nanoparticle surfaces result in NPs showing negative zeta-potential [49, 50]. This synthesis has been subsequently adapted by many researchers to allow for size control [48], and varied chemical methods have been done by another researchers [51-56]. While chemical methods of nanoparticle synthesis are commonly employed due to their relative convenience, other utilized methods involving ultrasonic waves [57-60], microwaves [61-64], laser ablation [65-68], solvothermal method [69-72], electrochemical and photochemical reduction [73-79] and different biosynthesis method [80-85] have also been explored for making AuNPs.

1.8 Localized surface plasmon resonance

When AuNPs are illuminated by resonance light, a part of the incident light is absorbed in moving the conduction band electrons towards the nanoparticle surface [86]. This leads to move a negative charge on one side, and an equal positive charge at the other side of the NPs, therefore creating a dipole. The dipole

creates an electric field inside of the nanoparticle and gives rise to a linear restoring force. The restoring force on the electrons forces them to return to the equilibrium position. As a result, a dipolar oscillation of electrons is produced, which is known as plasmon resonance frequency [87].

The collective oscillation of conduction band free electrons in AuNPs are known as plasmons [88] (Figure 1.3). As a consequence of these dipole oscillations, light is radiated from the NPs in the form of scattering [89]. Additionally, the dipolar oscillations are produced on the surface of AuNPs, thus this circumstance is called as LSPR [86].

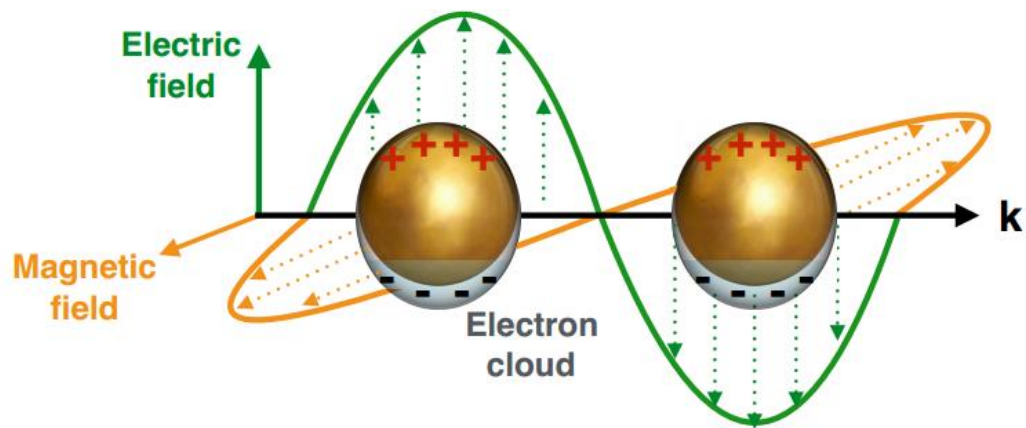


Figure 1. 3 Extinction of particles plasmons through the polarization of metallic nanoparticles. At the resonance frequency the plasmons are oscillating with 90° phase difference. The k-axis represents the light wave direction.

1.9 Plasmonic heat

Heat generation from AuNPs induced by light absorption have been regarded as side effects that needed to be minimized. However, it has been realized recently that the heat creation is effective and local. The potential applications by using this heat become popular quickly in the field of

nanotechnology such as photothermal cancer therapy. As discussed in the previous section, AuNPs show strong scattering and absorption of light at specific wavelength owing to their LSPR. The heating effect is proportional to the increasing effective absorption cross section in the region of the LSPR [90].

The high-energy of the excited plasmon can decay in two possible forms: One is a radiative decay, which corresponds to the elastic scattering of light (re-emission (scattering) of photons), and the other is a non-radiative decay, which results into the temperature (energetic charge carriers in the form of heat) increase of the AuNP [91] (Figure 1.4).

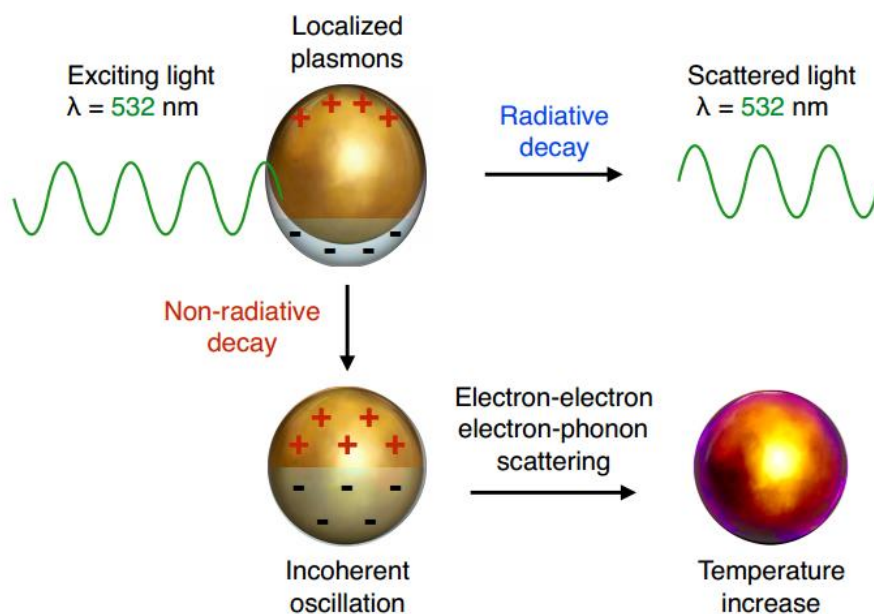


Figure 1. 4 Decays of the localized surface plasmon. The radiative decay results in elastically scattered light of the same wavelength as the incident light. The nonradiative decay is connected to the loss of phase of oscillating electrons. Electron-electron and electron phonon interactions lead to an increase of the temperature of the AuNPs.

Specifically, the non-radiative decay is linked to incoherently oscillating electrons and transfers the energy from LSPR to phonons due to electron-electron and electron-phonon interaction. The result of this process leads to the raised the temperature of the AuNP. The generated heat, then, diffuses away from the surface of the hot AuNP. This heat diffusion leads to the increase of the temperature around the AuNP.

1.10 Nanoplasmonic Optical Switch

Recent advancements in chemical biology, nanotechnology, and plasmonics now enable new light-sensitive tools of sub-nanometer and nanometer size scales to directly interface with intracellular processes. For example, nanoplasmonic optical antennae can be used as carriers of oligonucleotide cargo. Initially, oligonucleotide functionality is inactivated. Using light illumination as a remote trigger to release free oligonucleotides and “activate” their functionality, endogenous intracellular genes can be silenced on-demand.

Gold nanoplasmonic optical antennae, in the visible spectral region, are attractive candidates for intracellular control. Due to strong and sharp resonance peak of visible wavelength regime in their optical properties, AuNP efficiently convert light energy into surface-localized temperature, otherwise known as photothermal conversion [92-97], when the incident light is matched to their plasmon resonance wavelength. In the presence of this incident light, the conduction electrons of the antennae collectively oscillate in phase on resonance and subsequently make collisions with the metal lattice, thereby dissipating heat [98]. Heat transfer from the surface of antennae to the surrounding cellular environment is highly localized, decaying exponentially within a few nanometers [99-102] and therefore is thought to have minimal adverse effects on cells.

Several strategies, employing different carrier and cargo types. In this dissertation short single stranded DNA, otherwise known as antisense DNA, can be hybridized to a thiolated complementary sense strand, bound to a gold nanosphere's surface through the gold-thiol covalent bond, and photothermally dehybridized using continuous-wave incident light that is matched to the plasmon resonance wavelength of the gold nanosphere (Figure 1.5). This strategy of photothermal dehybridization using continuous-wave illumination offers notable advantages. For instance, no chemical modifications are made to the antisense DNA strand itself since a thiolated complementary strand is used to directly conjugate to the carrier's surface. Because chemical modifications can interfere with nucleic acid functionality and gene silencing efficacy, unmodified antisense DNA is highly desirable. Also maintaining surface coverage with complementary strands after illumination, prevents reattachment of antisense DNA strands back onto the carrier since rehybridization events are thermodynamically unfavorable due to steric hinderances and electrostatic repulsive forces at the carrier's surface [103]. Nanoplasmonic optical antennae enable "nanoplasmonic control" of genetic activities with sequence-specificity and spatiotemporal resolution. In this dissertation, sphere-shaped gold nanoplasmonic optical antennae are primarily utilized. Sphere-shaped nanoplasmonic optical antennae carrying genetic cargo are internalized in living cells.

However, gene interference with the precise spatial and temporal resolution, minimal photodamage, as well as the selective coupling of the optical transmission frequency to different nanoscale transmitters have not yet been accomplished in microalgae cells. Here, we present a new remote control switch of gene interference in these cells by using oligonucleotides on a nanoplasmonic carrier-based optical switch (ONCOS), short interfering oligonucleotides, and green laser transmitter.

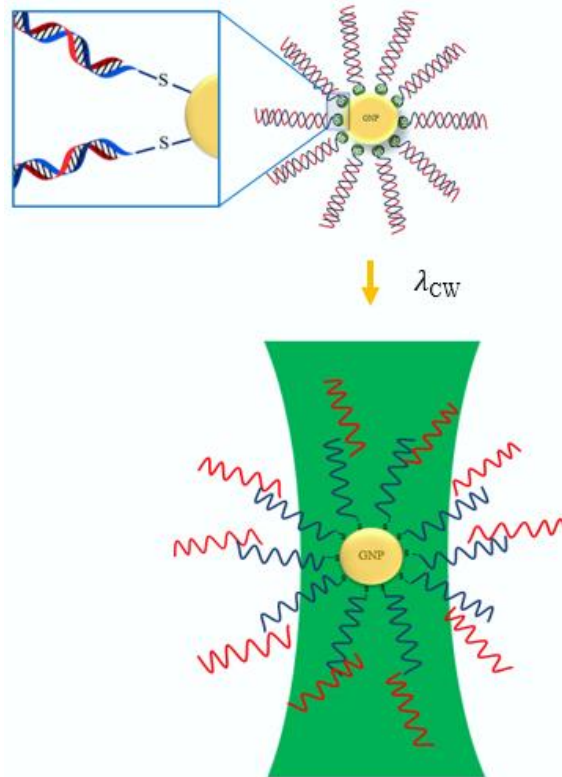


Figure 1. 5 Photothermal dehybridization of antisense DNA from AuNP using continuous-wave illumination.

1.11 Usage of AuNPs for the photothermal protein production as a new application in engineered biological systems

One of the many challenges in the development of engineered biological systems is to control gene expression [104]. Since most genes have specific biological function, it is of interest in the development of engineered biological systems to be able to control both in space and time the state of on and off of a gene expression [105]. Control of gene expression can occur at any both the transcription and the post-transcription stages [106], however, one of the most common involves post-transcription regulation which refers controlling the translation of mRNA into a protein [107]. In living cells, there are various

mechanisms that have been developed and engineered in order to controlling gene expression; mechanisms can be through external stimuli such as changes in temperature [108] or induction by light, or internal stimuli such as changes in the environmental pH [109], the use of chemical inducers [110] and changes in other culture conditions [111]. However, the internal induction mechanisms, although very efficient usually induce an irreversible on-off state, and the external mechanisms such as temperature are usually slowly reversible and lack space control specificity. Therefore, a lot of research have been focused on working with light-controlled gene expression, since light is a stimulus that induces a fast-switching non-invasive gene expression mechanisms with a highly space-specificity, especially when working with lasers. [112, 113]. Light can be naturally absorbed by many photoreceptor proteins found in biological systems such as plants, bacteria, fungi, and higher eukaryotes [114]. The structure of these photoreceptor proteins has two distinct parts with a specialized role. The light-sensitive part of these photoreceptor proteins has small molecules called chromophores, which are small molecules capable of receiving light and then transferring energy to another part of these photoreceptor proteins (which are connected to DNA) [115]. This mechanism for receiving light through chromophores finally leads to changes in the expression of the gene and, consequently, changes in the transcriptome pattern of the organism [116]. The existence of two major types of electronic and vibrational transitions, as well as the placement of these chromophores together, in order to increase the efficiency [117], leads to the formation of a variety of photoreceptors that can only absorb a certain spectrum of light. For example, red and far-red sensing phytochromes, cryptochromes and phototropins responsive to blue/UV-A and/or UV RESISTANCE LOCUS 8 (UVR8) photoreceptors responsive to UV-B are photoreceptors that exist in plant cells [118]. However, there are limitation of using these photoreceptors in the engineering of light-controlled gene expression systems; for example, chromophores are light spectra and their response is limited to exposure to the specific wavelengths. Therefore, when developing

complex gene expression systems, there is a need to incorporate expression of a variety of chromophores, leading in many cases to an instability of these molecules after being stimulated by the light [119]. Moreover, some modified fluorescent proteins such as green fluorescent proteins, based on the same chromophores (the basis of fluorescent proteins work is the chromophores), in addition to emitting fluorescent light they induce a series of unwanted biochemical side effects such as the production of reactive oxygen species (ROS) [120].

These various limitations associated with the use of chromophores to control gene expression in biological systems, led this work to search alternative systems that would allow versatility of absorption spectra to develop complex gene expression control. Therefore, this work explored the use of non-toxic metallic NPs, which are opto-thermal energy converter systems and are capable of interacting with biological systems. Metallic NPs have extraordinary optical properties that differ greatly from those of the bulk macroscopic metal [30]. In specific, AuNPs present a wide absorption spectrum that can be easily tuned since it directly depends on the size, shape and surface chemistry of the nanostructure. AuNPs due to having intense optical absorbance and large absorption cross section, can absorb optical energy in specific wavelength and convert it to thermal energy with high efficiency [121]. The result of this process leads to elevate the temperature of the AuNPs. The generated heat, then, diffuses away from the surface of the hot AuNPs and leads to the increase the temperature of the surrounding medium [87, 88, 91, 122, 123]. Although, to date, these superior optical properties or in another word plasmonic photothermal heating has not been successfully used except for some of applications as diagnostic reagents [33], drug carriers [34], contrast agents [35], radiosensitizers [33, 37] and specially photothermal therapy agents [36], we used the heat generated from AuNPs for a new application in name photothermal protein production for the first time in this study.

1.12 RNA thermometer

In photothermal protein production application, the main and primary aim is to produce different kind of proteins with various role in all engineered microorganisms contain switchable expression system such as RNA thermometers. RNA thermometers are structurally simple and sensitive to temperature changes. RNA thermometers are thermosensors which can sense temperature changes. Actually they are located in the 5'-untranslated region (5'-UTR) of mRNAs and can control the expression of downstream genes by regulate gene expression by temperature-induced changes in RNA conformation [124]. At low temperature (or in another word in a temperature-dependent manner) the mRNA will masks ribosome binding site [Shine–Dalgarno (SD) sequence] within the 5'-UTR and, in this way, prevents ribosome binding and translation and when temperature increase, the RNA secondary structure melts locally, thereby ribosomes can be joined to SD to start translation [125]. In this study, by computational design and in vivo screening, a RNA element capable of temperature-dependent induction of gene expression is constructed that regulate bacterial (*Escherichia coli* (*E. coli*) DH5 α) gene expression by a shift in the growth temperature. They construct single small stem-loop structure containing the ribosome binding site which works efficiently at specific temperatures. It can melt at specific temperature and be translated to a fluorescent protein. Therefore, our synthesized AuNPs in this work are particularly appealing candidates as a switchable temperature source that can provide needed temperature.

1.13 Microalgae Lipid

Microalgae as photosynthetic unicellular using water and atmospheric CO₂ are very efficient in converting sunlight into chemical energy and eventually, production of valuable chemical component such as proteins, carbohydrates and

especially lipids [126, 127]. During the process of photosynthesis nonpolar lipids such as triacylglycerol (TAG) (Figure 1.6:a and b) are stored in microalgal cells [128]. It has widely been accepted that these commercially beneficial and valuable compounds mainly serve as energy storage in microalgae cells [10, 128-130]. Through the process of transesterification (Figure 1.6:c), TAG can be easily converted into fatty acid methyl esters which are important and versatile form of biodiesel [131]. One of the best ways to produce high content of microalgal lipids and subsequently high amount of biofuel in future is microalgae efficient cultivation in mass scale [132]. But, as we know this work require large scale arable land. On the other hand, in compression with microalgae culture increasing to high production of lipids and eventually high amount generation of biofuel, enhancement of microalgae lipids through different method can be effective and sustainable way in future. Hence, it is very important to apply practicable method to raise lipid accumulation in microalgae cells [133].

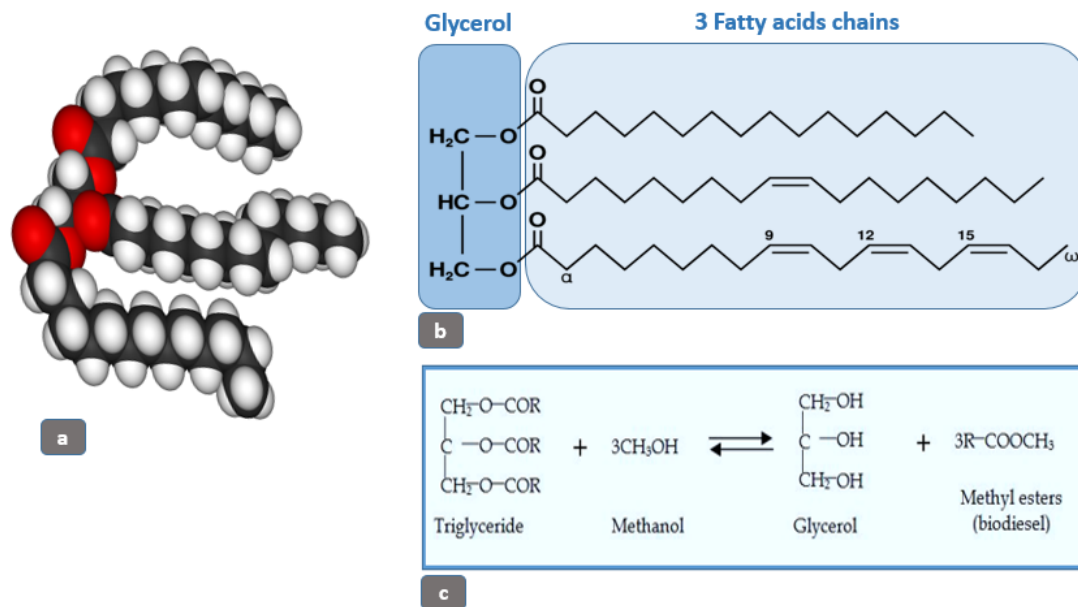


Figure 1. 6 Structure of TAG and convert it to biodiesel. (a) Three-dimensional model of a typical TAG molecule. (b) Linear structure of TAG. (c) General equation (Eq.) for transesterification of triglycerides to produce biodiesel.

The production and accumulation of microalgal lipids not only causing to survivorship of microalgae cells but also play important role to supply requirement energy to do crucial working such as cell division and DNA metabolism [134].

1.13.1 Lipids in *Chlamydomonas reinhardtii* (*C. reinhardtii*)

With increased industrial interest in microalgal production of biofuels, feed, food, and chemicals, research on lipid metabolism using *C. reinhardtii* as a model system has accelerated in recent years [135]. The unicellular microalga *C. reinhardtii* is no exception and accumulates TAGs, especially under nutrient deprivation or other environmental stress factors [136, 137]. *C. reinhardtii* has been studied in more detail compared to any other alga, resulting in the availability of molecular and genetic tools, annotated genome information, and an ever-increasing library of mapped mutants [138-140]. For this reason, *C. reinhardtii* has become a model system to investigate microalgal lipid metabolism, and research in this field has particularly gained traction due to potential interest in the production of biofuels and high-grade lipids [138, 141, 142].

Generally, lipids which produce by microalgae and especially *C. reinhardtii*, can be divided into two groups, polar lipids (such as glycerophospholipids) which have important role in cell structure (Structural lipids) and non-polar lipids (neutral lipids) which mainly known as storage lipids (such as TAGs). Structural lipids typically have long chain fatty acids that can be polyunsaturated fatty acids (PUFAs). These fatty acids which are include important source of Eicosapentaenoic acid (EPA), docosapentaenoic acid (DPA) and docosahexaenoic acid (DHA) have been found to have many benefits, not only due to their potential for biofuels production but also because of their valuable role in treatment of some diseases such as atherosclerosis, Parkinson and Alzheimer

[94]. These polar lipids also plays a major role in the mitochondrial supercomplexes [143].

Polar lipids and some sterols have a crucial role in cell membrane construction. It assists to provide a selective permeability barrier between different intracellular organelles [144]. These lipids also have special roles in maintaining optimal membrane fluidity for a wide variety of metabolic and biosynthetic processes and participate directly in several different intracellular membrane fusion events. Moreover, these structural lipid have significant function in cell signaling pathways and play key role responding to changes in the cellular environment [126, 144]. By contrast, as was noted above, TAGs have a pivotal role as energy storage in microalgae cells. In microalgae, CO₂ fixation process provides basic energy and required carbon skeletons for metabolism, growth, storage and maintenance throughout the daily cycle [145].

C. reinhardtii during light period capture energy from sunlight and then convert it to important organic carbon compounds like pyruvate, glucose, xylose, acetate and amino acids, which less than 10% of these compounds can be metabolized to produce fatty acids in the chloroplast in the light [146, 147].

Eventually, fatty acids ultimate product can be used to produce phosphatidic acid and diacylglycerol in the endoplasmic reticulum (ER) and the chloroplast, which their essential role was known in cellular metabolism. Since many elements and conditions may influence on accumulation of TAG, in specific situation such as nutrient destitution, ER-derived diacylglycerol can be used to assemble of TAG over the ER membranes in the cytosol (Figure 1.7). [133, 148-152]. These TAGs which are principally formed in light period in ER and reserve in them, again reused for polar lipid constructing in the darkness time [153].

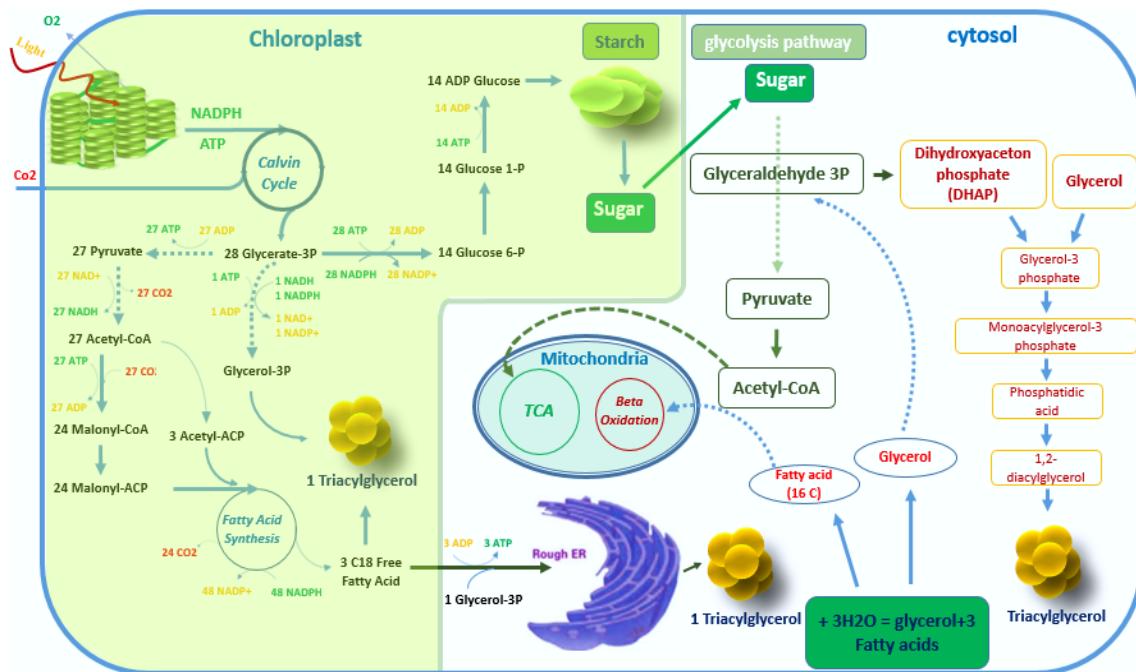


Figure 1. 7 The figure illustrates two possible pathways for TAG formation following the assumed route in the chloroplasts or over the ER membranes in the cytosol.

Constituted TAGs in microalgae cells typically contain saturated and monounsaturated fatty acids [154] and while, until recently it was believed that red alga (*Porphyridium cruentum*) is only alga, which can accumulate PUFA in TAGs [155], recently some species of green microalgae such as *Parietochloris incisa* have indicated more ability to produce high amount of omega-6 long-chain polyunsaturated fatty acids (n-6 LC-PUFA) [156, 157]. Also, there are another species (e.g., *Pavlova lutheri*, *Nannochloropsis oculata*, *Thalassiosira pseudonana*, and *Phaeodactylum tricorutum*) which is reported that their accumulated TAGs are contain lesser extent of PUFA [158, 159].

When we investigate more facts of TAGs, we can find that these may have additional performance except energy storage activation. They may have an indirect role in the reorganization of membrane in response to a sudden change

in the environmental situation. Because, in these conditions, TAGs can aid polar lipids through give them special acyl group to enable them for fast adaptive membrane reorganization [160, 161].

1.13.2 *Carnitine-acylcarnitine translocase* gene

The transport of solutes across the inner mitochondrial membrane is catalyzed by a family of nuclear-encoded membrane-embedded proteins called mitochondrial carriers (MCs). *carnitine/acylcarnitine translocase* (CACT) (Gene ID:5724426) is members of the MCs family involved in fatty acid metabolis [162]. This protein is essential for fatty acid oxidation, a multistep process that breaks down (metabolizes) fats and converts them into energy. Fatty acid oxidation takes place within mitochondria, which are the energy-producing centers in cells.

A group of fats called long-chain fatty acids cannot cross the mitochondrial membranes to β -oxidation without assistance. The fatty acid first should be change to acyl-COA and then must be attached to a substance known as carnitine to acyl-carnitine complex to enter mitochondria. The CACT protein transports them into mitochondria. Carnitine is then removed from the long-chain fatty acid and transported back out of mitochondria by the CACT protein (Figure 1.7). *Carnitine-acylcarnitine translocase* deficiency prevents the shuttle-like action of carnitine from assisting fatty acids across the mitochondrial membrane and therefore there is decreased fatty acid catabolism. The result of this is an increased lipid content within cells [163].

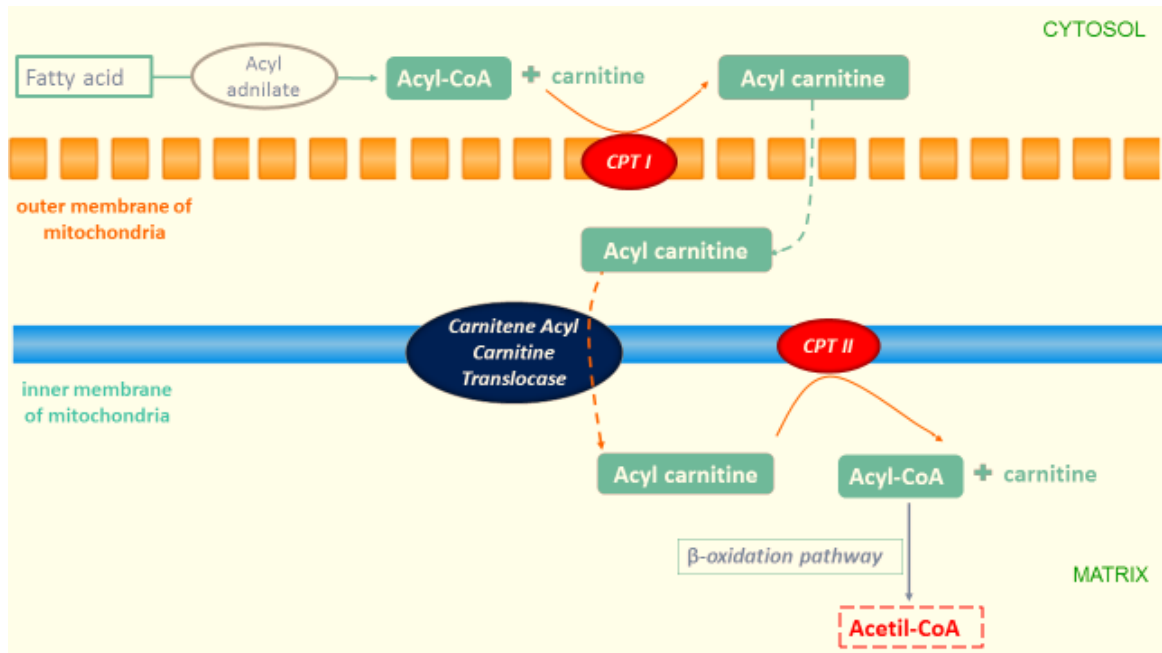


Figure 1. 8 Activation and transition of fatty acids into matrix of mitochondria [164].

CHAPTER 2

Background

It is believed that climate change is currently the most pressing global environmental problem. It is widely accepted that using fossil fuels has caused global warming; therefore fossil fuels as a source of energy should be replaced with renewable, clean energy sources to reduce CO₂ and greenhouse gas emissions [165]. Other detrimental effects of global warming include a potential increase in sea level and subsequent submerging of lowlands, deltas and islands, as well as changing of weather patterns [166]. Another issue is the energy crisis, in which the world suffers from lack of energy security due to depletion of the finite fossil fuel resources. The continued use of fossil fuels as a primary source of energy is now widely recognized to be unsustainable because of depleting resources and the contribution of these fuels to environmental pollution [167]. The main alternative to fossil fuel is biofuels.

The most common biofuels are biodiesel and bioethanol, which can replace diesel and gasoline, respectively, in today's cars with little or none modifications of vehicle engines. They are mainly produced from biomass or renewable energy sources and contribute to lower combustion emissions than fossil fuels per equivalent power output. They can be produced using existing technologies and be distributed through the available distribution system. For this reason biofuels are currently pursued as a fuel alternative that can be easily applied until other options harder to implement, such as hydrogen, are available [168]. The production of biodiesel has received much attention worldwide and was one of the first alternative fuels to become known to the public [169]. Biodiesel

that is produced from transesterification of triacylglycerides with monohydric alcohols [170], is renewable biofuel, which is derived from oil crops such as soybeans, canola oil, palm oil and corn oil, waste cooking oil and microalgae[171-174]. Global production of biodiesel is expected to reach 41.4 Bln L by 2025 corresponding to a 33% increase from the 2015 level (Figure 2.1) [175].

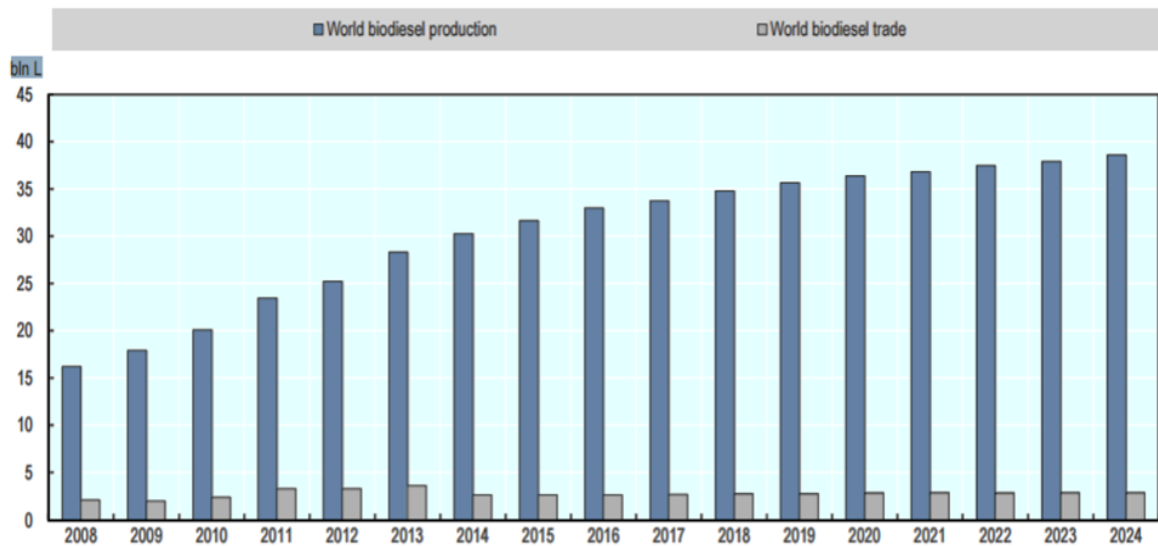


Figure 2. 1 World biodiesel production and trade.

The European Union is expected to be the major producer of biodiesel (Figure 2.2). Other significant players are the United States, Brazil, Argentina and Indonesia [175]. Mexico is one of eight countries that cover major expanding biofuel markets, as well as different world regions with varying levels of development [176].

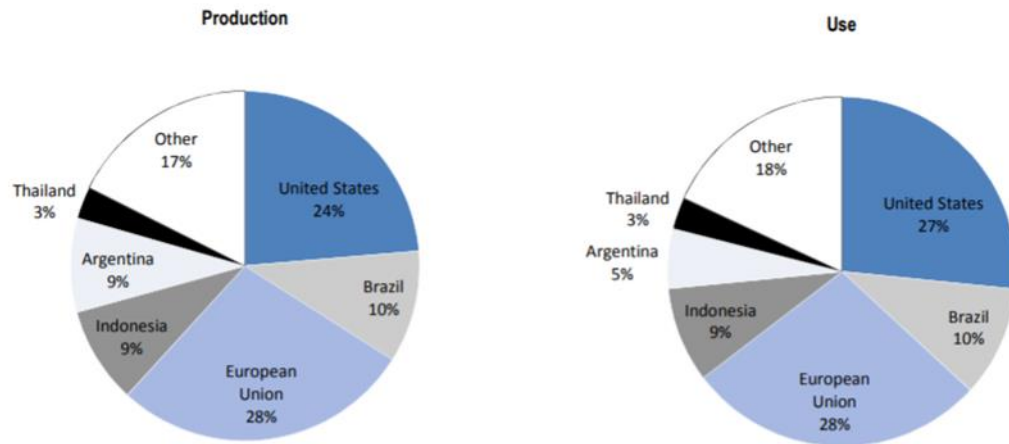


Figure 2. 2 Regional distributions of world biodiesel production and use in 2025 [175].

The first idea of blending vegetable oils with conventional diesel fuels came from Rudolf Diesel and Henry Ford. The idea of using microalgae as a source of fuel is not new [177, 178], but it is now being taken seriously because petroleum is non-renewable source energy and, more significantly, the emerging concern about global warming that is associated with burning fossil fuels. The oil content and biomass production from algae is far superior to that of terrestrial plants such as soybean and corn [179]. Even the most widely used oil crops including oil, palm, and sugarcane cannot match the amount of lipids for biodiesel that algae can produce when compared on a percent dry weight basis [180]. Oil content in microalgae can exceed 80% by weight of dry biomass [13]. Furthermore, lipids from algae are rich in saturated and unsaturated fatty acids such as oleic (18:1), palmitic (16:0), stearic (18:0), and linoleic (18:2) acids [181], making it ideal not only for fuel production, but also as a high value food product.

Some strains of microalgae contain high amounts of oil, which could be extracted and purified and converted to fuels. To improve biofuel production from microalgae, engineering solutions to optimize the productivity of any microalgae cultivation system and chose the suitable strains for biofuel

production are important [182]. However, many researchers worked on the enhancement of lipid amount in microalgae till now. They are using many different methods in this case. Biochemical engineering approach is one of the methods for enhancing lipid production of microalgae through controlling the nutritional or cultivation conditions such as environmental temperature [183-185]. Temperature is an important and easily-controlled environmental factor affecting algal growth and the formation of temperature-dependent components within the cells such as fatty acids. Many microalgae have the ability to grow over a wide temperature range, which is particularly true for *Chlorella* sp. that can adapt to 5°C – 42°C. Yet for the optimal growth temperature, it is species and/or strain specific. For example, *C. vulgaris* growth was negatively affected at temperature above 30°C, and further temperature increase (38°C) led to cell death [186]. For *C. sorokiniana* UTEX 2805, it can grow better under 40°C – 42°C than lower temperature (28°C), while for *C. sorokiniana* 211-32 (SAG) the maximum biomass was obtained under 28°C [187, 188].

Also when the marine microalgae *Chaetoceros* sp. FIKU035, *Tetraselmis suecica* FIKU032 and *Nannochloropsis* sp. FIKU036 were cultured at different temperatures (25, 30, 35 and 40 °C), results showed that the specific growth rate, biomass and lipid content of all microalgae decreased with increasing temperature. With regards to fatty acids, the presence of saturated fatty acids (SFAs) in *T. suecica* FIKU032 and *Nannochloropsis* sp. FIKU036 decreased with increasing temperature, in contrast with PUFAs. Moreover, *Chaetoceros* sp. FIKU035 was the species that could grow at 40°C [189]. Therefore, environmental temperature's effect on microalgal growth is definitely one of the major factors that need to be evaluated. Besides, nutrient media characteristics, such as carbon source, nitrogen source, and their initial concentrations, are also extremely important factors affecting cell growth and lipid accumulation. For example under nitrogen-deficient conditions, *P. tricornutum* produced a large amount of SFAs, mainly as palmitic acid (C16:0) [190].

Genetic engineering approaches that are based on transgenic microalgae are the other methods that used to increase of lipid amount in microalgae. The fast developments of microalgal biotechnology permit the isolation and use of key genes for genetic transformation [183, 191]. Using of this method reported by many researchers such as Dunahay *et al.* [191] and Sheehan *et al.* [192]. Some success has been achieved related to generate overexpression mutants; for example, starch mutant strains were observed to have significantly higher TAG contents [193], There has also been an attempt to modify the specific fatty acid composition within the cell to achieve a distribution that is more desirable for downstream processes. To that effect, *Phaeodactylum tricornutum* was modified through heterologous expression of two thioesterases to bias fatty acid production towards lauric and myristic acid [182, 194]. They were able to demonstrate significant upregulation in shorter chain fatty acids and also that 75-90% of the synthesized fatty acids was further incorporated into TAG. This same strategy was successful in plants as modified lipid composition was carried out in *Brassica napus*, *Arabidopsis thaliana*, *Glycine max*, and *Nicotiana tobacum* [194].

One of the attractive and promising biotechnological route that is using by scientists to gene expression control is gene interface which is promising method for enhancement of lipid now. In this case, accumulate and enhancement of lipid in microalgae will do due to prevent of expression of genes which have key roles in decrease of lipid amount through different pathways. Due to having promising effective effect on accumulate of lipid, this method done by researchers lately.

For example Trentacoste [195] reported that the targeted knockdown of a multifunctional lipase/phospholipase/acyltransferase increased lipid yields without affecting growth in the diatom *Thalassiosira pseudonana*.

Moellering, E. R. and C. Benning [196] focused on the model green alga *C. reinhardtii* and investigated accumulation of TAGs and the formation of lipid droplets during nitrogen deprivation. They reported that repression of the major

lipid droplet protein gene expression using an RNA interference (RNAi) approach led to increased lipid droplet size, but no change in TAG content. Moreover, examination of the artificial silencing effects of the five homologous genes (CrDGAT2-1 to CrDGAT2-5) on lipid content in *C. reinhardtii* was done by Deng (136). They demonstrated that silencing of CrDGAT2-4 resulted in increase in oil content. Also Deng, X., *et al.* (2013) [197] demonstrated that Silencing of *Chlamydomonas citrate synthase* gene increases TAG content in *C. reinhardtii*. They found that the regulation of *Chlamydomonas citrate synthase* gene can indirectly control the lipid content of algal cells and then propose that increasing oil by suppressing *Chlamydomonas citrate synthase* expression in microalgae is feasible.

In another study, CrCO gene which is homolog of *CONSTANS (CO)* gene is an important gene that regulates both plant photoperiod and flowering time [198, 199], is evaluated and silenced via RNAi. The silencing of this gene led to an increase in lipid content and an increase in TAG level by 24% [199]. By the same token, we want to investigate one of the important proteins called *carnitine acylcarnitine translocase* which has more importance in β -oxidation process and finally catabolism of lipids. Silencing of *carnitine acylcarnitine translocase* gene expression has not been done to increase of lipid and accumulate in microalgae so far. Although different gene has been studied through conventional methods of gene silencing, there is a new remote control switch of gene interference by using ONCOS, short interfering oligonucleotides, and a green laser transmitter. Gene interference by ONCOS occurs at the translational step.

In fact, the application of RNAi using AuNPs principally involves delivery of microRNAs (miRNAs) and small interfering RNAs (siRNAs) [200, 201]. For example, Seferos *et al.* [201], synthesized a functionalized AuNPs with thiol-modified oligonucleotides and used them to gene silencing. They saw that dense shell of oligonucleotides on the surface of these NPs inhibits degradation by

nucleases and also this higher density of oligonucleotide on the particle surface led to rapid cellular uptake of these polyvalent nucleic acid AuNPs (pNA–AuNPs). In another studies, RNase-free polyvalent siRNA–AuNPs were synthesized and delivered into HeLa cells [200]. This method also is done on BT474 breast carcinoma cells and blocking the translation of the ERBB2 mRNA by Lee [202]. They show that it is possible to gain highly precise spatial control and temporal tunability of translational events, which are otherwise impossible using conventional RNAi techniques. Moreover, Huschka *et al.* [203] demonstrated resonant light-induced release of single-stranded DNA (ssDNA) from Au nanoshells. In this experience, continuous wave (CW) laser radiation at 800 nm released the nonthiolated DNA strand from the nanoshell surface. As well, Huschka *et al.* [204] designed Antisense Oligonucleotide and siRNA based on Gold Nanoshell. They reported that Light-triggered delivery resulted in ~47% and ~49% downregulation of the targeted GFP expression by antisense oligonucleotide (AON-GFP) and siRNA-GFP, respectively. More recently, Vinhas *et al.* [205], conjugate AuNPs with a ssDNA oligonucleotide that selectively targets the e14a2 *BCR-ABL1* transcript expressed by K562 cells. They showed that this gold (Au)-nanoconjugate had great efficacy in gene silencing that induced a significant increase in cell death. Depending on the amount of heat generated and transferred to the surroundings, it can compromise or destroy cells. Regarding the functionalization of AuNPs with synthetic and biological compounds, covalent attachment via interaction between sulfur and gold (the S–Au binding) is a strong and effective method to anchor these structures on AuNPs' surface. Taking into account this background, we propose silencing *Carnitine-acylcarnitine translocase* gene by using ONCOS. Because through this route we will gain highly precise spatial control and temporal tunability of translational of target mRNA.

CHAPTER 3

Hypothesis and Objectives

3.1 Hypothesis

Our hypothesis is that we can control optically gene expression using metallic NPs such as AuNPs that have extraordinary optical properties (surface plasmon resonance). This method of gene expression optical control can be used for engineered microorganisms such as *E. coli* DH5 α TM that have temperature-sensitive part on the 5'-UTR of their mRNAs to produce a reporter protein (fluorescent protein) or in other word photothermal protein production for the first time. Also, this method can be used in another unicellular microorganisms such as microalgae such that *Carnitine-acylcarnitine translocase* gene of these organisms can be silenced with time-precision using ONCOS, leading to lipid accumulation in them.

3.2 Objectives

3.2.1 General objective

Photothermal protein production for the first time and introduction of this method as a new and controllable gene expression model. Also, increase accumulation of lipids in microalgae (*C. reinhardtii*) through opto-remote gene silencing using ONCOS.

3.2.2 Specific objectives

1. To synthesis and characterize the spherical AuNPs.
2. To test the AuNPs stability for long times.
3. Toxicity test of AuNPs to ensure that have not any toxicity
4. Toxicity test of AuNPs to ensure that have not any toxicity effect in biological system.
5. Simulation of temperature production and evaluation of AuNPs heat distribution.
6. Experimentally heat up the AuNPs by Laser and LED light source and make a temperature profile for the released temperature of AuNPs.
7. To test the Photothermal application of obtained AuNPs in biological system such as *E. coli* DH5 α TM and unicellular microalgae in order to evaluate its feasibility.

CHAPTER 4

Experimental Methodology

4.1 Materials and Reagents

JENAerGLAS 125, 250 and 500 mL Erlenmeyer flasks, 96-well plates, micropipettes of 2-20, 20-200, 100-1000 and 5-500 μl (Eppendorf) with their respective tips (Neptune), 1.5 mL tubes (Neptune) for microcentrifuge, 16 x 125 mm screw-capped test, bacteria culture media: Luria–Bertani (LB) Broth, Miller (Difco™), TAP medium [Tris(hydroxymethyl)-aminomethan ($\text{H}_2\text{NC}(\text{CH}_2\text{OH})_3$), Ammonium Chloride (NH_4Cl), Magnesium Sulfate Heptahydrate ($\text{MgSO}_4 \cdot 7\text{H}_2\text{O}$), Calcium Chloride Dihydrate ($\text{CaCl}_2 \cdot 2\text{H}_2\text{O}$), Dipotassium Phosphate (K_2HPO_4), Monopotassium Phosphate (KH_2PO_4), Ethylenediaminetetraacetic acid, Disodium Dihydrate ($\text{Na}_2\text{EDTA} \cdot 2\text{H}_2\text{O}$), Zinc Sulfate Heptahydrate ($\text{ZnSO}_4 \cdot 7\text{H}_2\text{O}$), Boric acid (H_3BO_3), Manganese(II) Chloride Tetrahydrate ($\text{MnCl}_2 \cdot 4\text{H}_2\text{O}$), Iron(II) Sulfate Heptahydrate ($\text{FeSO}_4 \cdot 7\text{H}_2\text{O}$), Cobalt(II) Chloride Hexahydrate ($\text{CoCl}_2 \cdot 6\text{H}_2\text{O}$), Copper(II) Sulfate Pentahydrate ($\text{CuSO}_4 \cdot 5\text{H}_2\text{O}$), Ammonium Molybdate Tetrahydrate ($(\text{NH}_4)_6\text{MoO}_3$), Acetic acid (CH_3COOH), Gold trichloride (AuCl_3), Trisodium citrate, Deionized water (18 M Ω), Disodium phosphate (Na_2HPO_4), Monosodium phosphate (NaH_2PO_4), Dithiothreitol (DDT), sense sequence, antisense sequence, phosphate-buffered saline (PBS). All of materials will provide from Proveedores CTR, Recitec and Probiotec companies.

4.2 Equipment

Shaking incubator (Lab Companion), refrigerator and freezer (Norlake), erlenmeyer flasks, Autoclave (Electric model No, 75X), magnetic stirrer (HP-

3000), pH meter (210-A), MASTECH MS6610 Digital Lux Meter, green LED chip with a peak wavelength of 520-525 nm, Readers (Thermo Scientific™ Varioskan™ LUX), confocal microscopy, UV-visible spectrophotometer (2120 UV Plus), Plate Reader (MULTISKAN GO), NAP5 purification columns (GE Healthcare), temperature-controlled shaker (IB-11E), Professional multimeter RMS. The development of the project to be developed will be carried out in Research Center in Biotechnology and Nanotoxicology located in the research and technological innovation park.

4.3 Synthesis of AuNPs

To synthesize AuNPs, Turkevich *et al.* method or in another word citrate reduction method was used [206]. 300 ml of 0.5 mM aqueous gold chloride solution was prepared in beaker and was boiled on heater stirrer until steaming. As soon as steaming was observed, 30 ml of aqueous 38.8 mM trisodium citrate solution was added to beaker. Immediately, after adding trisodium citrate solution, the solution became colorless and then was changed into dark, violet-red and maroon respectively. Finally, synthesized gold nanoparticle solution were brought to room temperature to cool down and shift color to red.

4.4 Characterization of the obtained nanoparticles

Among different technics to characterize NPs, Ultra Violet-Visible (UV-vis) spectroscopy [207], zeta potential analysis, transmission electron microscope are most common. UV-vis spectroscopy is a very useful, applicable and reliable technique for the primary characterization of synthesized AuNPs and also, AuNPs have unique optical properties which can have interact with specific wavelengths of light [207]. That is why we have used this technic as primary characterization

to observe SPR of AuNPs. We also have used conventional TEM and selected area electron diffraction (SAED) using an FEI-TITAN 80–300 kV microscope operated at an accelerating voltage of 300 kV to characterization of AuNPs shape and structure. In relation to the particle size, TEM images were used to measure synthesized AuNPs diameter and estimate particle size distribution of them using the manual microstructure distance measurement software. The elemental composition of the particles was analyzed by energy dispersive X-ray spectroscopy (EDS) analyzer integrated in the transmission electron microscope. Additionally, we have used Zetasizer (Nano ZS90 model) to measure zeta-potential of synthesized AuNPs to evaluate their stability in suspension.

4.5 Laser and LED light source and their temperature profile statistical analysis

4.5.1 Set-up the Laser for temperature profile measurements

To obtain complete temperature profile, a CW green laser (532 nm wavelength) has been employed to activate aqueous dispersions of AuNPs (Figure 4.1). 200 μ l suspensions of AuNPs loaded in a semi micro UV-cuvette (Cat. No. 7591 50) and directly was illuminated by CW green laser. Moreover, deionized water as a control experiment in same volume (200 μ l) was loaded in same cuvette and was illuminated by CW green laser (532 nm wavelength). Temperature was measured before and after laser illumination by using professional RMS Digital Multimeter sensitive sensors and then the temperature changes were recorded.

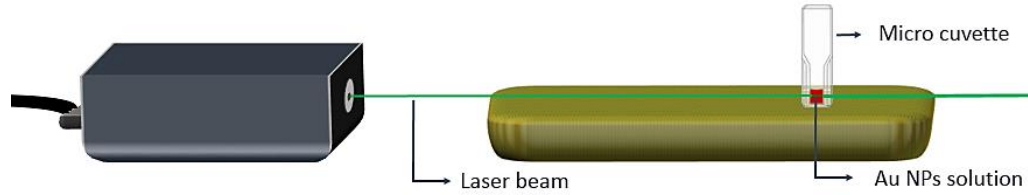


Figure 4. 1 Experimental setup for measuring the temperature profile of gold nanoparticle solutions.

4.5.2 Statistical analysis for Laser temperature profile

The design of experiment was carried out by MINITAB statistical software version 18 based on full factorial design. Factorial designs are preferred over traditional one factor at a time method, because they offer better estimates on the effect of each factor, can easily estimate the interactive effect between factors, offer more experimental information and do so using less resources (i.e. time, material). In this study, the design included three separate factors with several levels and three repetitions; CW laser with two different powers (100 and 300 mW), two various concentration of the gold nanoparticle aqueous (44 ppm and 88 ppm) and two level of the time (10 and 20 minutes). In order to identify effective variables in change temperature of AuNPs solution, Pareto analysis was used. Also to illustrate how these factor affect that, a regression model was developed and related analysis was done. All of the experiments were analyzed at a 95% confidence interval using MINITAB statistical software.

In addition, in order to investigate the regression model performance, two random tests were performed in three replication and residual standard error percentage (RSE %) was calculated (Eq. 4.1) as follow [208]:

$$RSE (\%) = \frac{(Actual\ value - Predicted\ value)}{Predicted\ value} \times 100 \quad \text{Eq. 4.1}$$

4.5.3 Set-up and assessing the LED chip suitability and feasibility for large scale use

To set-up and assessing the LED chip suitability and feasibility for large scale use, the green LED chip with a peak wavelength of 520-525 nm, $P_{LED} = 50\text{ W}$ and a viewing angle of 140° was mounted onto a heat sink with an incorporated same size cooling fan and driven only by electric power (Figure 4.2). To investigation of LED potency and functional capability to stimulate aqueous suspension of AuNPs and making of temperature profile, the LED light was put in front of the semi micro UV-cuvette (are transparent for experiments between 230-900 nm) contain different concentration and volume of AuNPs dispersions. The LED light was directly illuminated on the cuvette in different distance from samples and during various illumination time. Temperature changes immediately were measured and recorded using sensitive sensor of professional RMS Digital Multimeter.

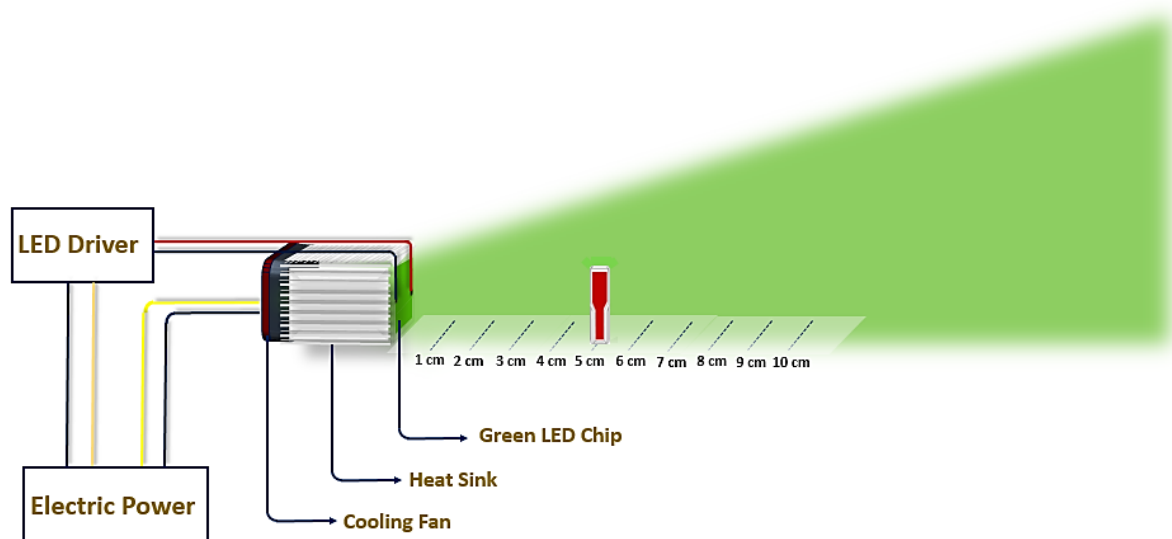


Figure 4. 2 Experimental setup for measuring the temperature profile of AuNPs solutions.

4.5.4 Experimental temperature profile for LED

In order to identify effective variable on increasing temperature of AuNP solution, statistical approaches were used. In first step for screening the various factors which had significant effect on temperature change, full factorial design was used by design expert software (version 11.0.5, STAT-EASE, Minneapolis, MN, USA). Then, following screening and identifying the significant factor, in order to achieve optimal AuNP photothermal treatment, Central Composite Design (CCD) and Response Surface Methodology (RSM), which are based on the mathematical and statistical techniques, were employed.

4.5.5 Theory and simulation for LED

Because of having AuNPs characteristics such as shape, diameter and etc, we simulated the light matter interaction with the AuNPs as well as heat generation of AuNP ensemble using finite element method and the software COMSOL Multiphysics.

4.6 Strains of used bacteria

To demonstrate temperature production in surrounding of gold nanoparticle surface and also use this temperature to heat up bacteria and subsequently related single small stem-loop structure on mRNA, *E. coli* DH5 α TM was used.

4.7 Growth Media of Bacteria

4.7.1 LB medium

LB broth (10 g/L Tryptone, 5 g/L yeast extract and 10 g/L Sodium Chloride) was used to grow *E. coli* cultures. To make 200 ml of LB broth, 5 g of LB broth powder was weighed and dissolved in 200 ml of purified water. It was mixed thoroughly and autoclaved at 121°C and after cool down, was kept in refrigerator (at 4°C).

4.8 Culture the bacteria strain

E. coli DH5 α TM cells were taken from bacteria precultured medium (20 μ l) and were grown in LB medium (5 ml) with 5 μ l kanamycin (50 mg/ml) at 37°C under continuous shaking (150 rpm). Cell density of the cultures after 12 h, was set to OD₆₀₀ = 0.5.

4.9 Design of genetic temperature sensor for *E. coli* DH5 α TM

In order to prove the optogenetic phenomena, a synthetic gene, which is controlled by a constitutive promoter, an RNA thermometer, the mCherry protein with a LVA tag, and a transcription terminator is designed in the laboratory of Dr. Jose Ruben Morones Ramirez, Universidad Autónoma de Nuevo León, Monterrey, Mexico (Figure 4. 3).



Figure 4.3 Genetic temperature sensor structure; The constitutive promoter BBa_J23119 for a constant production of RNA, the U6 RNA thermometer conformed by a Shine-Dalgarno (SD) sequence, an anti-SD sequence, and a spacer sequence, the mCherry protein as reporter with a LVA tag to avoid the mCherry accumulation, and a T7 transcriptional terminator.

Nucleotide sequence of synthetic temperature sensor is:

>Temperature sensor sequence

```

GAATTCGCGGCCGCTTCTAGAGttgacagctagctcagtcctaggtataatgctagcggatccT
CTCCTTCaaaaaAAAAAAAAAAAAAAAAAAAAAAAAAAAAAAAAAGGAGATATACCCA
TGGTTAGCAAAGGTGAAGAAGATAATATGGCAATTATTAAGAATTTATGCG
TTTTAAAGTTCATATGGAAGGTAGCGTTAATGGTCATGAATTTGAAATTGAA
GGTGAAGGTGAAGGTCGTCCGTATGAAGGTACCCAGACCGCAAAACTGAA
AGTTACCAAAGGTGGTCCGCTGCCGTTTGCATGGGATATTCTGAGCCCGC
AGTTTATGTATGGTAGCAAAGCATATGTTAAACATCCGGCAGATATTCCGGA
TTATCTGAAACTGAGCTTTCCGGAAGGTTTTAAATGGGAACGTGTTATGAAT
TTTGAAGATGGTGGTGTGTTACCGTTACCCAGGATAGCAGCTTACAGGAT
GGTGAATTTATTTATAAAGTTAAACTGCGTGGTACCAATTTTCCGAGCGATG
GTCCGGTTATGCAGAAAAAACAATGGGTTGGGAAGCAAGCAGCGAACGT
ATGTATCCGGAAGATGGTGCACCTGAAAGGTGAAATTAACAGCGTCTGAAA
CTGAAAGATGGTGGTCATTATGATGCAGAAGTTAAAACCACCTATAAAGCA
AAAAACCGGTTTCAGCTGCCGGGTGCATATAATGTTAATATTAAACTGGATA
TTACCAGCCATAATGAAGATTATACCATTGTTGAACAGTATGAACGTGCAGA
AGGTCGTCATAGCACCGGTGGTATGGATGAACTGTATAAACTGGTTGCATA

```

AACTAGTAGCGGCCGCTGCAGCATAACCCCTTGGGGCCTCTAAACGGGTC
TTGAGGGGTTTTTTGAAGCTT

The previously reported U6 RNA thermometer [124] was used in this designed synthetic gene. This thermosensor have a theoretical optimal temperature of 37°C (on state), and at 30°C (off state) there is no protein production [124]. On the other hand, the mCherry protein was used as a reporter. This monomeric protein can be measured by fluorescence, (with a peak fluorescent excitation and emission at 587 nm and 610 nm, respectively), have a maturation time of 15 minutes [209] and its labeled with a LVA degradation tag for a constant degradation.

4.10 Toxicity test of AuNPs on *E. coli* DH5 α

Since we intended to use the *E. coli* DH5 α TM bacteria in photothermal protein production application, toxicity effect of the AuNPs at different concentration (60, 70, 80 and 88 ppm) was investigated. The standard broth micro-dilution (BMD) method using 96-well microtiter plates [211] was performed as it was recommended by the Clinical and Laboratory Standards Institute (CLSI) to detect the sensitivity of the standard strains into AuNPs, with a minimum inhibitory concentration (MIC). Briefly, *E. coli* DH5 α TM cells was took from bacteria pre-cultured medium (20 μ l) and were grown LB medium (5 ml) with 5 μ l kanamycin (50 mg/ml) at 37 °C under continuous shaking (150 rpm). Then, AuNPs were dissolved in water and different concentration of them is made (60, 70, 80 and 88 ppm). LB medium as negative control were also prepared. 100 μ l of different concentration of AuNPs diluted in LB (100 μ l) containing *E. coli* DH5 α TM strains suspension (1 \times 10⁸ CFU/mL) and then incubated at 37 °C for 24 h. Finally, the bacterial growth was measured as turbidity with MultiskanTM GO Microplate Spectrophotometer at 600 nm.

4.11 Photothermal protein production by LED in *E. coli* DH5 α

Based on the computational design, we founded that stem-loop structure containing the ribosome binding site can be provisionally opened and works efficiently at 37°C. Beside, based on achieved temperature profile and related analysis in last sections, we found that we can obtain a given specific absorption rate (SAR) and thermal response in solution (it means bacteria surrounding) and finally achieve optimal AuNPs photothermal protein production through changing and regulation of main effective factors such as distance of LED light source and intended sample and also select and apply the appropriate concentration of AuNPs, volume of solution and illumination time. Based on our achieved regression model (Eq. 5.6) and analysis of response surface curve (Figure 5.9), we found that intended temperature (37°C) in 2800 μ l of AuNPs (with final concentration of 44 ppm) can be obtained in distance of 5 cm. In the next step, in order to examination of LED light source, thermal response of AuNPs, stem-loop opening and finally efficiently of photothermal protein production, our experiment is done in three different conditions including (A); under illumination, (B); without illumination and (C) Incubation condition (with the regulated temperature at 37°C (the exact needed temperature that stem-loop structure containing the ribosome binding site can be opened and works efficiently)). Samples detail of each one of condition that mentioned above are summarized below:

(A) Under illumination condition that had two samples (Sample 1 and Sample 2);

Sample 1) a cuvette containing the 1400 μ l AuNPs (with final concentration of 44 ppm) and 1400 μ l *E. coli* DH5 α TM strains (with final OD = 0.1) as main test.

Sample 2) a cuvette contain only 2800 μ l *E. coli* DH5 α TM strains as control.

(B) Without illumination condition that had two samples (Sample 3 and Sample 4);

Sample 3) a cuvette containing the 1400 μl AuNPs (with final concentration of 44 ppm) and 1400 μl *E. coli* DH5 α^{TM} strains (with final OD = 0.1) as control.

Sample 4) a cuvette contain only 2800 μl *E. coli* DH5 α^{TM} strains as control.

(C) Incubation condition that had one samples (Sample 5);

Sample 5) a cuvette contain only 2800 μl *E. coli* DH5 α^{TM} strains as positive control.

Optical density (OD) measurements were recorded at 600 nm using a UV–Vis spectrophotometer (LMAI-1-ES-3) every 1h and then growth curves were generated for each one of samples. Also, relative fluorescence units (RFU) of produced mCherry protein in their exponential phase were quantified.

4.12 Strain of used microalgae

For silencing of *Carnitine-acylcarnitine translocase* gene in microalgae, we used *C. reinhardtii* (ATCC[®] PRA-142TM), strain of CC-503 cw92 mt⁺.

4.13 Growth Media of microalgae

4.13.1 TAP medium for culturing of *C. reinhardtii*

TAP-Medium can be used for those microalgae such as *C. reinhardtii* which use NH_4^+ instead of NO_3^- as a nitrogen source. Such microalgae lack the nitrate reductase which would enable them to reduce nitrate via nitrite to ammonium. For

1000 mL final culture medium, was added the following quantities (Volume) of stock solutions (SL) prepared at the given concentrations to 850 mL dd-H₂O [212-215] (Table 4.1).

For Trace elements solution, first at all, Na₂EDTA.2H₂O was dissolved in 100 mL dd-H₂O by heating to 60-80 °C. Then pH was adjusted with KOH to 5.0. All trace elements were added separately and the pH value was checked constantly (the pH value should not increase above 6.8). Solution was let stand at 4 °C; when the color was changed from orange to red after approx. 2 weeks, it was filtered and was used to mix with the other reagents to make TAP medium and rest of it stored at -20°C to use in next time. In next step, was added one component after the other until each one has completely mixed and finally was filled up to 1000 mL. Medium was adjusted to final pH of 6.0 and was autoclaved at 121°C for 20 minutes. All stock solutions (unsterilized) and TAP medium (sterilized) was stored at 4°C.

Table 4. 1 Volume and concentration of TAP-Medium stock solutions.

Stock Solution (SL)	Volume	Component		Concentration in SL	Conc. in final Medium
Tris base	2.42 g	Tris(hydroxymethyl)-aminomethan $\text{H}_2\text{NC}(\text{CH}_2\text{OH})_3$			$2.00 \cdot 10^{-2}\text{M}$
TAP-salts	25 mL	Ammonium chloride NH_4Cl		$15 \text{ g} \cdot \text{L}^{-1}$	$7.00 \cdot 10^{-3}\text{M}$
		Magnesium Sulfate Heptahydrate $\text{MgSO}_4 \cdot 7\text{H}_2\text{O}$		$4 \text{ g} \cdot \text{L}^{-1}$	$8.30 \cdot 10^{-4}\text{M}$
		Calcium Chloride Dihydrate	$\text{CaCl}_2 \cdot 2\text{H}_2\text{O}$	$2 \text{ g} \cdot \text{L}^{-1}$	$4.50 \cdot 10^{-4}\text{M}$
Phosphate solution	1 mL	Dipotassium phosphate	K_2HPO_4	$28.8 \text{ g} \cdot 100 \text{ mL}^{-1}$	$1.65 \cdot 10^{-3}\text{M}$
		Monopotassium phosphate	KH_2PO_4	$14.4 \text{ g} \cdot 100 \text{ mL}^{-1}$	$1.05 \cdot 10^{-3}\text{M}$
Trace elements	1 mL	Ethylenediaminetetraacetic acid, disodium dehydrate $\text{Na}_2\text{EDTA} \cdot 2\text{H}_2\text{O}$		$5.00 \text{ g} \cdot 100 \text{ mL}^{-1}$	$1.34 \cdot 10^{-4}\text{M}$
		Zinc Sulfate Heptahydrate	$\text{ZnSO}_4 \cdot 7\text{H}_2\text{O}$	$2.20 \text{ g} \cdot 100 \text{ mL}^{-1}$	$1.36 \cdot 10^{-4}\text{M}$
		Boric acid	H_3BO_3	$1.14 \text{ g} \cdot 100 \text{ mL}^{-1}$	$1.84 \cdot 10^{-4}\text{M}$
		Manganese(II) chloride tetrahydrate	$\text{MnCl}_2 \cdot 4\text{H}_2\text{O}$	$0.50 \text{ g} \cdot 100 \text{ mL}^{-1}$	$4.00 \cdot 10^{-5}\text{M}$

		Iron(II) Sulfate Heptahydrate_ $\text{FeSO}_4 \cdot 7\text{H}_2\text{O}$	$0.50 \text{ g} \cdot 100 \text{ mL}^{-1}$	$3.29 \cdot 10^{-5} \text{ M}$
		Cobalt(II) Chloride Hexahydrate_ $\text{CoCl}_2 \cdot 6\text{H}_2\text{O}$	$0.16 \text{ g} \cdot 100 \text{ mL}^{-1}$	$1.23 \cdot 10^{-5} \text{ M}$
		Copper(II) sulfate pentahydrate_ $\text{CuSO}_4 \cdot 5\text{H}_2\text{O}$	$0.16 \text{ g} \cdot 100 \text{ mL}^{-1}$	$1.00 \cdot 10^{-5} \text{ M}$
		Ammonium molybdate tetrahydrate $(\text{NH}_4)_6\text{MoO}_3$	$0.11 \text{ g} \cdot 100 \text{ mL}^{-1}$	$4.44 \cdot 10^{-6} \text{ M}$
Acetic acid, conc.	1 mL	Acetic acid	CH_3COOH	

4.14 Microalgae Cultivation and Maintenance

800 ml cylindrical glasses were used for culturing. The initial amount of algae inoculum was about 5% of the total medium volume. Cultures were grown in a standard shaking incubator (LSI-3016R) with a shaking speed of 140 rpm at a temperature of 25°C and a light intensity of 60 $\mu\text{mol}/\text{m}^2/\text{s}$ (under alternate 14 h light and 10 h dark cycle).

4.14.1 Analysis of Samples

4.14.1.1 Cell Density

The light-scattering properties of *C. reinhardtii* cells is used to measure the optical density (OD) of the algal culture. OD is a direct measure of the algal cell density. In this case, 1 ml sample of *C. reinhardtii* was extracted daily and analyzed under the appropriate wavelength: at 680 nm where *C. reinhardtii* showed the highest peak for chlorophyll or at 750 nm to avoid photosynthetic absorption peak interference. Each experiment was repeated three times and curves of cell density for both OD₆₈₀ and OD₇₅₀ were drawn.

4.14.1.2 Cell Count

The cell count involves manually counting the number of cells under a microscope using Hemocytometer. *C. reinhardtii* cell count carried out with three repetitions in each experiment and growth curve of that was drawn.

4.14.1.3 Dry Weight and Biomass Concentration

Algal dry weight is one of the most critically needed measurements for determination of microalgal biomass at high concentrations. For this purpose, a calibration curve was prepared as follows:

20 ml samples of the algal suspension in three repetitions were collected on the daily basis during the duration of the experiment. Each sample was first centrifuged (10,000 rpm, 20 minutes), washed and centrifuged the second time. The concentrated algal broth was poured into watch glass and placed into the oven at temperature of about 60°C for a period of about 24 hours till its weight became constant. Afterwards, the watch glass with algae were weighted (W_s). The dry watch glass weight was measured (W_0). Finally, the dry cell weight was calculated using Eq. 4.2.

$$\text{Dry cell weight} = W_s - W_0 \quad \text{Eq. (4.2)}$$

The dry weight calibration curve, in next chapter, was created according to the above mentioned procedure.

4.15 Preparation of oligonucleotide-conjugated AuNPs

4.15.1 Required oligonucleotide

All synthetic oligonucleotides, including the sense and antisense sequence were purchased from T4 Oligo (Mexico) and their sequences are shown in Table 4.2. All antisense sequences are not labeled with dye.

Table 4. 2 Modified DNA oligonucleotides and their melting temperatures (T_m).

Strand	Sequence (5' to 3')	T_m (°C)	Modification	Length of production
Sense (15 bp)	ACACCTTATGGAGCC	54.9°C	3'-(CH ₂) ₆ -thiol	-
Antisense (15 bp)	GGCTCCATAAGGTGT	54.9°C	3'-(6-FAM)	-
F primer of CACT gene	CGAGGAACACCTTATGGAGCC	64.6°C	-	263 bp
R primer of CACT gene	TGGCTGACTGTAAGCG	64.5°C	-	
F primer of alpha tubulin 1 (TUA1) gene	ATGGAGGAGGGTGAGTTCTC	63.2°C	-	157 bp
R primer of alpha tubulin 1 (TUA1) gene	ACTACACTTGCTGCTACCCT	63.5°C	-	

4.15.2 Attachment of DNA to AuNPs

4.15.2.1 Thiol-Modified Oligonucleotide Reduction and purification

In the first step, the disulfide bonds of thiol-modified oligonucleotides were reduced with DDT (Thermo fisher science R0862) to achieve the active sulfhydryl form (Figure 4.4).

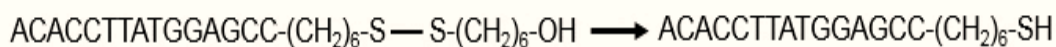


Figure 4. 4 Example disulfide bond reduction of a 3'-Thiol-Modifier C6 S-S oligonucleotide.

Then, the activated sulfhydryl forms of oligonucleotides were purified using NAP10 purification columns (GE Healthcare).

4.15.2.2 Conjugation of sense and antisense oligonucleotides to switches

To conjugate sense oligonucleotides to surface of the AuNPs, 10 μL of 100 μM thiolated, sense oligonucleotides was incubated with 2000 μL of AuNPs (6.52×10^{11} particles/ml or 1.08 nM) and 40 μL of PBS (pH 7.4) on a rocker for 8 h. The sense oligonucleotides attached to the switches through the thiol (-SH) group on the 3' end (Figure 4.5).

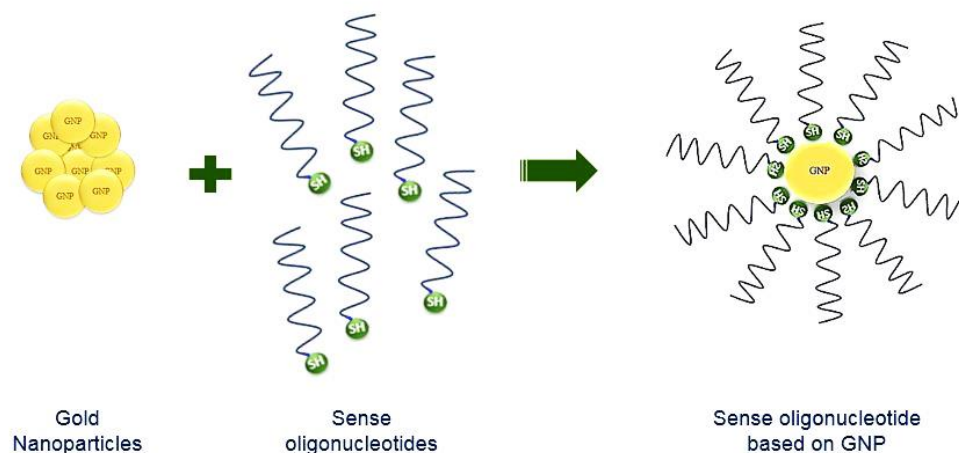


Figure 4. 5 Conjugation of sense oligonucleotide to AuNPs surfaces.

To hybridize antisense oligonucleotides to the sense oligonucleotides, 10 μL of 100 μM antisense oligonucleotides were added to the switch-containing solution. This mixture was then heated for 2 minutes at 80°C and then heated for 15 minutes at 65°C . The mixture was finally incubated at room temperature on a rocker for 8 hours to ensure maximum hybridization (Figure 4.6).

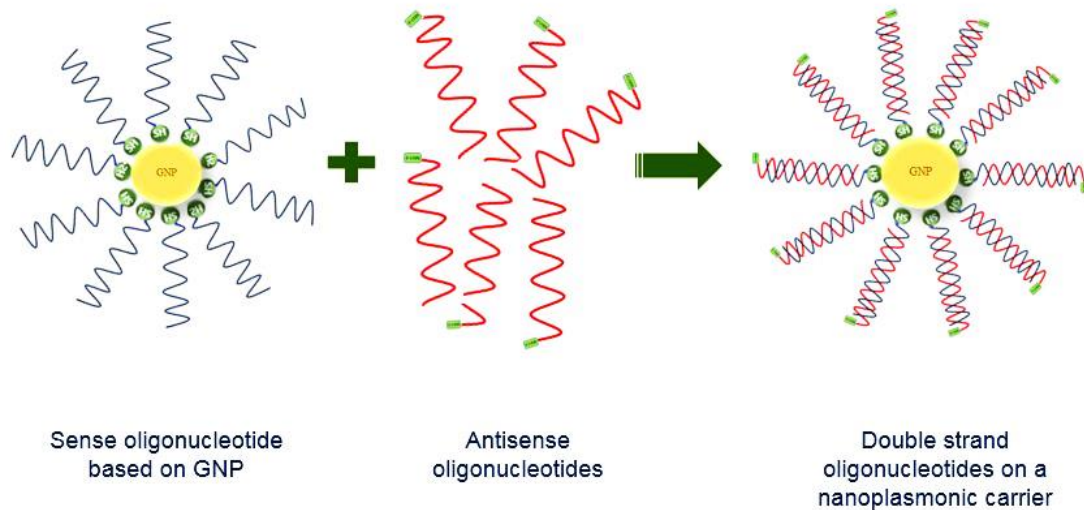


Figure 4. 6 Conjugation of antisense oligonucleotide to sense strand.

4.16 In-vitro test of antisense photothermal dehyridization

In order to confirm *in vitro* photothermal dehyridization of antisense strands from the switches to verify that photothermally generated heat lead to antisense releasing and gene silencing in living microalgae cells, we used an oligonucleotide (15 bp) with known melting temperatures (54.9°C): (15 bp sense) 5'-ACACCTTATGGAGCC-3'-(CH₂)₆-thiol, (15 bp antisense) 5'-GGC TCCATAAGGTGT -3'-6-FAM. Because, the temperature profile of AuNPs was experimentally and statistically characterized, 200 µL switches with length of 15 bp was illuminated separately in a specific distance for 15 minutes. The fluorescence intensity of the conjugated switches was measured by Microplate Readers (Fluoroskan™ Microplate Fluorometer).

4.17 Switches delivery into the microalgae cells

Generally, import of exogenous DNA into the unicellular, green alga *C. reinhardtii* is limited by their rigid cell wall. Although various methods, such as glass beads agitation, electroporation, and microparticle bombardment, have been successfully used [19, 216-220] to import of DNA into the plant cells such as microalgae, there is not any successful report about ssDNA or dsDNA-functionalized AuNPs (DNA-AuNPs) delivery into the microalgae cells. However, we imported the switches into the *C. reinhardtii* cells by electroporation following the protocol from Invitrogen using GeneArt® MAX Efficiency® reagent. Preparation of sample was performed according to the manufacturer's instructions with some modifications. The basic modification included kind of sample (dsDNA-functionalized AuNPs instead of linear DNA or plasmid), and other modifications included kind of electroporation device (Eppendorf Eporator®), DNA concentration and sample size.

Microalgae strains were subcultured in 200 ml of TAP medium until they reached to the early exponential phase and reached a cell density more than of 2×10^6 cell/ml (total amount was 45×10^7 cell in 200 mL of TAP medium). The cells were then harvested by centrifugation (for 2500 rpm and 5 min) followed by washing twice with 10 mL GeneArt® MAX Efficiency® Transformation Reagent. After that they were resuspended at a cell density of 25×10^7 cells/ml, and 400 μ l microalgal cells were mixed with 800 μ L switches in a microtube and then divided into ice-colds 0.2 cm cuvette for electroporation process. This was followed by electroporation using the Eppendorf Eporator® electroporation system at 500 V and 600 Ω . They incubated on the bench for 15 minutes and then transferred to 10 ml TAP-40 mM sucrose medium and allowed to recover for 12–16 h in the dark at 25 °C and shaking at low speed. Then cells were harvested, resuspended in 400 μ l TAP medium. (confirmation of switches delivery is done by confocal microscopy).

4.18 Experimental setup for photothermal releasing of antisense oligonucleotide to gene silencing

After entering the switches into the microalgae cells, the green LED chip (with a peak wavelength of 520-525 nm, $P_{LED} = 50 W$ and a viewing angle of 140°) was positioned in front of them. The green LED chip was used to illuminate the 400 μ l microalgae cells containing switches (with final concentration of 43 μ g/ml AuNPs) at a distance of 1.7 cm for 10.8 minutes to reach surrounding temperature of AuNPs surface up to T_m of sense and antisense oligonucleotide ($T_m = 55^\circ\text{C}$) which are conjugated on the AuNP surfaces. It is necessary to note that, mentioned illumination time duration, the distance of sample and LED source light are selected and used based on the final concentration of AuNPs switches and the regression equation which obtained from experimental temperature profile of LED source light.

Then, samples in three repetitions are incubated at 25°C (normal growth temperature of *C. reinhardtii* strain) for 2.5 h. In this experiment, we also prepared control samples; The cells that not received any switches and have not been exposed to any LED illumination. Afterwards, the samples are incubated at 25°C for 2.5 h (this experiment is carried out with three repetitions in each experiment).

4.19 RNA extraction and quantification

RNA extraction was facilitated by Invitrogen™ TRIzol™ reagent (Cat. No. 15596026) from Invitrogen following the protocol in the technical manual. RNA concentrations were measured using a Shimadzu BioSpec-Nano Micro-Volume Spectrophotometer. Then, DNase treatment was performed using DNase I, RNase-free kit from Invitrogen™ (Cat. No. MAN0012000), following the protocol in the technical manual to remove genomic DNA from the RNA preparation.

Generation of cDNA was performed using SuperScript™ IV First-Strand Synthesis System from Invitrogen™ (Cat. No. 18091050), following the protocol in the technical manual. Gene-specific primers were designed to amplify fragments of approximately 157–263 bp in length. For the quantification of gene expression, Real-time PCR (RT-PCR) was carried out on AriaMx Real-time PCR System using the SYBR Green dye; innuMIX Real-time PCR DSGreen Standard (Analytic Jena). RT-PCR reactions were carried out in a total volume of 20 µl, with 10 µl mentioned SYBR Green PCR Master Mix, 1 µl of a 5 µM primer of each one of forward and reverse primers, 100ng of cDNA as template and sterilized Milli-Q water up to 20 µl. RT-PCR program is shown in table 4.3.

Table 4. 3 Thermocycler program (RT-PCR) used for the quantification of gene expression.

Step		Temperature	Time (s)	Cycles
Hot Start		95°C	120	1
Denaturation		95°C	15	40
Annealing		60°C	30	
Extension		72°C	30	
Melt	Denaturation	95°C	30	1
	Annealing	65°C	30	
	Extension	95°C	30	

The alpha tubulin 1 (TUA1) gene was served as internal control for the quantification assays. For gene expression analysis by RT-PCR, the expression values were calculated according to the Livak method [221]. See Table 4.2 for all primer sequences used in this work. It is worth mentioning that threshold values were determined manually and normalized between plates. All RT-PCRs were run

in triplicate (also this experiments had three biological repetition). Finally, in order to enable further understanding of CACT gene silencing effect on cellular lipid formation increase, *C. reinhardtii* cells were stained (2h after silencing) with a Nile Red fluorescent dye (Sigma-Aldrich); microalgae cells (200 μ l) were added with 50 μ l of Nile Red dye (10 μ g mL⁻¹ DMSO stock) and incubated for 10 min in the dark and room temperature followed by washing with sterilized Milli-Q water. Then, the slides with stained microalgae sample were prepared and observed under a fluorescence microscope (Leica DM500 microscopes) at 596 nm excitation.

CHAPTER 5

Results

5.1 Microalgae Growth analysis

Photoheterotrophic growth of *C. reinhardtii* is one of the common options used by many researchers. In this experiment, a photoheterotrophic culture was prepared and the samples were kept in the standard shaking incubator (LSI-3016R). The optical densities of samples (both OD₆₈₀ and OD₇₅₀), number of cells and biomass concentration were measured every 24 hours. growth curves of each one of them is shown in figure 5.1. As can be seen in figure 5.1 (A) and (B), there isn't any difference between their growth model. Both growth curves demonstrate that after the culturing, the algal cells entered their logarithmic growth phase and after four days entered slowly their stationary phase in mixotrophic condition. Also figure 5.1 (C) shows that *C. reinhardtii* has highest number of cell in the five days after cultivation.

The linear relationship between the optical density and cells number was obtained after regression analysis and is given by Eq. 5.1 and 5.2 for OD₆₈₀ and OD₇₅₀ respectively.

$$\text{Cell numbers (cells/ mL)} = 14574x + 1178.7 \quad R^2 = 98 \quad (\text{Eq. 5.1})$$

$$\text{Cell numbers (cells/ mL)} = 20526x - 289.5 \quad R^2 = 98 \quad (\text{Eq. 5.2})$$

Which x is the numeric amount of OD₆₈₀ and OD₇₅₀ in each equation.

So, indirect measurements of cell count of *C. reinhardtii* can be determined easily through UV-Vis spectrophotometer. The growth curve related to biomass production data after 10 days is presented in figure 5.1 (D).

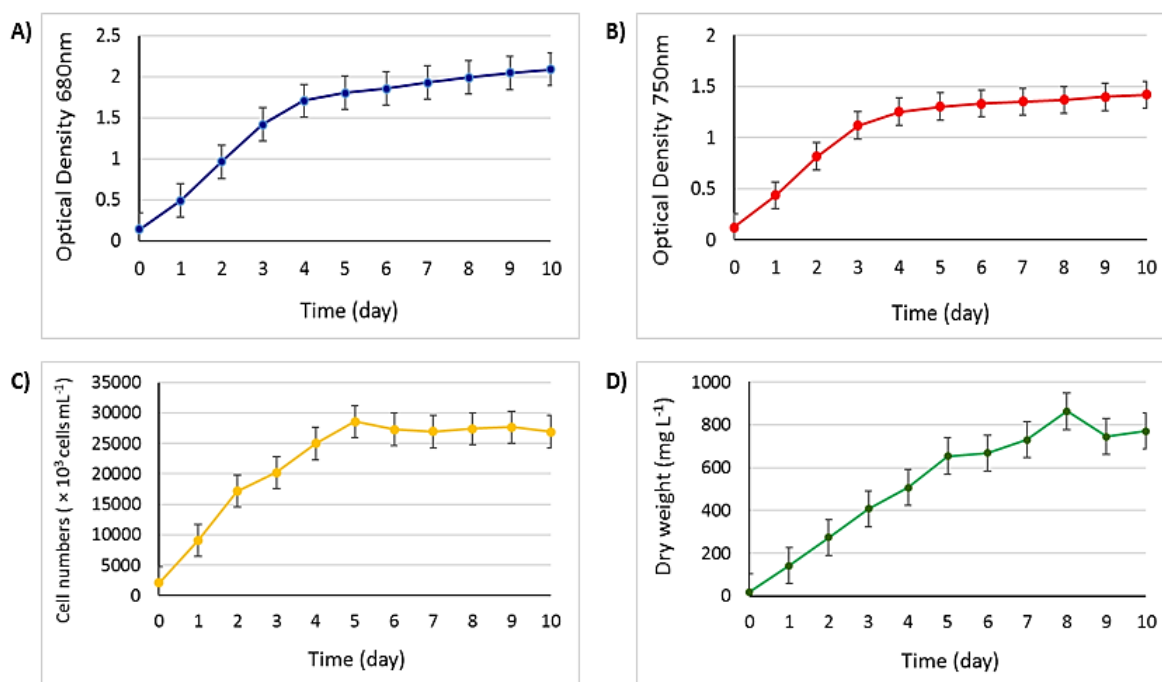


Figure 5. 1 Cell growth profile of *C. reinhardtii* in TAP growth medium. (A) and (B) cell growth (O.D. 680 nm and 750 nm respectively), (C) cell count growth curve and (D) biomass accumulation during the experiment. Error bars represent standard deviations from three independent growth experiments (Each point in the curves represent the mean of three replicates \pm standard deviation (n = 3)).

5.2 Characterization of the obtained nanoparticles

5.2.1 UV–Vis Spectra Analysis

The initial detection of the gold nanoparticles was done by UV–visible absorption, which is a useful technique to characterize nanoparticles. For metallic

nanoparticles, absorption wavelengths in the range of 300–800 nm are normally used for characterization [222]. Solution of the gold nanoparticles was red (Figure 5.2) originated from the excitation of surface plasmon resonance (SPR) of the nanoparticles [81]. This color strongly depends on the concentration and the size of the nanoparticles. However, the UV–vis spectra of the reaction sample was recorded instantly after the synthesis and is depicted in Figure 5.3. As it can be seen, gold nanoparticles exhibited optical absorbance around 523 nm which has been previously demonstrated to be a characteristic of gold nanoparticles [223-225]. Also, to survey stability of synthesized gold nanoparticle, UV–visible absorption of them was measured after 4 months. As shown in figure 5.3, this absorption is same first absorption (was recorded instantly after the synthesis).

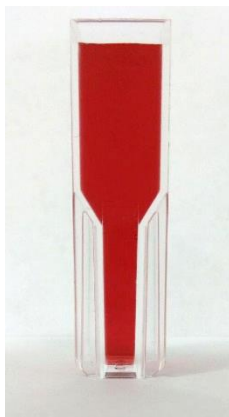


Figure 5. 2 Surface plasmon resonance (SPR) excitation of the nanoparticles.

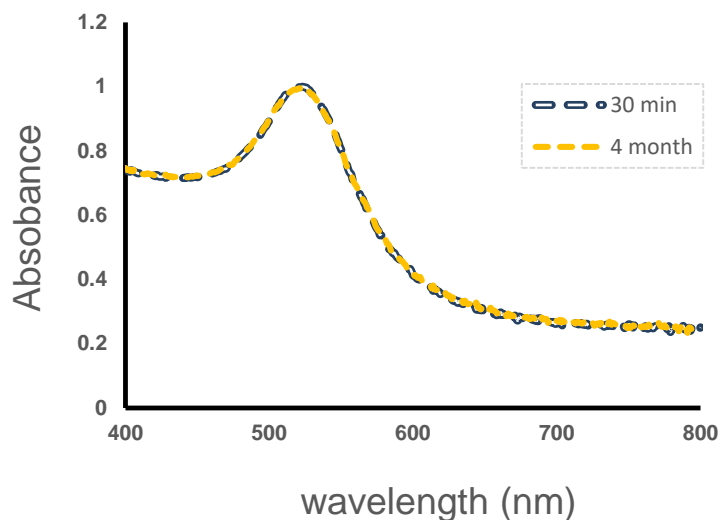


Figure 5. 3 UV–vis absorption spectrum of AuNPs; 30 minutes and after 4 months later synthesis.

5.2.2 Transmission Electron Microscopy Analysis

TEM was used for the determination of shape, average size, and particle size distribution of the synthesized AuNPs. As can be seen from figure 5.4 (A) and (B), the synthesized particles are spherical and approximately are homogeneous in nature. The high-resolution Transmission electron microscopy (HRTEM) image in figure 5.4 (C) shows that the lattice fringe was distinguishable, which also confirms the formation of Au crystals.

5.2.3 Selected-area electron diffraction pattern (SAED)

SAED analysis confirmed the crystalline nature of the AuNPs with the *n* (fcc) phase. Spotty rings which were observed corresponding to (111), (200), (220) and (311) planes of the fcc crystalline lattice of AuNPs (figure 5. 4 (D)).

Furthermore, the analysis of particles distribution determined an average size of the synthesized AuNPs to be 20.44 nm (Figure 5.5).

5.2.4 Energy dispersive X-ray spectroscopy (EDS)

As shown in figure 5.6, characterization of the NPs by EDS analysis exhibits Au atoms which confirmed the presence of gold nanoparticle. In this analysis other elements such as oxygen (O), carbon (C) and copper (Cu) were detected, where the oxygen is due to the air present in the chamber [226] and copper and carbon corresponds to the TEM holding grids [227].

5.2.5 Zeta-potential of synthesized AuNPs

Figure 5.7 shows the zeta potential measurement of the synthesized AuNPs by citrate method. The result revealed that the zeta potential value of AuNPs was determined as -26.6 mV, a measure of stability of the NPs. This high absolute value of zeta potential confirmed the formation of high negative charges on the surface of AuNPs. Negative charges which resulted from citrate, can cause strong repellent forces among particles to prevent aggregation and precipitation of NPs [228].

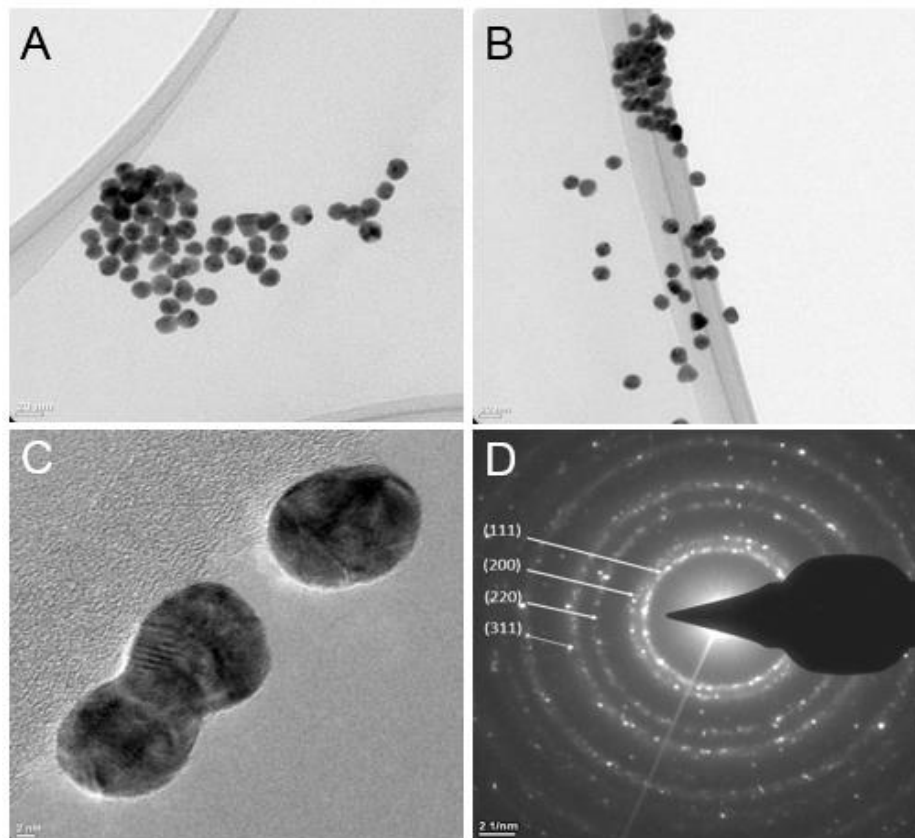


Figure 5. 4 (A), (B) TEM, (C) HRTEM and (D) SAED pattern of synthesized AuNPs.

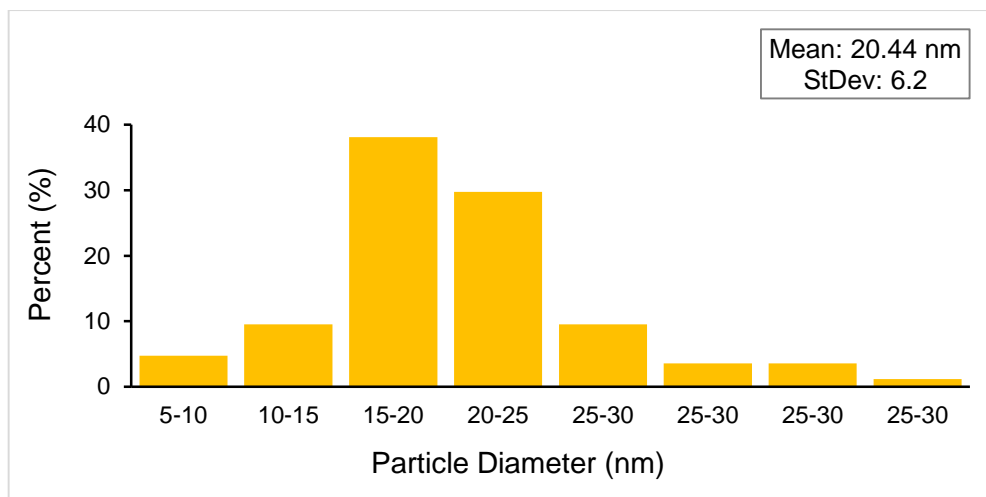


Figure 5. 5 Particle size distribution of the synthesized AuNPs.

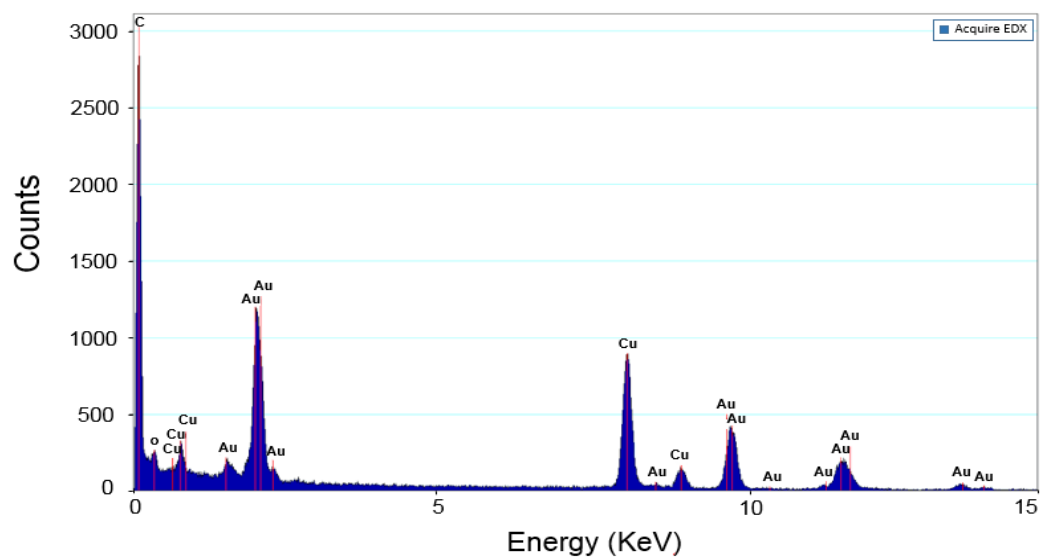


Figure 5. 6 EDS spectrum of synthesized AuNPs.

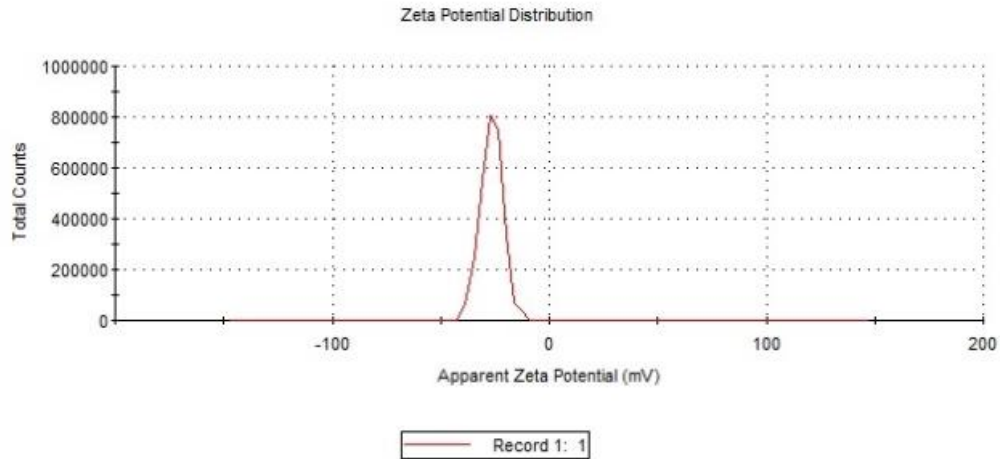


Figure 5. 7 Zeta potential of synthesized AuNPs.

5.3 Effect of different AuNPs concentration, Laser illumination time and Laser power amounts on temperature changes of colloidal AuNPs

In order to show effective variables on increasing temperature of AuNPs solution, Pareto analysis was used for three factors and their interaction. In this case, a reference line exists in chart that indicates statistical significance factors. Indeed, bars that interrupt the reference line are statistically significant. Here the Pareto chart (Figure 5. 8) illustrated that the main effect of all factors were significant at 0.05 level. In addition to mentioned effects, the effect of time \times laser power as only significant interaction effect was the other effective variable that they modified the AuNPs solution temperature. Hence, we took a deeper look into these significant variables by other statistical analysis.

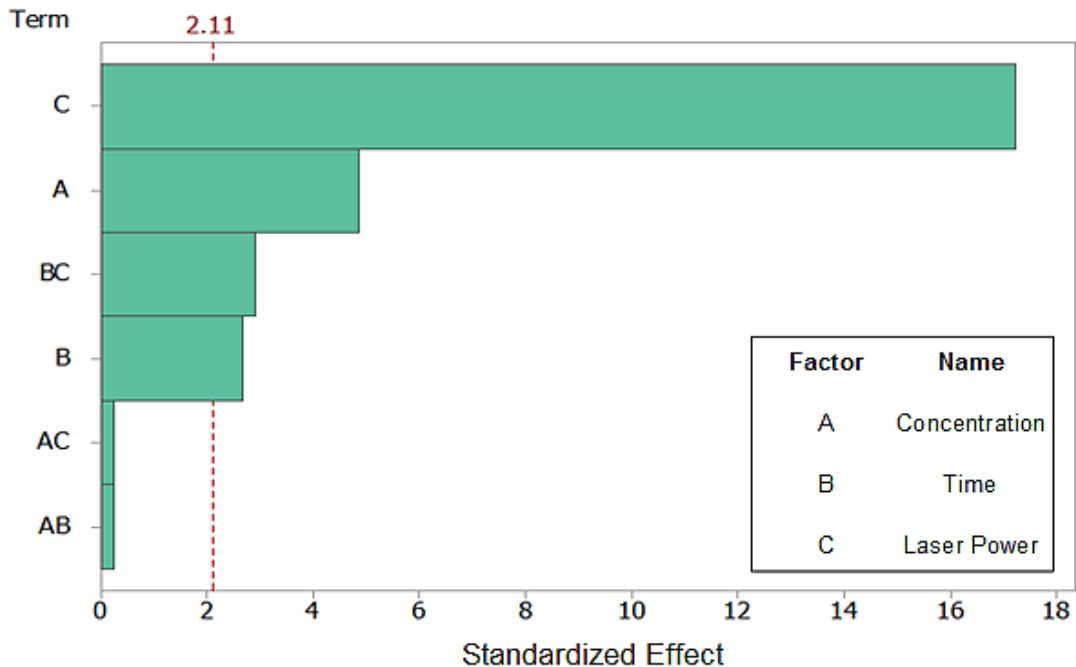


Figure 5. 8 Pareto chart showing the main effects of the various factors and their interaction on the temperature change of the colloidal AuNPs.

In next step in order to investigate how the variables affect the response and what the relationship is between variables and their response, the regression analysis was done. For this aim, we have applied the significant factor that identified from Pareto interpretations section. Hence, the relationships were identified between temperature, as a response or dependent variable, and significant factor, as independent variables. The regression model in terms of coded factors in the form of linear equation as follows:

$$y = 13.83 + 1.667 x_1 + 0.917 x_2 + 5.917 x_3 + x_2x_3 \quad \text{Eq. 5. 3}$$

Where x_1 , x_2 , x_3 and Y represent the concentration of AuNPs solution, time illumination of laser light, laser power and the temperature change, respectively.

By the same token, ANOVA as an essential step for the model analysis, was done and the results were shown in table 5.1. It was done in order to compare the effect of significant factor by comparing the variance of parameters and the F-test. Whatever the F value in ANOVA is bigger, the regression coefficient will be bigger in equation and consequently, the factor will be more significant and efficacious in response. According to that, the laser power was the most effective factor in change temperature of AuNPs solution and had the biggest coefficient in the model. This can also be theoretically confirmed. Theoretical calculations show that the maximum temperature at the surface of a small enough AuNP (where retardation effects can be ignored) is obtained as follows [229]:

$$\Delta T_{max} (I_0) = \frac{R_{NP}^2}{3k_0} Re \left[i\omega \frac{1-\varepsilon(r)}{8\pi} \left| \frac{3\varepsilon_0}{2\varepsilon_0+\varepsilon_m} \right|^2 \right] \frac{8\pi \cdot I_0}{c \sqrt{\varepsilon_0}} \quad \text{Eq. 5. 4}$$

Where R_{NP} and c is the radius of AuNPs and velocity of light, respectively, ω is the frequency of the incident light, K_0 is the thermal conductivity of the solution. $\varepsilon(r)$ is the local dielectric constant, ε_0 is the dielectric constant of the solution and $\varepsilon(\omega)$ is the frequency dependent dielectric constant of AuNP. I_0 is the intensity of the LASER beam directly proportional to the LASER power. The equation shows that the temperature of a single AuNPs rises linearly with light intensity.

Table 5. 1ANOVA result for the experimental parameters which affecting temperature of AuNPs solution.

Source	DF	Adj SS	Adj MS	F-Value	P-Value
Model	4	951.00	237.750	93.46	0.00000
Concentration	1	66.67	66.667	26.21	0.00000
Time	1	20.17	20.167	7.93	0.01104
Laser Power	1	840.17	840.167	330.27	0.00000
Time × Laser Power	1	24.00	24.000	9.43	0.00628
Error	19	48.33	2.544		
Lack-of-Fit	3	11.00	3.667	1.57	0.23523
Pure Error	16	37.33	2.333		
Total	23	999.33			

P-values less than 0.05 indicate model terms are significant.

After laser power, the concentration of GNP solution was the most effective variable in AuNPs temperature change. The concentration effect can be explained theoretically by considering the physics of ensemble heating. For an ensemble of AuNPs with concentration c , the total volumetric heat flux Q generated by all NPs can be approximated as:

$$Q = c \cdot \sigma_{abs} \cdot I_0 \quad \text{Eq. 5. 5}$$

Where σ_{abs} is the absorption cross section of single AuNPs. As it can be seen, the heat (and so the temperature) is linearly proportional to the concentration. However, LASER light is attenuated in the solution according to Beer-Lambert law. The LASER intensity in the solution is exponentially decreased with a decay constant of $\tau = c \cdot \sigma_{abs}$. Considering these two facts indicates that although increasing AuNPs concentration results in linear increase of the total heat, the intensity is attenuated along the solution with higher number of AuNPs [230]. Finally, the other factors including time \times laser-power interaction and time illumination had the most effect on the response and the biggest coefficient value in equation after them, respectively. It should be noted that the positive sign of all significant regression coefficients implied that all the terms had a direct relationship with AuNPs temperature change. It indicated that the mean of the dependent factor tended to increase or decrease when the value of each independent variable increased or decreased, consequently. Therefore, more temperature production and more intensive in the photothermal phenomenon of the GNP solution was because of increasing the value of each independent variable. Also, the results of ANOVA regression showed the statistical significance of the applied model and its lack of fit that were investigated by F-test. These results depicted that the obtained linear model was high significant (p-value < 0.0001) and lack of fit is not significant (p-value > 0.05). Furthermore, both the correlation coefficient value (95.16%) and adjusted R^2 (94.15%), which indicate the correlation between the model and experimental data, had large enough value. In another words they were close to value of 100% that represented a very good fit of the linear model for experimental data. Also, in order to validation the obtained regression model, predicted values of ΔT obtained based on uncoded regression model (Table 5.2). Then the average of experimental data were compared to predicted values by calculating the RSE% (Eq. 4.2). The results of RSE% showed that the difference between experiments and predicted value were no significant (RSE values were lower than 4). However, there was a very good

fit between linear model and experimental data. Hence, the model can be used to determine ΔT with good accuracy and precision in the range of the factors values.

Table 5. 2 Predicted and actual values of ΔT for the confirmation the regression model.

set	AuNPs Concentration (ppm)	Illumination Time (minutes)	Laser power (mW)	Predicted ΔT ($^{\circ}\text{C}$)	Actual ΔT ($^{\circ}\text{C}$)	RSE (%)
					r ₁ =13	
1	44	20 minutes	200	13.1	r ₂ =14	3.8
					r ₃ =14	
					r ₁ =17	
2	88	10 minutes	250 mW	17.05	r ₂ =17	1.5
					r ₃ =18	

r is replication of experiment

It should be noted that when water, as a negative control, exposed the laser light, there was not any changing in temperature. It means that all the increasing in AuNPs solution temperature were arising from optical properties of AuNPs.

5.4 LED and statistical analysis

In order to identify effective variable on increasing temperature of AuNP solution, statistical investigation was done on four factors including concentration

and volume of AuNP solution, time illumination of light and distance of AuNP container from LED. Table 5.3 shows the mention experimental variables at different levels.

Table 5. 3 Four experimental variables screened by full factorial design at different levels.

Variable	Units	Levels		
		1	2	3
Time	minute	5	10	15
Concentration	ppm	22	44	88
Distance	cm	3	5	10
Volume	μl	200	1400	2800

The analysis of Variance (ANOVA) was conducted to recognize which of the factors in temperature change of AuNP solution were significant (Table 5.4). The results demonstrated that the main and interaction effects of all factors were significant.

Table 5. 4 ANOVA for the experimental parameters of full factorial design.

Variable	SS	df	MS	F-value	p-value
Concentration (X ₁)	409.71	2	204.85	247.57	< 0.0001
Volume (X ₂)	89.57	2	44.79	54.12	< 0.0001
Distance (X ₃)	3283.61	2	1641.80	1984.14	< 0.0001
Time (X ₄)	245.49	2	122.74	148.34	< 0.0001

X ₁ X ₃	89.08	4	22.27	26.91	< 0.0001
X ₁ X ₄	17.58	4	4.39	5.31	0.0012
X ₂ X ₃	29.82	4	7.45	9.01	< 0.0001
X ₂ X ₄	22.44	4	5.61	6.78	0.0002
X ₃ X ₄	95.87	4	23.97	28.97	< 0.0001

R² = 0.99; Adjusted R² = 0.98; SS, sum of squares; DF, degrees of freedom and MS, mean square. P-values less than 0.05 indicate model terms are significant.

Following screening and identifying the significant factor, in order to achieve optimal AuNP photothermal treatment, CCD and RSM, which are based on the mathematical and statistical techniques, were employed. They used to both exploring the relationship between the response and independent variables and optimization of significant factors (time illumination of light, distance of AuNP container from LED, concentration and volume of AuNP solution). These four factors were investigated at five different levels and a set of 81 experiments were accomplished. After the tests were completed, statistical methods were used to analyze the experimental data. Design Expert software was used to perform the design and analyze the experiment. Also, the mathematical relationship between the temperature change as a dependent variable and the others as independent variables, was described by using the following second-order polynomial model:

$$Y = \beta_0 + \sum \beta_i x_i + \sum \beta_{ii} x_i^2 + \sum \beta_{ij} x_i x_j \quad (\text{Eq. 5.5})$$

Where Y was the dependent or predicted response, x_i and x_j were the coded independent factors, β_0 was the interception coefficient; β_i was the linear coefficient and β_{ii} and β_{ij} were quadratic and interaction coefficients respectively.

ANOVA was another step for the model analysis. As shown in Table 5.5, the statistical significance of the applied quadratic model and its lack of fit were

investigated by F-test and it implied that the model was high significant (p-value < 0.0001) and lack of fit is not significant (p-value > 0.05). Also, correlation coefficient value (98.42%) especially adjusted R² (96.95%), which indicate the correlation between the observed and predicted response values, reflected a very good fit for the quadratic model. The ANOVA demonstrated that the main effect of all factors, the concentration × distance and time × distance interactions and also second order effects of x_1^2 , x_3^2 and x_4^2 were significant. So, these factors had a key role on thermal response of AuNP solution. Based on mention regression model (Eq. 5.5), ANOVA (Table 5.5) and regression coefficients, the relationships between temperature changed and variables were fitted as follows:

$$Y = 5.42 + 2.47 x_1 + 0.95 x_2 - 3.02x_3 + 1.2 x_4 - 0.93x_1x_3 - 0.45x_3x_4 + 0.43 x_1^2 + 1.78x_3^2 + 0.31 x_4^2$$

(Eq. 5.6)

Where in this equation, Y represents the temperature change, x_1 , x_2 , x_3 and x_4 are concentration of AuNP solution, volume, time illumination of light and distance of AuNP container from LED, respectively.

In order to illustrate the major interactive effects on thermal response of AuNP solution, 3D response surface plot was used. The figure 5. 9 (A) depicts the time × distance combined effect and shows that temperature of AuNP solution was enhanced by decreasing the AuNP solution distance from LED source because distance had a negative coefficients with the increasing AuNP solution temperature. Furthermore, increasing in its temperature was reached when the time of LED illumination was raised. Although according to the previous section the time factor had lower main effect compared to distance on temperature change (Table 5. 5). Another effective interactive effect on temperature change was concentration × distance (Figure 5. 9 (B)). It provides the mention results related to the distance factor and also the effect of concentration in the presence

of the distance. Indeed, when the distance and concentration were decreasing and increasing sequentially, the temperature enhanced up to maximum amount. The concentration of AuNP factor was more effective than the time illumination factor on increasing the temperature of this solution (Table 5. 5). It led to a great reduction in AuNP solution temperature when at a constant distance the concentration was reduced that this reduction was more than reduction of temperature when at a constant distance the time illumination was decreased.

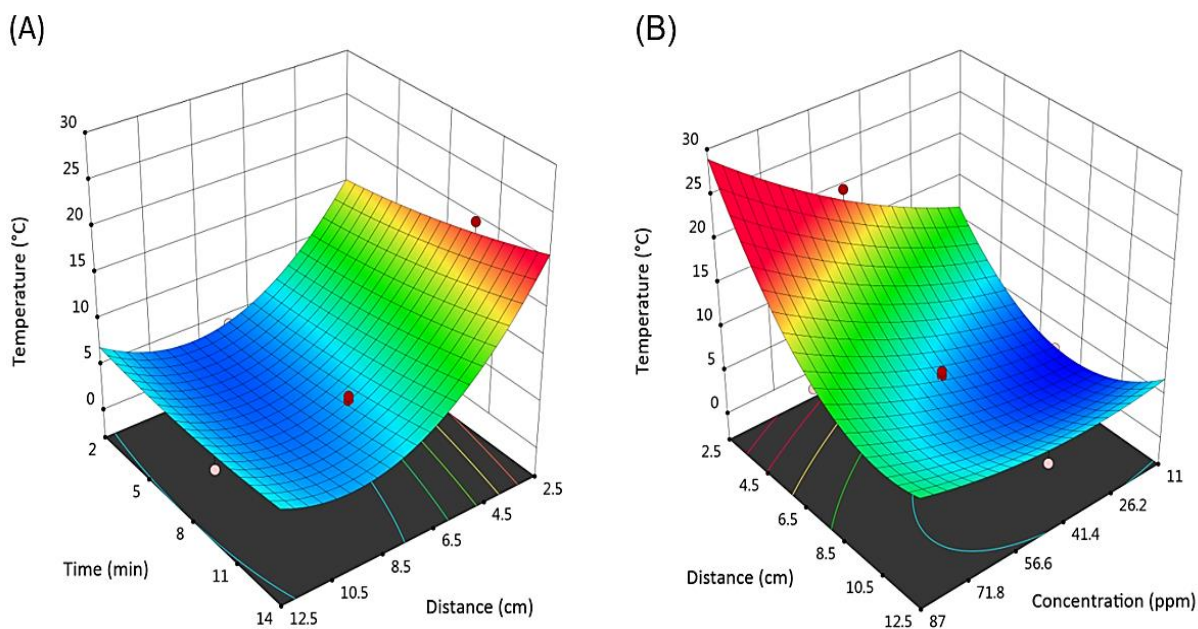


Figure 5. 9 Response surface curve for interaction effect of: (A) Time and distance factors when concentration and volume were maintained at 49 ppm and 1525 μl , respectively. (B) Distance and concentration factors when time and volume were maintained at 10 minutes and 1525 μl , respectively.

In order to validate the performance of regression model for predicting the specific changes temperature, we used one of experimental test parameters (44 ppm concentration, 2800 μl AuNPs, 10 minutes illumination and distance = 5 cm) which led to obtained $\Delta T = 12^\circ\text{C}$. Predicted value of response surface that is based on regression model, was $\Delta T = 11.8^\circ\text{C}$ which this results suggested that the quadratic model and response surface predictions were in good agreement

with the experimental results and can be used as prediction equation with good accuracy and precision in amplitude of study.

Table 5. 5 Analysis of variance (ANOVA) for response surface quadratic model.

Source	SS	df	MS	F-value	p-value	
Model	527.67	14	37.69	66.87	< 0.0001	significant
Concentration (x_1)	146.03	1	146.03	259.07	< 0.0001	
Volume (x_2)	21.66	1	21.66	38.43	< 0.0001	
Distance (x_3)	218.41	1	218.41	387.47	< 0.0001	
Time (x_4)	34.56	1	34.56	61.31	< 0.0001	
x_1x_2	0.4900	1	0.4900	0.8693	0.3659	
x_1x_3	13.69	1	13.69	24.29	0.0002	
x_1x_4	0.4900	1	0.4900	0.8693	0.3659	
x_2x_3	0.6400	1	0.6400	1.14	0.3035	
x_2x_4	0.0400	1	0.0400	0.0710	0.7936	
x_3x_4	3.24	1	3.24	5.75	0.0300	
x_1^2	5.15	1	5.15	9.14	0.0086	
x_2^2	0.9219	1	0.9219	1.64	0.2204	

x_3^2	87.23	1	87.23	154.76	< 0.0001	
x_4^2	2.61	1	2.61	4.63	0.0482	
Residual	8.45	15	0.5637			
Lack of Fit	6.25	10	0.6247	1.41	0.3685	not significant
Pure Error	2.21	5	0.4417			
Total	536.12	29				
<hr/>						
Quality of quadratic model						
<hr/>						
Correlation coefficient (R^2)			0.9842			
Adjusted R^2			0.9695			
Predicated R^2			0.9270			
<hr/>						

5.5 Theory and simulation

In order to simulation of the light matter interaction with the AuNPs, at first, we calculated the cross sections of absorption, scattering, and extinction of one Au NP with diameter 20.44 nm by plane electromagnetic wave excitation. The analytical solution of scattering for simple spheres is known from Mie theory. However, we need to take into account the intrinsic broadening of absorption spectrum observed in the measurements (See figure 5. 10). We included broadening of gold by combining Drude model and experimental bulk permittivity of gold following the same method in reference [231]. We took the Drude

parameters as $\Gamma_{bulk,D} = 0.076 \text{ eV}$ and $\omega_p = 8.9 \text{ eV}$, where $\Gamma_{bulk,D}$ and ω_p are the broadening and plasma frequency, respectively. The experimental bulk permittivity of gold has been taken from literature reference [232]. Figure 5. 10 shows our calculations of the cross sections for the AuNP in solution. The solution is treated as water with relative permittivity of $\epsilon_{water} = 1.8$.

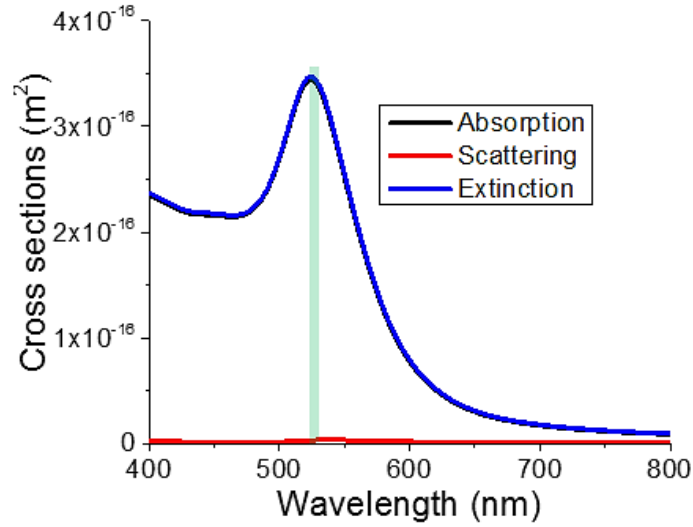


Figure 5. 10 Extinction, absorption, and scattering cross sections for a 20.44 nm AuNP in water. The green vertical line shows the LED wavelength excitation range.

In the next step, we need to consider time dependent heat dissipation resulted from ensemble of AuNPs in solution based upon the absorption of one AuNP. In the absence of convection, time dependent heat equation reads,

$$\rho(\vec{r})c(\vec{r})\frac{\partial T(\vec{r},t)}{\partial t} = \vec{\nabla} \cdot (k(\vec{r})\vec{\nabla}T(\vec{r},t)) + Q_{heating}(\vec{r},t) = 0 \quad (\text{Eq. 5.7})$$

In Eq. 5.7, \vec{r} represents the local position and t is time. T is the local time dependent temperature. Local thermal properties are defined as thermal conductivity, k , density, ρ , and specific heat capacity, c . $Q_{heating}$ is the local collective volumetric heat flux corresponding to resistive losses in the system. In our model, the resistive losses only come from the AuNPs since gold is the only material with non-zero imaginary part of permittivity. For ensemble of metal NPs $Q_{heating}$ can be defined as reference [230]:

$$Q_{heating}(\vec{r}) = \rho_{AuNP}(\vec{r}) \cdot \sigma_{abs-AuNP} \cdot I_{LED}(\vec{r}) \quad (\text{Eq. 5.8})$$

Where in Eq. 5.8, ρ_{AuNP} is number density of AuNPs in solution, $\sigma_{abs-AuNP}$ is the absorption cross section of AuNP, and I_{LED} is the local LED intensity. In experiment, the solution is at distance x . LED light is diverging, and we approximate the LED power reduction at the position of the ensemble solution by inverse square law of light as $I_{LED}(\vec{r} \equiv \vec{x}) \propto 1/(4\pi x^2)$. Additionally, the light intensity decays in the absorptive solution according to Beer-Lambert law. Therefore, the intensity of LED will decay in the solution proportional to $\exp(-\alpha r)$ where α is the absorbance decay constant. We solved Eq. 5.4 using parameters of our experimental setup. We chose the parameters as $d = 5$ cm, $\rho_{AuNP} = 3.26 \times 10^{17}$ 1/m³, $\sigma_{abs-AuNP} = 3.46 \times 10^{-16}$ m² at wavelength 522nm, and $P_{LED} = 50$ W where P_{LED} is the LED power at $\vec{x} = 0$. The number density of 3.26×10^{17} 1/m³ corresponds to 44 ppm concentration of AuNPs in solution. In experiment, a cuvette with cross section area of 10mm \times 12.2mm is filled with 2800 μ l solution. If we assume the cuvette as rectangular prism, then it is filled up to about 2.24 cm. The entire system is in contact with air as the ambient medium. Time dependent calculations of the temperature is shown in figure 5. 11 for two different concentrations 44 ppm and 88 ppm. The temperature increases linearly at early

times and then reaches steady state at longer times (hours). The inset of figure 5. 11 shows decent linear behavior at early times (less than an hour).

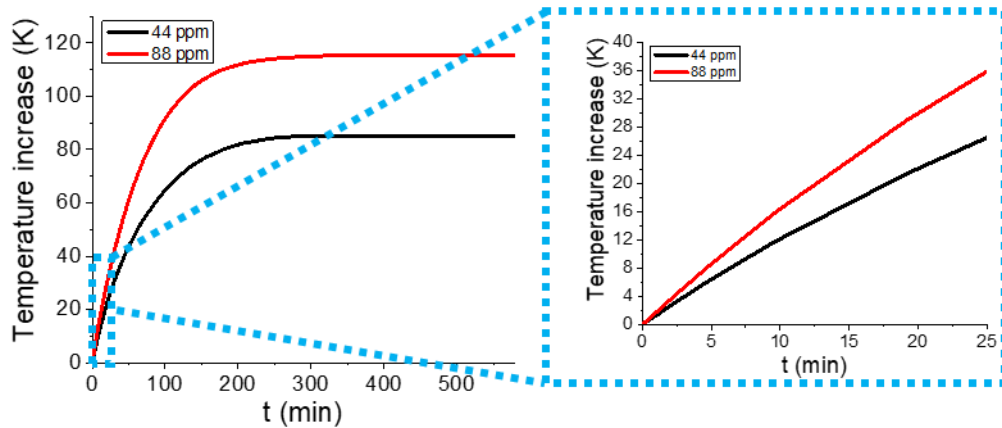


Figure 5. 11 Time dependent temperature calculations for two concentrations of 44 ppm and 88 ppm. The inset is the zoom in plot for early times. It shows linear behavior.

Figure 5. 12 (A) shows our calculation of local collective heating $Q_{heating}(\vec{r})$ by the incident of LED in $+x$ direction for 44 ppm. As it is seen, the heat decays following Beer-Lambert law and inverse square law along x axis. Figure 5. 12 (B) is the temperature profile along x axis going through the middle of the cuvette for increasing early times less than one hour. We would have a flat temperature profile inside the solution if the heat decay was absent. It is depicted in figure 5. 12 (B) that the temperature at opposite walls of the cuvette differ by 1 – 2 °C.

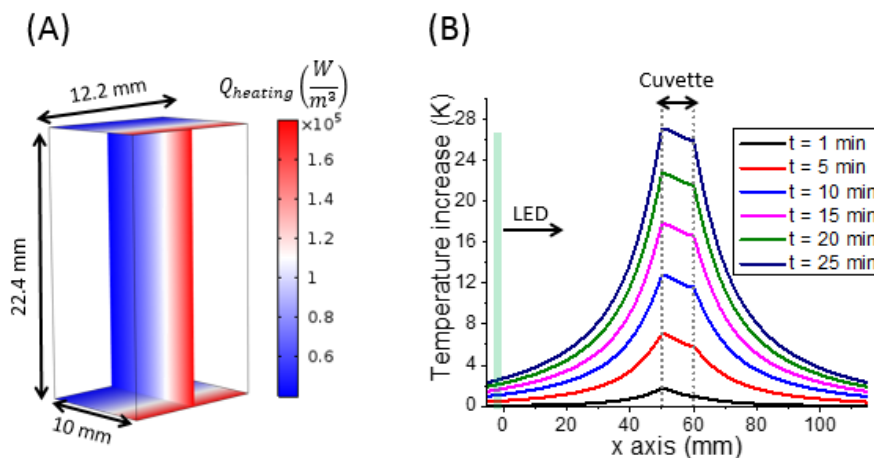


Figure 5. 12 (A) Calculated local collective heating of ensemble of AuNPs in the cuvette of 10mm×12.2mm×22.4mm. The LED excitation is along positive x axis at wavelength of 522 nm. (B) Temperature profile of the middle of cuvette along x axis for increasing time. The position of LED and cuvette is also shown.

In this evaluation in order to compare the theoretical and experimental approaches, we also simulated heat generation from our AuNPs. For this case, we used one of experimental test parameters (44 ppm concentration, 2800 μl AuNPs, 10 minutes illumination and distance = 5 cm) which its ΔT result was about $\Delta T = 12^\circ\text{C}$. Figure 5. 13 (A) is the simulation of temperature distribution at $t = 10$ minutes along xz plane. The geometry of the cuvette is shown as three dimensional black lines. However, simulation result showed that the maximum temperature increase in figure 5. 13 (A) inside the solution reaches about $\sim 12.7^\circ\text{C}$ which is in excellent agreement with our observations. It is noteworthy to mention that the maximum temperature is the local collective temperature derived based upon the maximum temperature generated on the surface of AuNPs (Figure 5. 13 (B) and (C)).

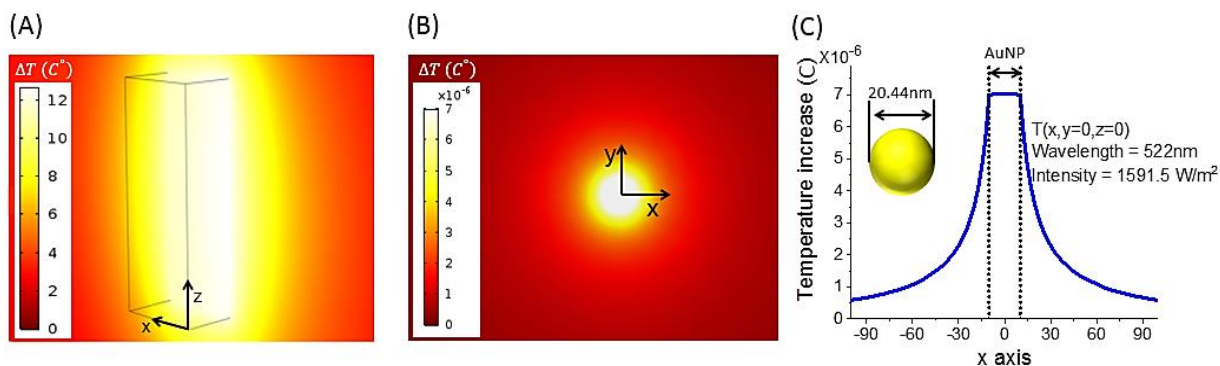


Figure 5. 13 (A) Temperature distribution along xz plane at $y=11.2$ mm at $t=10$ minutes. (B) Steady state temperature distribution of one AuNP in water at wavelength 522 nm with diameters 20.44 nm. (C) Temperature profile of AuNP along x axis for the same intensity of LED applied to the ensemble of AuNPs. Inset shows the geometry of AuNP.

5.6 Toxicity test of AuNPs on *E. coli* DH5 α

As seen in figure 5. 14, all of different concentrations of synthesized AuNPs have not remarkable toxicity effect on *E. coli* DH5 α TM. These results are consistent with previous work which is done by Dasari *et al.* [225]. They have tested antibacterial effect of AuNPs on three strain of bacteria including *Escherichia coli*. They have reported that AuNPs alone do not inhibit bacteria growth. Morales-Avila *et al.* [233] also have tested AuNPs and AuNPs Functionalized with the Ubiquicidin (29–41) with nanoparticle concentration of up to 182 ppm on *E. coli* and *Pseudomonas aeruginosa* and have reported that no inhibition of bacterial growth was observed with this nanoparticle and this concentration.

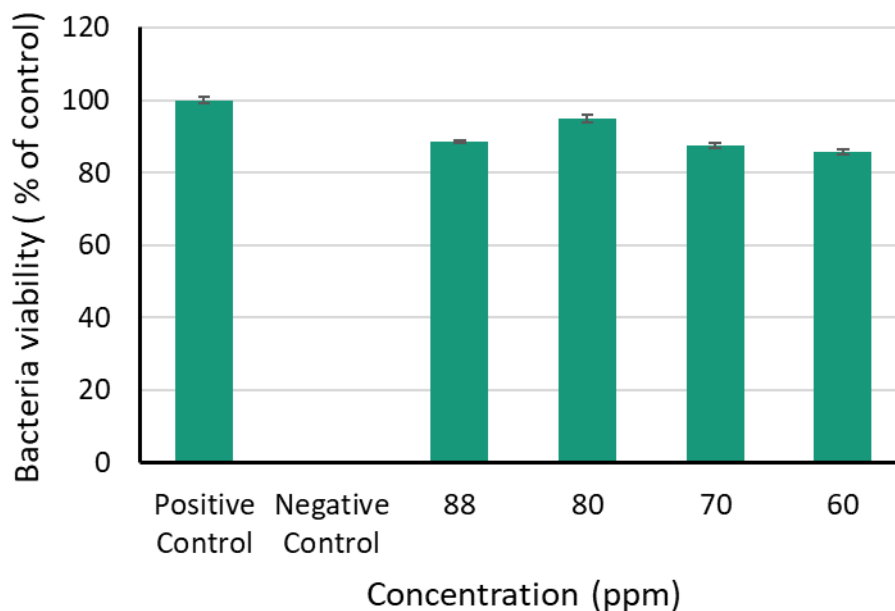


Figure 5. 14 Toxicity effect of different concentrations of AuNPs on *E. coli* DH5 α TM.

5.7 Photothermal protein production by LED in *E. coli* DH5 α

Optical density (OD) measurements (Figure 5. 15) demonstrate that the existence of both illumination and nanoparticle factors caused that the bacteria grew and reached the maximum growth rate very fast (Figure 5.15 (A)). Furthermore, the bacteria in this condition were able to grow and have maximum OD more than same bacteria which grew without GNP, without illumination or both of them (Figure 5.15 (B), (C) and (D) respectively) and were a little bit less than the maximum OD of bacteria that were grown in the Incubator (37 °C).

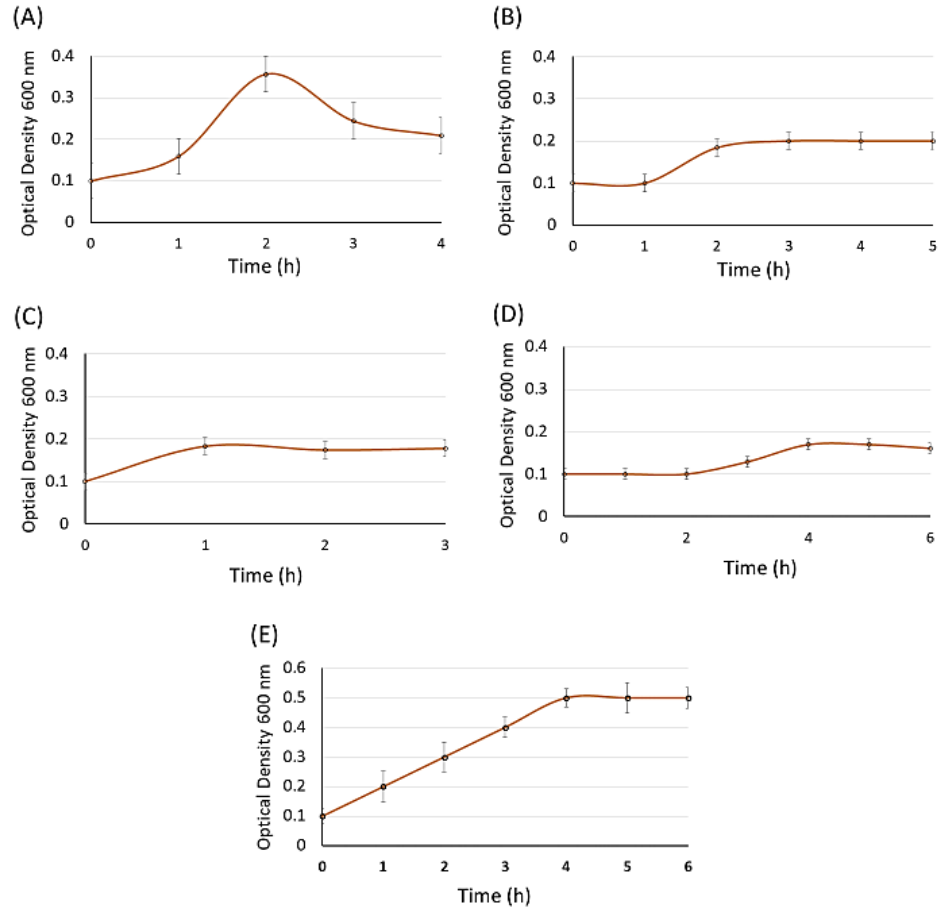


Figure 5. 14 (A), Sample 1 including GNP and *E. coli* DH5 α^{TM} Bacteria under LED light illumination. (B), Sample 2 including *E. coli* DH5 α^{TM} under illumination. (C), Sample 3 containing GNP and *E. coli* DH5 α^{TM} Bacteria without LED light illumination. (D), Sample 4 which Its content is only *E. coli* DH5 α^{TM} without LED light illumination.

Moreover, because bacteria in their exponential phase have maximum growth rate, RFU of produced mCherry protein in this phase with three repetitions, excitation and emission wavelength of 587 and 610 nm respectively were quantified for each one of samples using Microplate Readers (Thermo ScientificTM VarioskanTM LUX) and SkanItTM Software. As shown in figure 5. 16, using of AuNPs and LED as light source for illumination of them led to efficiently working of stem-loop structure containing the ribosome binding site and consequently a

large amount of mCherry protein production. Difference of produced mCherry protein amount in sample 1 is significant compared to samples 1, 2, 3 and 4. This is very higher than sample 5 produced mCherry protein amount but is not significant statistically. This result showed using of AuNPs and LED as light source for providing the required temperature (37 °C) is even more effective than using of incubator that can provide exact required temperature.

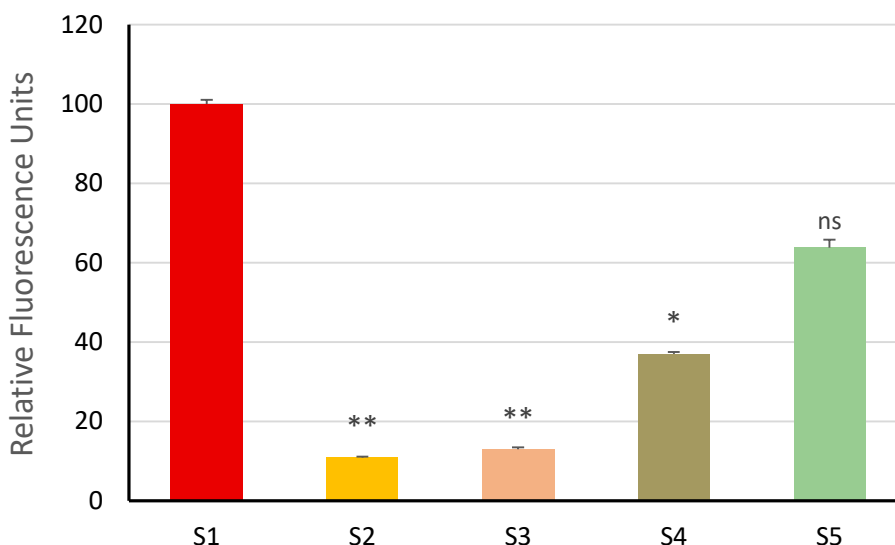


Figure 5. 15 The average RFU of the mCherry proteins of *E. coli* DH5 α TM. Comparison of Produced mCherry protein in the main sample (S1) against samples S2, S3, S4 and S5 were performed. Data are expressed as mean \pm SEM, n= 3 well; *P < 0.05 and **P < 0.01 vs. S1.

5.8 Conjugation of sense and antisense oligonucleotides to switches

Conjugation process of sense oligonucleotides to surface of the AuNPs and antisense to the sense strands was monitored using UV-vis absorbance spectroscopy. The citrate-ssDNA ligand exchange process was monitored using

UV- vis absorbance spectroscopy. This is feasible due to the fact that replacing the citrate capping ligand with the thiolated sense oligonucleotide and also hybridization of antisense oligonucleotide to sense strand resulted in the solution color change into pale red (Figure 5. 17) and a small but observable red shift of the nanoparticle's SPR band (Figure 5. 18).

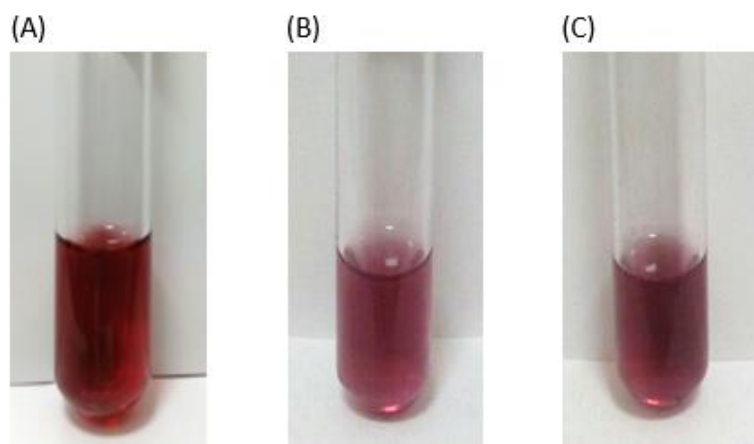


Figure 5. 16 Color change of AuNPs solution in the switches synthesis process. (A) Pure AuNPs. (B) Conjugation of AuNPs to sense oligonucleotides. (C) Conjugation of antisense oligonucleotides to AuNPs + Sense oligonucleotides.

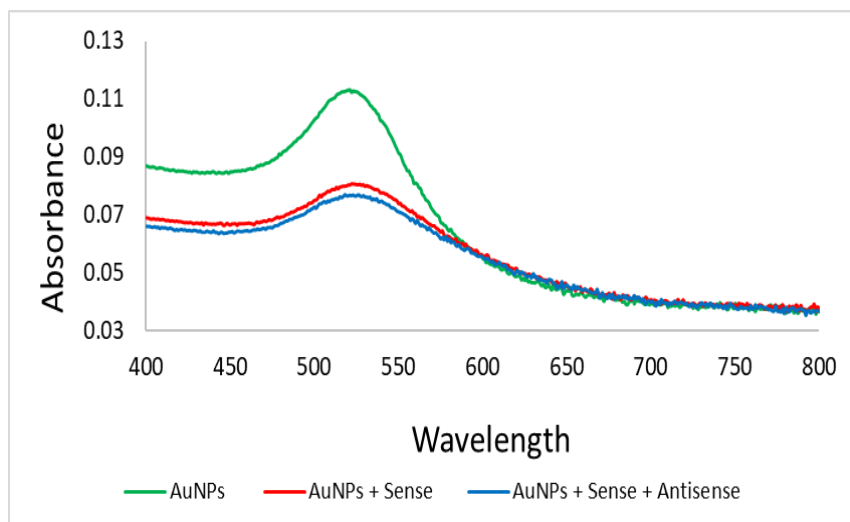


Figure 5. 17 Changes in the UV-vis absorption spectrum when an aqueous dispersion of 20.44 nm AuNPs is treated with thiolated sense oligonucleotides and then with the antisense oligonucleotides, showing a decrease in absorption rate and a small red shift of the SPR band indicative of ligand exchange [234].

5.9 In-vitro confirmation of antisense photothermal dehybridization

The temperature on the surface of the switches is experimentally and statistically characterized. That is why, an oligonucleotide (15 bp) with known melting temperatures (54.9°C) is used. As seen in figure 5. 19, when the temperature on the switches reaches the melting temperature of this oligonucleotide, the fluorometer measurements showed that the fluorescent intensity decreases sharply, indicating that the antisense oligonucleotides have been released into solution [202]. This in-vitro test result can give us hope for the feasibility of antisense photothermal dehybridization in the microalgae cells (in-vivo) which receive the switches (dsDNA-functionalized AuNPs).

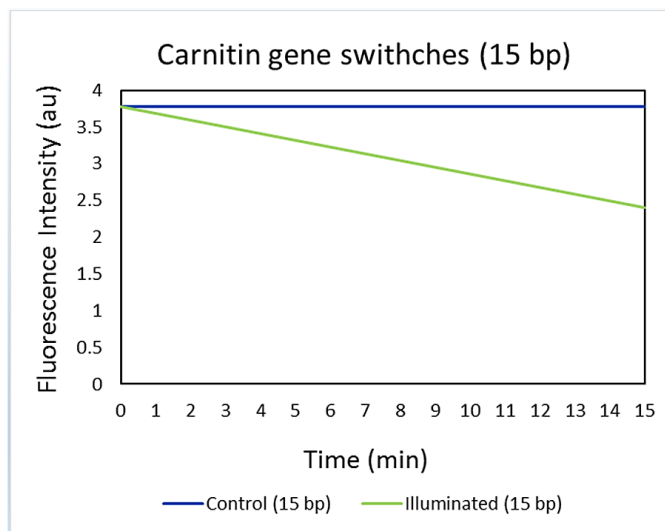


Figure 5. 19 Photothermal dehybridization of 15 bp oligonucleotides with known melting temperatures (54.9°C). Antisense oligonucleotides are 6-FAM-labeled.

5.10 Confirmation of switches delivery into the microalgae cells and RNA quantification

Confocal microscopy images represent internalization of dsDNA-functionalized AuNPs into the microalgae cells in 14 hours (Figure 5. 20). Our results show that the internalization of switches into the microalgae cells is facilitated by an optimized protocol in this thesis and MAX Efficiency® Transformation Reagent (this reagent increases the permeability of the microalgae cell wall). As it can be seen in the figure 5. 20, dsDNA-functionalized AuNPs localized in one section of inside some cells (Cells + Switches (Zoom 10x) – Merged) while some of them are localized in two section of inside some cells (Cells + Switches (Zoom 13x) – Merged).

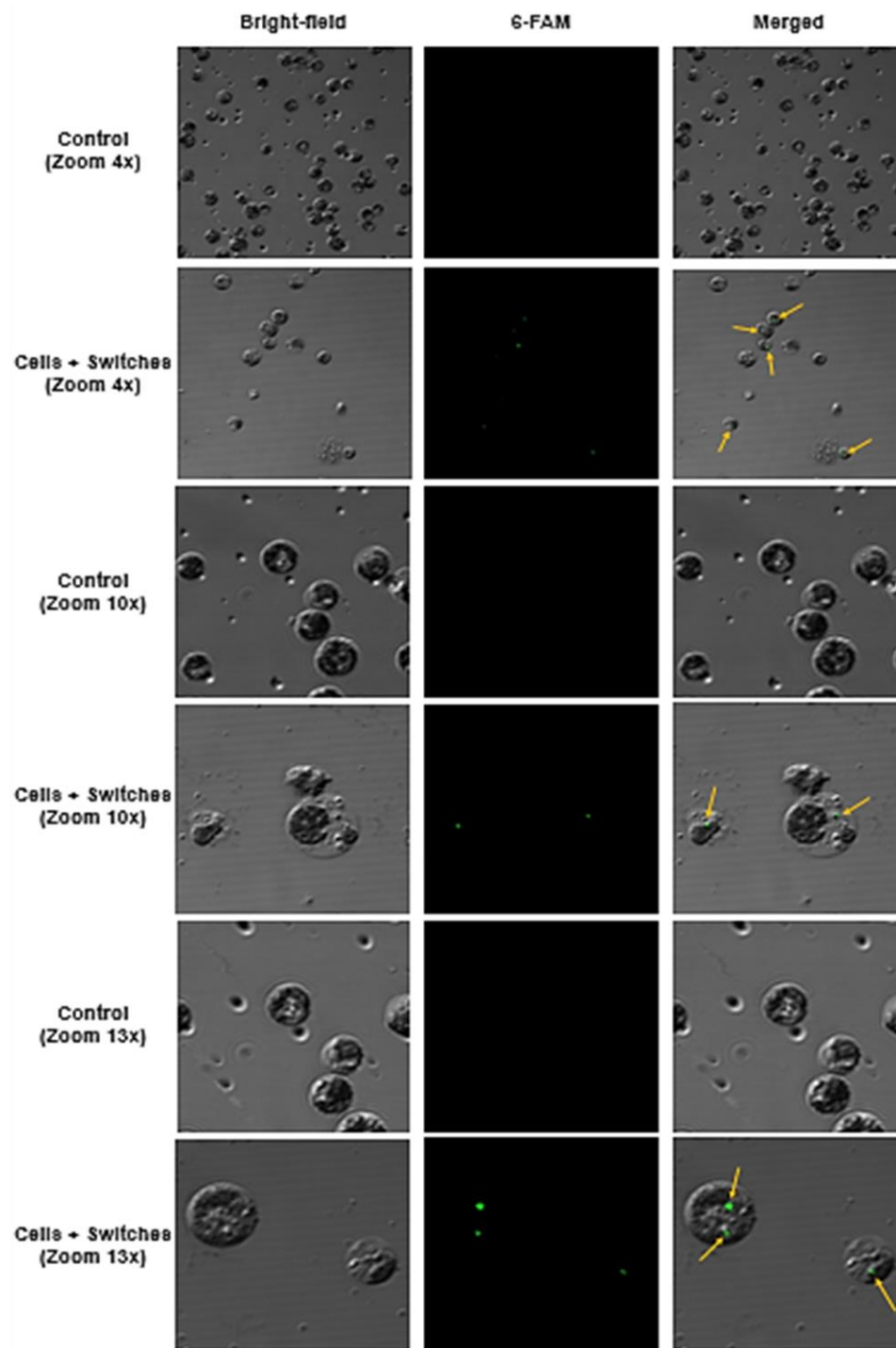


Figure 5. 18 Confocal microscopy images; dsDNA-functionalized AuNPs successfully delivered into the microalgae cells.

Then, to evaluate the effectiveness of the gene silencing through antisense oligonucleotide (ASO) delivery, the abundance of target gene-specific mRNA by comparative RT-PCR in microalgae cells that received dsDNA-functionalized AuNPs was analyzed. The results revealed that there was a significant difference in the levels of mRNA expression control and treated groups. As shown in figure 5. 21, the CACT mRNA abundance decreased up to 90.7% in comparison with control samples that didn't receive any dsDNA-functionalized AuNPs, indicating high-efficiency silencing by this method. This result confirmed that LED light sources could heat up the surface of AuNPs up to melting temperature of the sense and ASOs that were located on the NPs. This produced temperature led to release the ASOs well and released oligonucleotides could conjugate on the first section of CACT mRNAs. This event led to significantly high silencing in the required time (on-demand silencing).

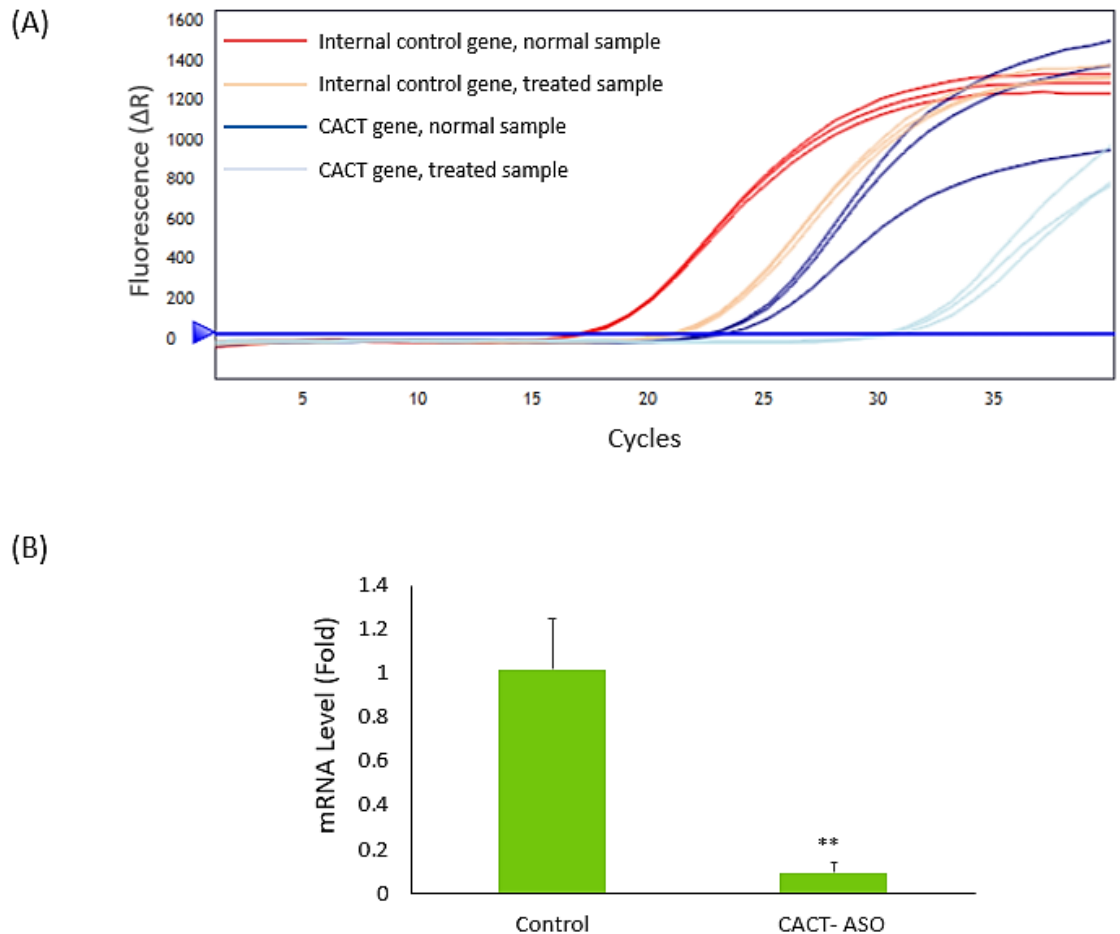


Figure 5. 19 comparative RT-PCR; (A) Amplification curves against PCR cycle number (Triplicate data are shown for each experiment). (B) The mRNA abundance of CACT gene in *C. reinhardtii* cells that received dsDNA-functionalized AuNPs (To be more precise, received ASOs); The expression of CACT gene in compare to control, revealed decreased expression of this gene in exact time that the cells illuminated by LED light source to gene silencing. Data are expressed as mean \pm SEM; n= 3 well for each group; **P < 0.01 vs. control (non-treated dsDNA-functionalized AuNPs) cells.

Eventually, in order to enable further understanding of CACT gene silencing effect on cellular lipid accumulation, *C. reinhardtii* cells which were stained with Nile red fluorescent dye, were visualized using fluorescence microscopy. As our prediction and hypothesis based on that on-demand ASOs delivery can be led to CACT gene silencing in the exact time that this event can be led to lipid structures increase in the microalgae cells ultimately. As it can be seen in figure 5. 22, Nile

red staining of lipid bodies confirmed our claim such that substantial accumulation of lipids (compared to control sample), mostly in the form of TAG can be observed.

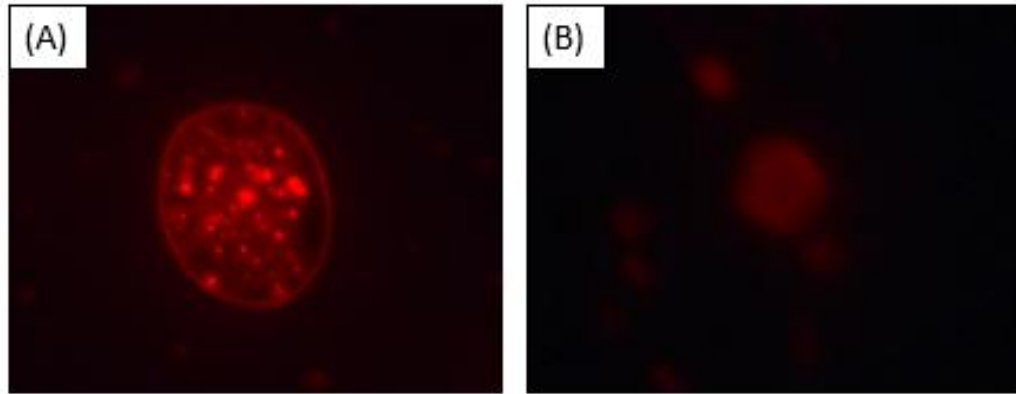


Figure 5. 20 Fluorescence images of Nile red-stained *C. reinhardtii* cells, 2h after gene silencing; (A) Cells that received dsDNA-functionalized AuNPs and contain too many shiny points that are related to lipid bodies (B) Control samples contains cells that didn't receive any dsDNA-functionalized AuNPs.

CHAPTER 6

Discussion

The project comprises two major sections; Photothermal gene expression in *Escherichia coli* and gene silencing in *Chlamydomonas reinhardtii*. In both sections the plasmonic resonance feature of AuNPs is used. Gold nanoplasmonic optical antennae, in the 532 nm spectral region, are attractive candidates for intracellular control. Compared to any other chromophores, smaller AuNPs, sizes between 2 to 20 nm have higher absorbance with a possibility of reaching high light-to-heat conversion efficiency. With the development of nanoscience, the optical properties of AuNPs have shown tremendous interest in plasmon-based technologies. Localized surface plasmons can be excited by optical excitation, leading to the device development of small-scaled optical antenna with enhanced electric fields. Metallic NPs have extraordinary optical properties that differ greatly from those of the bulk macroscopic metal [30]. In specific, AuNPs present wide absorption spectra that can be easily tuned since it directly depends on the size, shape and surface chemistry of the nanostructure. AuNPs due to having intense optical absorbance and large absorption cross section, can absorb optical energy in specific wavelength and convert it to thermal energy with high efficiency [121]. In this work, when we illuminated AuNPs by incident light, a collective oscillation of free conduction electrons was produced in AuNPs which is known as a plasmon resonance. A part of high-energy of the excited plasmon due to phonon-phonon (at a time scale of 100–380 ps) and electron-phonon (at a time scale of 2–5 ps) interaction was decay in non-radiative form producing a large amount of highly localized thermal energy. The result of this process led to elevate the temperature of the AuNPs. The generated heat, then, diffuses away from the surface of the

hot AuNPs and led to the increase the temperature of the surrounding medium [87, 88, 91, 122, 123]. So, using applications and features of AuNPs that mentioned above, we created engineered microorganisms contain a switchable expression system in order to gene expression remote control in special time. This work establishes a promising new biological system that uses a LED instead of laser device as a new, cheaper, harmless, switchable method, non-destructive for living organisms (in most of wavelength and time period) and especially feasible in large scale to stimulate AuNPs for the photothermal protein production as a novel biological application. We demonstrated high efficiently working of stem-loop structure in this system. Taking into account the mentioned unique features of introduced gene expression system and obtained excellent results in this study, we applied this expression system for genes which have a crucial role in organisms and extending this method to other prokaryotic or eukaryotic cells. Also, it is noteworthy that, except the photothermal protein production as a novel biological application, we used the extraordinary optical properties of AuNPs for silencing of the gene that we should have its expression and function in all the stages of the organism's life especially in the early stages of their life, and then, depending on time we stopped its activity and expression. For this application, we had some challenges that we solve them step by step. One of these challenges was kind of our cells. The cells that we worked on them were a kind of plant cells that had rigid cell walls. So, the cell wall was a big hurdle to entering our switches (dsDNA-functionalized AuNPs). We solved this problem using an optimized protocol in this thesis and a kind of reagent that increased the permeability of the microalgae cell wall.

It is shown in this dissertation that short single-stranded DNA, otherwise known as antisense strand, can be hybridized to a thiolated complementary sense strand, bound to a spherical AuNPs surface through the gold-thiol covalent bond, and photothermally dehybridized using LED continuous-wave incident light that is

matched to the plasmon resonance wavelength (532 nm) of the spherical AuNPs (Figure 1. 5).

As it is shown in the results, the surface of the AuNPs because of strong gold-thiol covalent bonds, the surface of the AuNPs were remains covered with the thiolated complementary sense strands (the antisense oligonucleotides just released from their complementary strands) after illumination (Figure 5. 20). This happen was crucial because it led to that the AuNPs had not any cytotoxicity effects (was remained as being biocompatible) on the microalgae cells and didn't kill the cells while, bare gold nanoparticles have been shown to interact with proteins and induce mis-folding at physiological conditions.

Also in the results it is shown that this applied strategy of photothermal dehybridization of antisense strands using LED continuous-wave incident light offered several notable advantages that helped to the obtained results; we used the unmodified (it means chemical modifications) antisense strand (Figure 4. 6) that it caused that we have not any inefficiency in gene silencing process (Figure 5. 22). In more detail, in the gene silencing process that is done (5. 11), using light illumination as an activator remote to photothermally dehybridize antisense DNA and "activate" their functionality, the unmodified antisense was released into the cytosol successfully. Then the released antisense strand was bound to start codon section of the corresponding mature mRNA. Afterwards, the mRNA/antisense DNA heteroduplex was formed and was recognized and degraded by cytosolic RNase H enzymes, thereby silencing of the CACT gene was achieved (Figure 5. 22 (B)). It is noteworthy that since RNase H, is ubiquitously present in both the cytosol and the nucleus [235, 236]. So, as an alternative model [235] we can suggest that unbound antisense strands went into the nucleus. In the nucleus, the antisense strands that were arrived bound to the pre-mRNA and after forming of pre-mRNA/antisense hetero duplex, were recognized and degraded by nuclear RNase H enzymes.

It is noteworthy that, following CACT gene silencing through this mentioned method and mechanism, as our prediction and hypothesis fatty acids increased considerably. It is notable that substantial accumulation of lipids, mostly in the form of TAG observed through Nile red staining (Figure 5. 23). Actually, with silencing of CACT gene and subsequently lack of CACT protein synthesis, it is expected that the fatty acids can't enter the matrix of the mitochondria to breaking through Beta-oxidation cycle. Consequently, it is expected that just fatty acids can be increased between the inner and outer membrane of the mitochondria. But, there are some other pathways that lead to accumulation of TAG in addition to fatty acids. Actually, after stopping the Beta-oxidation pathway because of lack of entering the fatty acids into the matrix of the mitochondria, Acetyl-CoA as a final product of beta oxidation pathway couldn't be produced. On the other hand, since Acetyl-CoA is an essential ingredient for the Krebs cycle, so decreasing Acetyl-CoA led to increasing Oxaloacetate (Figure 6.1).

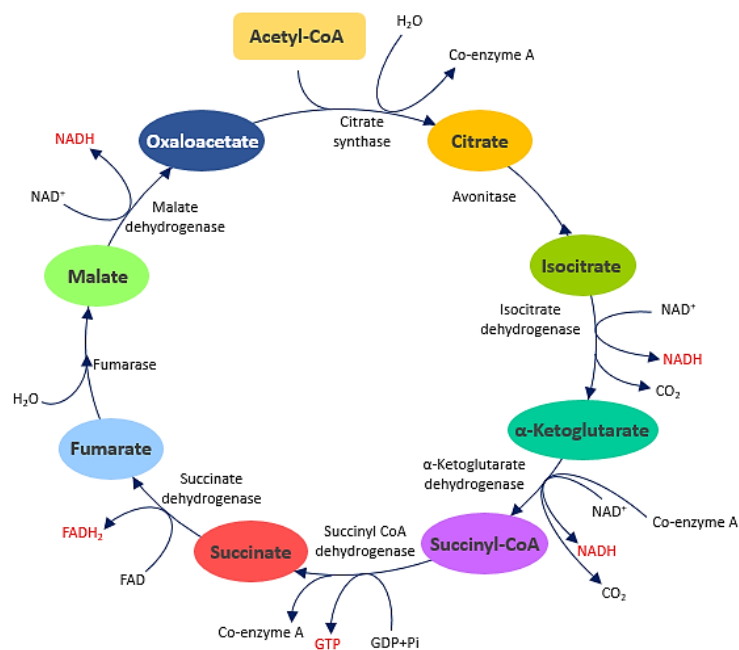


Figure 6. 1 Krebs cycle; Necessity of Acetyl-CoA to start Krebs cycle.

In the next step, Oxaloacetate during a two-way reaction could be converted to the Phosphoenolpyruvate (Figure 6.2). In this step Phosphoenolpyruvate, during some two-way reactions could be converted to the Dihydroxyacetone phosphate (Figure 6.2).

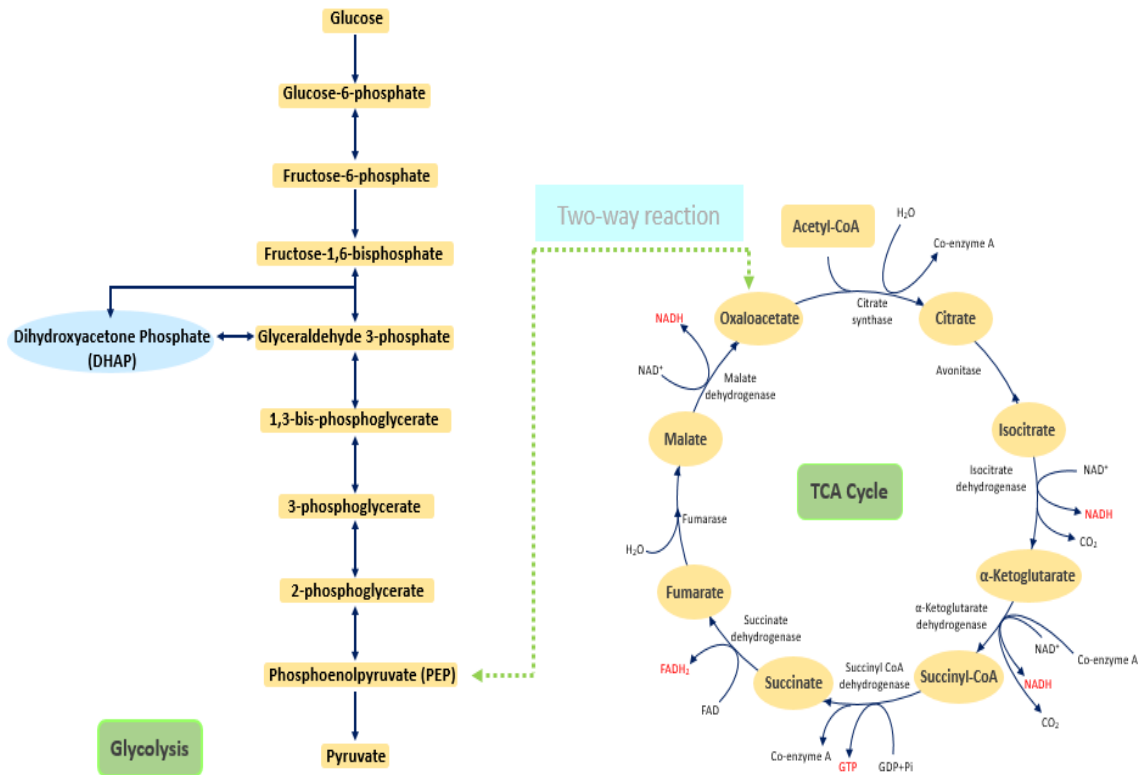


Figure 6. 2 Conversion of Oxaloacetate to PEP pathway.

Eventually, produced Dihydroxyacetone phosphate in combination of Glycerol could be converted to TAG (Figure 6.3). Because of these mentioned complex reactions we could see a substantial accumulation of lipids, mostly in the form of TAG (Figure 5. 23) as a final product of CACT gene silencing.

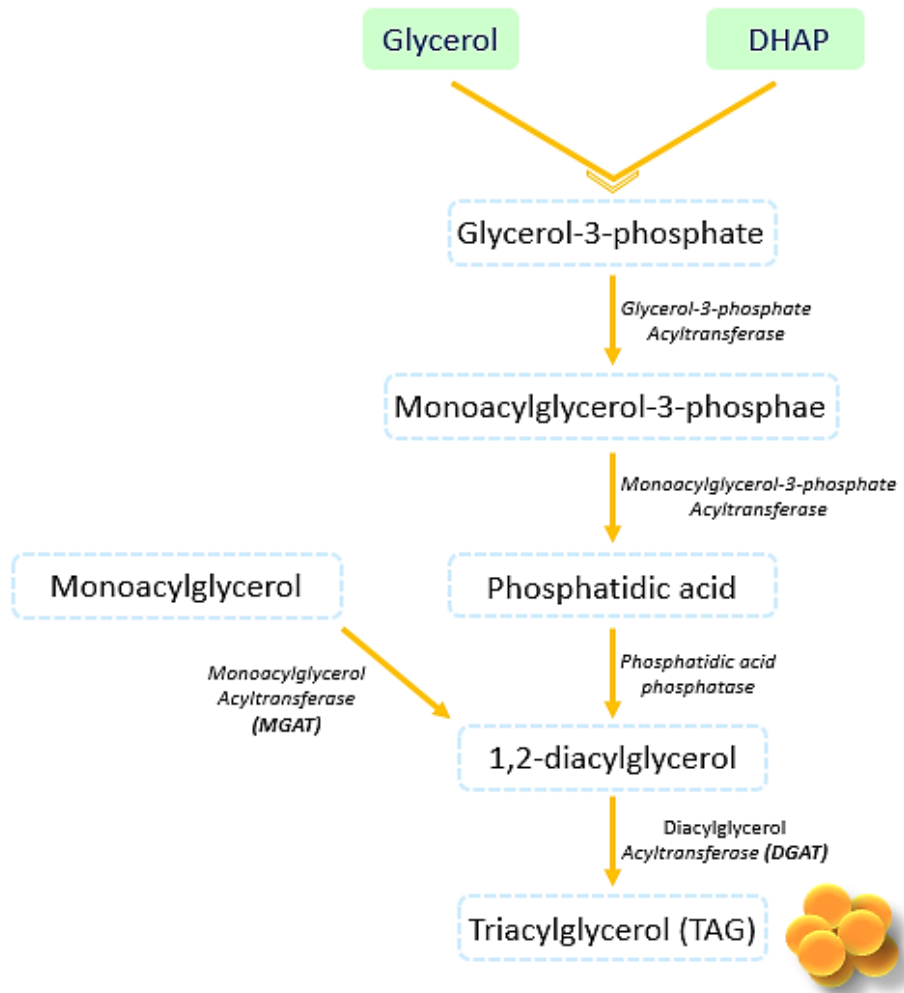


Figure 6. 3 TAG synthesis pathway; synthesis of TAG from DHAP that is one of the intermediate compounds of Glycolysis.

However, this study was a multidisciplinary work that linked some different specialty groups such as mechanical and electrical engineering group, electrical and computer engineering group, photonic group and nanobiotechnology group in order to help perform some parts of this study and present novel results. The novelty of this study about the photothermal releasing of the antisense oligonucleotides to silencing of the gene is in two major cases;

1) kind of used light source and its scalability; the present study showed that LED light source can be a promising alternative source instead of laser device to provide enough temperature in large scale using switchable AuNPs.

2) kind of target gene that its repression leads to increase the lipid amount that is a valuable compound in microalgae cells, while in other cases, this method is using in order to silence some genes and consequently cancer cell death.

CHAPTER 7

Conclusions

Increasing the multidisciplinary nature of scientific research will be the key to solving complex issues not yet understood. Micro-scale technology is a powerful tool for addressing many challenges in the field of engineering. With the development of nanoscience, the optical properties of AuNPs have shown tremendous interest in plasmon-based technologies. Localized surface plasmons can be excited by optical excitation, leading to produce temperature.

In the present study, AuNPs, which was prepared by Turkevich *et al.* method, was detected by UV–visible absorption in the first step. As obtained results, AuNPs exhibited optical absorbance around 523 nm which has been previously demonstrated to be a characteristic of AuNPs [223-225]. Moreover, the stability of these AuNPs was confirmed that this issue demonstrates that trisodium citrate playing an important role to stabilize AuNPs even for four months. Also, through TEM pictures, we observed that the size distribution of AuNPs with average size of 20.44 nm, was in ranges from 7 to 40 nm. In this work, in order to stimulation of the AuNPs to produce heat and making of temperature profile, we used two kind of the light source; CW Laser and LED. Then, in order to the investigation of Laser and LED potency and functional capability and also identify effective variable on increasing temperature of AuNPs solution, statistical approaches were used. About the Laser, based on a statistical evaluation, we identified different crucial factors that are effective in temperature change of AuNPs solution. Our results indicated that laser power, concentration of AuNPs, time \times laser power interaction and time illumination, were the most effective in

temperature change of AuNPs solution, respectively. Then we applied the significant variables to present a regression model in order to predict the heat generation amount from the same AuNPs surface. This model is chosen according to the F test, lack-of-fit-test, and adjusted R^2 value. Also, RSE% values were lower than 4 that showed the model can be used to determine ΔT of AuNPs solution with good accuracy and precision in the range of the values of the factors. In addition, it is confirmed and justified theoretically. We also statistical analyzed the produced temperature from surface of the AuNPs when they illuminated by LED as a light source. The results demonstrated that the main and interaction effects of all factors were significant. Finally, based on presented regression model (Eq. 5.5), ANOVA (Table 5.5) and regression coefficients, we could present a powerful regression model that shows the relationships between temperature changed and variables. This results and model can help researchers when they have the necessity to know about released temperature amount from same AuNPs for applying them in biological systems or another field. In this evaluation in order to compare the theoretical and experimental approaches, we also simulated heat generation from our AuNPs. In the present work is demonstrated that the maximum temperature increase inside the gold nanoparticle solution was in excellent agreement with our observations. There are some reports that showed some of nanoparticles such as Ag, CuO, ZnO, Se, Pd, FeO and especially AuNPs in some concentration, turn out to be highly toxic for different organisms [237-242]. Thus, because we wanted to use the AuNPs as a switchable temperature source for photothermal protein production, we tested its toxicity effect on the *E. coli* DH5 α . The results showed that different concentrations of our synthesized AuNPs (88, 80, 70 and 60 ppm) have not remarkable toxicity effect on this strain of bacteria. Of course, It is worth noting that gold-thiol covalent bonds are stable after illumination, such that the carrier's surface remains covered with the thiolated complementary sense strands. With respect to cytotoxicity, this surface coating of complementary strands after illumination is critical and it causes that this structure of AuNPs will have not any toxicity effect in the microalgae cells.

So, this one of notable advantages of this strategy (photothermal dehybridization using CW laser or LED illumination) that is using for releasing antisense oligonucleotides in the microalgae cells. we demonstrated the feasibility of dehybridizing dsDNA attached to the gold nanostructures (*in vitro* test) by LED light source at selected wavelengths. This LED produced SPR heating can be used as a “remote trigger” to release antisense oligonucleotides from surface sense oligonucleotides that strongly attached to AuNPs. Also, for *in vivo* test (in microalgae cells), we showed that (by confocal images) the dsDNA-functionalized AuNPs were successfully localized in the microalgae cells and were prepared to release antisense strand to silencing the *Carnitine-acylcarnitine translocase* gene. Then, we showed efficiency of these localized structures such that they could receive the light from the LED light source and convert it to temperature on the surface of the AuNPs. Finally, the antisense oligonucleotides could release and did the CACT gene silencing up to 90.7%. Consequently, this event led to accumulation of lipid bodies in the microalgae cells (Figure 5. 23).

In this study, many works have been accomplished and results are obtained given the little time available but, undoubtedly, there are still many questions are yet to be answered, e.g.:

1. What is the best way to achieve a high yield loading of dsDNA onto AuNPs?
2. Is there better method to optimization switch delivery into the microalgae cells?
3. Is there any way to recovery of AuNPs after using as switchable NPs in photothermal bacteria protein production process?
4. Is there any way to recovery of AuNPs after using for switch delivery into the microalgae cell?

5. Is there any difficulty about protein purification in photothermal protein production or lipid purification in microalgae gene silencing process when we use the AuNPs?

These questions will hopefully be answered in future projects.

CHAPTER 8

References

1. Sarma, S.J., et al., *Microbial hydrogen production by bioconversion of crude glycerol: A review*. International Journal of Hydrogen Energy, 2012. **37**(8): p. 6473-6490.
2. Murta, A.L.S. and M.A.V. de Freitas, *CO₂ Emissions Avoided Through the use of Biodiesel in the Brazilian Road System*. International Journal of Energy Economics and Policy, 2018. **8**(2): p. 59-68.
3. Brennan, L. and P. Owende, *Biofuels from microalgae—a review of technologies for production, processing, and extractions of biofuels and co-products*. Renewable and sustainable energy reviews, 2010. **14**(2): p. 557-577.
4. Naik, S.N., et al., *Production of first and second generation biofuels: a comprehensive review*. Renewable and sustainable energy reviews, 2010. **14**(2): p. 578-597.
5. Kalnes, T., T. Marker, and D.R. Shonnard, *Green diesel: a second generation biofuel*. International Journal of Chemical Reactor Engineering, 2007. **5**(1).
6. Gordon, M.E. and A.T. Cook, *Challenge and Potential of Biofuels from Algae-ft*. Science, 2016. **2016**.
7. Ozkurt, I., *Qualifying of safflower and algae for energy*. Energy Education Science and Technology Part a-Energy Science and Research, 2009. **23**(1-2): p. 145-151.
8. Melis, A., *Solar energy conversion efficiencies in photosynthesis: minimizing the chlorophyll antennae to maximize efficiency*. Plant science, 2009. **177**(4): p. 272-280.
9. Scott, S.A., et al., *Biodiesel from algae: challenges and prospects*. Current opinion in biotechnology, 2010. **21**(3): p. 277-286.
10. Chisti, Y., *Biodiesel from microalgae beats bioethanol*. Trends in biotechnology, 2008. **26**(3): p. 126-131.

11. Cantrell, K.B., et al., *Livestock waste-to-bioenergy generation opportunities*. Bioresource technology, 2008. **99**(17): p. 7941-7953.
12. Medipally, S.R., et al., *Microalgae as sustainable renewable energy feedstock for biofuel production*. BioMed research international, 2015. **2015**.
13. Spolaore, P., et al., *Commercial applications of microalgae*. Journal of bioscience and bioengineering, 2006. **101**(2): p. 87-96.
14. Markou, G. and E. Nerantzis, *Microalgae for high-value compounds and biofuels production: a review with focus on cultivation under stress conditions*. Biotechnology advances, 2013. **31**(8): p. 1532-1542.
15. Damartzis, T. and A. Zabaniotou, *Thermochemical conversion of biomass to second generation biofuels through integrated process design—A review*. Renewable and Sustainable Energy Reviews, 2011. **15**(1): p. 366-378.
16. Demirbas, M.F., *Biorefineries for biofuel upgrading: a critical review*. Applied Energy, 2009. **86**: p. S151-S161.
17. Nigam, P.S. and A. Singh, *Production of liquid biofuels from renewable resources*. Progress in energy and combustion science, 2011. **37**(1): p. 52-68.
18. Zhu, L., *Microalgal culture strategies for biofuel production: a review*. Biofuels, Bioproducts and Biorefining, 2015. **9**(6): p. 801-814.
19. Qv, X.Y., Q.F. Zhou, and J.G. Jiang, *Ultrasound-enhanced and microwave-assisted extraction of lipid from *Dunaliella tertiolecta* and fatty acid profile analysis*. Journal of separation science, 2014. **37**(20): p. 2991-2999.
20. Chen, C.-Y., et al., *Cultivation, photobioreactor design and harvesting of microalgae for biodiesel production: a critical review*. Bioresource technology, 2011. **102**(1): p. 71-81.
21. Wang, J., H. Yang, and F. Wang, *Mixotrophic cultivation of microalgae for biodiesel production: status and prospects*. Applied biochemistry and biotechnology, 2014. **172**(7): p. 3307-3329.
22. Perez-Garcia, O. and Y. Bashan, *Microalgal heterotrophic and mixotrophic culturing for bio-refining: From metabolic routes to techno-economics*, in *Algal biorefineries*. 2015, Springer. p. 61-131.

23. Morales-Sánchez, D., O.A. Martínez-Rodríguez, and A. Martínez, *Heterotrophic cultivation of microalgae: production of metabolites of commercial interest*. Journal of Chemical Technology and Biotechnology, 2017. **92**(5): p. 925-936.
24. Perez-Garcia, O., et al., *EFFICIENCY OF GROWTH AND NUTRIENT UPTAKE FROM WASTEWATER BY HETEROTROPHIC, AUTOTROPHIC, AND MIXOTROPHIC CULTIVATION OF CHLORELLA VULGARIS IMMOBILIZED WITH AZOSPIRILLUM BRASILENSE 1*. Journal of Phycology, 2010. **46**(4): p. 800-812.
25. Kröger, M. and F. Müller-Langer, *Impact of heterotrophic and mixotrophic growth of microalgae on the production of future biofuels*. Biofuels, 2011. **2**(2): p. 145-151.
26. Bhatia, S., *Nanoparticles types, classification, characterization, fabrication methods and drug delivery applications*, in *Natural Polymer Drug Delivery Systems*. 2016, Springer. p. 33-93.
27. Mnyusiwalla, A., A.S. Daar, and P.A. Singer, *'Mind the gap': science and ethics in nanotechnology*. Nanotechnology, 2003. **14**(3): p. R9.
28. KUMAR, N., KUMBHAT, S., *Essentials in nanoscience and nanotechnology*. 2016, Hoboken, New Jersey: John Wiley & Sons, Inc. 2.
29. Kibeche, A., Dionne, A., Brion-Roby, R., Gagnon, C., & Gagnon, J., *Simple and green technique for sequestration and concentration of silver nanoparticles by polysaccharides immobilized on glass beads in aqueous media*. Chemistry Central Journal, 2015.
30. Alishah, H., et al., *Green synthesis of starch-mediated CuO nanoparticles: preparation, characterization, antimicrobial activities and in vitro MTT assay against MCF-7 cell line*. Rendiconti Lincei: p. 1-7.
31. Matea, C.T., et al., *A novel immunoglobulin G monolayer silver bio-nanocomposite*. Chemistry Central Journal, 2015. **9**(1): p. 55.
32. Luo, Y.-H., L.W. Chang, and P. Lin, *Metal-based nanoparticles and the immune system: activation, inflammation, and potential applications*. BioMed research international, 2015. **2015**.
33. Ning, L., B. Zhu, and T. Gao, *Gold Nanoparticles: Promising Agent To Improve The Diagnosis And Therapy Of Cancer*. Current drug metabolism, 2017.

34. Khoshnevisan, K., et al., *The promising potentials of capped gold nanoparticles for drug delivery systems*. Journal of drug targeting, 2017: p. 1-8.
35. Kumar, S., et al., *PEG coated and doxorubicin loaded multimodal Gadolinium oxide nanoparticles for simultaneous drug delivery and imaging applications*. International journal of pharmaceutics, 2017. **527**(1-2): p. 142-150.
36. Malekmohammadi, S., H. Hadadzadeh, and Z. Amirghofran, *Immobilization of Gold Nanoparticles on the Folate-Conjugated Dendritic Mesoporous Silica-Coated Reduced Graphene Oxide Nanosheets: A New Nanoplatform for Targeted Delivery and pH-Controlled release of Curcumin*. Soft matter, 2018.
37. Spyratou, E., et al., *Recent Advances in Cancer Therapy Based on Dual Mode Gold Nanoparticles*. Cancers, 2017. **9**(12): p. 173.
38. Ebara, M. and K. Uto, *Gold nanomaterials for gene therapy*, in *Polymers and Nanomaterials for Gene Therapy*. 2016, Elsevier. p. 189-214.
39. Faraday, M., X. *The Bakerian Lecture.—Experimental relations of gold (and other metals) to light*. Philosophical Transactions of the Royal Society of London, 1857. **147**: p. 145-181.
40. Hess, S.T., T.P. Girirajan, and M.D. Mason, *Ultra-high resolution imaging by fluorescence photoactivation localization microscopy*. Biophysical journal, 2006. **91**(11): p. 4258-4272.
41. Lidke, K.A., et al., *Superresolution by localization of quantum dots using blinking statistics*. Optics express, 2005. **13**(18): p. 7052-7062.
42. Zarei, A.R. and F. Barghak, *Application of the localized surface plasmon resonance of gold nanoparticles for the determination of 1, 1-dimethylhydrazine in water: Toward green analytical chemistry*. Journal of Analytical Chemistry, 2017. **72**(4): p. 430-436.
43. Stokes, G.G., XVI. *On the change of refrangibility of light.—No. II*. Philosophical Transactions of the Royal Society of London, 1853. **143**: p. 385-396.
44. Becquerel, E. *Des effets produits sur les corps par les rayons solaires*. in *Annales de Chimie et Physique*. 1843.
45. Turkevich, J., P.C. Stevenson, and J. Hillier, *The formation of colloidal gold*. The Journal of Physical Chemistry, 1953. **57**(7): p. 670-673.

46. Ji, X., et al., *Size control of gold nanocrystals in citrate reduction: the third role of citrate*. Journal of the American Chemical Society, 2007. **129**(45): p. 13939-13948.
47. Turkevich, J., P.C. Stevenson, and J. Hillier, *A study of the nucleation and growth processes in the synthesis of colloidal gold*. Discussions of the Faraday Society, 1951. **11**: p. 55-75.
48. Frens, G., *Controlled nucleation for the regulation of the particle size in monodisperse gold suspensions*. Nature physical science, 1973. **241**(105): p. 20.
49. Kumar, S., K. Gandhi, and R. Kumar, *Modeling of formation of gold nanoparticles by citrate method*. Industrial & Engineering Chemistry Research, 2007. **46**(10): p. 3128-3136.
50. Inoue, Y., et al., *Stepwise Preparation of Spherical Gold Nanoparticles Passivated with Cationic Amphiphiles*. Analytical Sciences, 2016. **32**(8): p. 875-880.
51. Rajan, A., A.R. Rajan, and D. Philip, *Elettaria cardamomum seed mediated rapid synthesis of gold nanoparticles and its biological activities*. OpenNano, 2017. **2**: p. 1-8.
52. Sachdev, S., et al., *Synthesis and assembly of gold and iron oxide particles within an emulsion droplet; facile production of Core@ Shell particles*. Colloid and Interface Science Communications, 2017. **16**: p. 14-18.
53. Azubel, M. and R.D. Kornberg, *Synthesis of water-soluble, thiolate-protected gold nanoparticles uniform in size*. Nano letters, 2016. **16**(5): p. 3348-3351.
54. Kuttner, C., et al., *Seeded Growth Synthesis of Gold Nanotriangles: Size Control, SAXS Analysis, and SERS Performance*. ACS applied materials & interfaces, 2018.
55. Anwar, A., et al., *Synthesis of gold nanoparticles stabilized by a pyrazinium thioacetate ligand: A new colorimetric nanosensor for detection of heavy metal Pd (II)*. Sensors and Actuators B: Chemical, 2018. **257**: p. 875-881.
56. Gasiorek, F.B., *Synthesis and functionalization of nanoparticles with biogenic amines and their biological application*. 2016.
57. Yusof, N.S.M. and M. Ashokkumar, *Sonochemical synthesis of gold nanoparticles by using high intensity focused ultrasound*. ChemPhysChem, 2015. **16**(4): p. 775-781.

58. Bahrani, S., et al., *Ultrasound-accelerated synthesis of gold nanoparticles modified choline chloride functionalized graphene oxide as a novel sensitive bioelectrochemical sensor: Optimized meloxicam detection using CCD-RSM design and application for human plasma sample*. Ultrasonics Sonochemistry, 2017.
59. Kumar, B., et al., *Ecofriendly ultrasound-assisted rapid synthesis of gold nanoparticles using Calothrix algae*. Advances in Natural Sciences: Nanoscience and Nanotechnology, 2016. **7**(2): p. 025013.
60. Bhosale, M.A., D.R. Chenna, and B.M. Bhanage, *Ultrasound Assisted Synthesis of Gold Nanoparticles as an Efficient Catalyst for Reduction of Various Nitro Compounds*. ChemistrySelect, 2017. **2**(3): p. 1225-1231.
61. Sunkari, S., et al., *Microwave-irradiated green synthesis of gold nanoparticles for catalytic and anti-bacterial activity*. Journal of Analytical Science and Technology, 2017. **8**(1): p. 13.
62. Chuang, K.-T. and Y.-W. Lin, *Microwave-Assisted Formation of Gold Nanoclusters Capped in Bovine Serum Albumin and Exhibiting Red or Blue Emission*. The Journal of Physical Chemistry C, 2017. **121**(48): p. 26997-27003.
63. Williams, M.G., D.A. Boyne, and M.H. Griep, *Rapid synthesis of high purity gold nanorods via microwave irradiation*. Materials Research Express, 2017. **4**(3): p. 035040.
64. Ngo, V.K.T., et al., *Preparation of gold nanoparticles by microwave heating and application of spectroscopy to study conjugate of gold nanoparticles with antibody E. coli O157: H7*. Advances in Natural Sciences: Nanoscience and Nanotechnology, 2015. **6**(3): p. 035015.
65. Scaramuzza, S., M. Zerbetto, and V. Amendola, *Synthesis of gold nanoparticles in liquid environment by laser ablation with geometrically confined configurations: Insights to improve size control and productivity*. The Journal of Physical Chemistry C, 2016. **120**(17): p. 9453-9463.
66. Vinod, M., R.S. Jayasree, and K. Gopchandran, *Synthesis of pure and biocompatible gold nanoparticles using laser ablation method for SERS and photothermal applications*. Current Applied Physics, 2017. **17**(11): p. 1430-1438.
67. Sengani, M., A.M. Grumezescu, and V.D. Rajeswari, *Recent trends and methodologies in gold nanoparticle synthesis—A prospective review on drug delivery aspect*. OpenNano, 2017. **2**: p. 37-46.

68. Khumaeni, A., W.S. Budi, and H. Sutanto. *Synthesis and characterization of high-purity gold nanoparticles by laser ablation method using low-energy Nd: YAG laser 1064 nm.* in *Journal of Physics: Conference Series*. 2017. IOP Publishing.
69. Zhao, X., et al., *Facile Synthesis of Gold Nanoparticles with Alginate and Its Catalytic Activity for Reduction of 4-Nitrophenol and H₂O₂ Detection.* *Materials*, 2017. **10**(5): p. 557.
70. Ahmad, T., et al., *Antifungal activity of gold nanoparticles prepared by solvothermal method.* *Materials Research Bulletin*, 2013. **48**(1): p. 12-20.
71. Li, J., Q. Wu, and J. Wu, *Synthesis of nanoparticles via solvothermal and hydrothermal methods.* *Handbook of Nanoparticles*, 2015: p. 1-28.
72. Choi, J., et al., *Facile Solvothermal Preparation of Monodisperse Gold Nanoparticles and Their Engineered Assembly of Ferritin–Gold Nanoclusters.* *Langmuir*, 2013. **29**(50): p. 15698-15703.
73. Zou, C.e., et al., *Electrochemical synthesis of gold nanoparticles decorated flower-like graphene for high sensitivity detection of nitrite.* *Journal of colloid and interface science*, 2017. **488**: p. 135-141.
74. Huang, C.-J., et al., *Electrochemically controlling the size of gold nanoparticles.* *Journal of The Electrochemical Society*, 2006. **153**(12): p. D193-D198.
75. Ahmed, S.R., et al., *Synthesis of gold nanoparticles with buffer-dependent variations of size and morphology in biological buffers.* *Nanoscale research letters*, 2016. **11**(1): p. 65.
76. Dong, S., et al., *Photochemical synthesis of gold nanoparticles by the sunlight radiation using a seeding approach.* *Gold bulletin*, 2004. **37**(3-4): p. 187-195.
77. Thirumalraj, B., et al., *Light-Controlled Photochemical Synthesis of Gelatin-Capped Gold Nanoparticles for Spectral Activity and Electro-oxidation of Quercetin.* *ChemElectroChem*, 2017. **4**(11): p. 2842-2851.
78. Rutherford, G., et al., *Photochemical Growth of Highly Densely Packed Gold Nanoparticle Films for Biomedical Diagnostics.* *ECS Journal of Solid State Science and Technology*, 2015. **4**(10): p. S3071-S3076.
79. Gonnelli, C., et al., *Green Synthesis of Gold Nanoparticles from Extracts of Cucurbita pepo L. Leaves: Insights on the Role of Plant Ageing,* in *Advances in Bionanomaterials*. 2018, Springer. p. 155-164.

80. Molnár, Z., et al., *Green synthesis of gold nanoparticles by thermophilic filamentous fungi*. Scientific reports, 2018. **8**(1): p. 3943.
81. Biao, L., et al., *Green Synthesis, Characterization and Application of Proanthocyanidins-Functionalized Gold Nanoparticles*. Nanomaterials, 2018. **8**(1): p. 53.
82. Gonzalez-Ballesteros, N., et al., *Green synthesis of gold nanoparticles using brown algae cystoseira baccata: Its activity in colon cancer cells*. Colloids and Surfaces B: Biointerfaces, 2017. **153**: p. 190-198.
83. Lee, S.Y., et al., *Biosynthesis of gold nanoparticles using Ocimum sanctum extracts by solvents with different polarity*. ACS Sustainable Chemistry & Engineering, 2016. **4**(5): p. 2651-2659.
84. Correa, S., A. Naranjo, and A. Herrera. *Biosynthesis and characterization of gold nanoparticles using extracts of Tamarindus indica L leaves*. in *Journal of Physics: Conference Series*. 2016. IOP Publishing.
85. Kim, S.-E., et al., *Near-Infrared Plasmonic Assemblies of Gold Nanoparticles with Multimodal Function for Targeted Cancer Theragnosis*. Scientific reports, 2017. **7**(1): p. 17327.
86. Gonçalves, M.S.T., *Fluorescent labeling of biomolecules with organic probes*. Chemical reviews, 2008. **109**(1): p. 190-212.
87. Hechler, D., R. Nitsch, and S. Hendrix, *Green-fluorescent-protein-expressing mice as models for the study of axonal growth and regeneration in vitro*. Brain research reviews, 2006. **52**(1): p. 160-169.
88. Jung, I., et al., *Surface plasmon resonance extension through two-block metal-conducting polymer nanorods*. Nature communications, 2018. **9**(1): p. 1010.
89. Stewart Jr, C.N., *Go with the glow: fluorescent proteins to light transgenic organisms*. Trends in biotechnology, 2006. **24**(4): p. 155-162.
90. Govorov, A.O. and H.H. Richardson, *Generating heat with metal nanoparticles*. Nano today, 2007. **2**(1): p. 30-38.
91. Fan, W. and M.K. Leung, *Recent development of plasmonic resonance-based photocatalysis and photovoltaics for solar utilization*. Molecules, 2016. **21**(2): p. 180.

92. Daniels, J.L., et al., *Synthesis and characterization of pHLIP® coated gold nanoparticles*. Biochemistry and biophysics reports, 2017. **10**: p. 62-69.
93. Yavuz, M.S., et al., *Measuring Temperature Change at Nanometer Scale on Gold Nanoparticles using Thermoresponsive PEGMA Polymers*. ChemNanoMat, 2017.
94. Silvero C, M.J.n., et al., *Selective Photoinduced Antibacterial Activity of Amoxicillin-Coated Gold Nanoparticles: From One-Step Synthesis to in Vivo Cytocompatibility*. ACS Omega, 2018. **3**(1): p. 1220-1230.
95. Dong, J., et al., *In situ curing of liquid epoxy via gold-nanoparticle mediated photothermal heating*. Nanotechnology, 2017. **28**(6): p. 065601.
96. Iyer, V. and T. Shetty, *Gold nanoshells: A ray of hope in cancer diagnosis and treatment*.
97. Link, S. and M.A. El-Sayed, *Shape and size dependence of radiative, non-radiative and photothermal properties of gold nanocrystals*. International reviews in physical chemistry, 2000. **19**(3): p. 409-453.
98. Chen, Y.-S., D. Yeager, and S.Y. Emelianov, *Photoacoustic Imaging for Cancer Diagnosis and Therapy Guidance*, in *Cancer Theranostics*. 2014, Elsevier. p. 139-158.nd
99. Guo, A., et al., *Diameter effect of gold nanoparticles on photothermal conversion for solar steam generation*. RSC Advances, 2017. **7**(8): p. 4815-4824.
100. Perigo, E.A., et al., *Fundamentals and advances in magnetic hyperthermia*. Applied Physics Reviews, 2015. **2**(4): p. 041302.
101. Amirsardari, Z., R.M. Aghdam, and M.R. Jahannama, *Role of surface thermal properties of HfB_2 nanoparticles on heat flow in MWCNT/novolac composites*. Bulletin of Materials Science, 2018. **41**(1): p. 11.
102. Takahashi, H., Y. Niidome, and S. Yamada, *Controlled release of plasmid DNA from gold nanorods induced by pulsed near-infrared light*. Chemical communications, 2005(17): p. 2247-2249.
103. Lee, E.S., *Nanoplasmonics-enabled On-demand Gene Regulation*. 2010, UC Berkeley.
104. Meric-Bernstam, F., et al., *Aberrations in translational regulation are associated with poor prognosis in hormone receptor-positive breast cancer*. Breast Cancer Research, 2012. **14**(5): p. R138.

105. Glasser, S.W. and L.M. Noguee. *Genetically engineered mice in understanding the basis of neonatal lung disease*. in *Seminars in perinatology*. 2006. Elsevier.
106. Bhattacharjee, S., et al., *Combinatorial control of gene expression*. BioMed research international, 2013. **2013**.
107. Ries, L., et al., *Genome-wide transcriptional response of Trichoderma reesei to lignocellulose using RNA sequencing and comparison with Aspergillus niger*. BMC genomics, 2013. **14**(1): p. 541.
108. Neugart, S., A. Krumbein, and R. Zrenner, *Influence of light and temperature on gene expression leading to accumulation of specific flavonol glycosides and hydroxycinnamic acid derivatives in kale (Brassica oleracea var. sabellica)*. Frontiers in plant science, 2016. **7**: p. 326.
109. Denison, S.H., *pH regulation of gene expression in fungi*. Fungal Genetics and Biology, 2000. **29**(2): p. 61-71.
110. Gatz, C., *Chemical control of gene expression*. Annual review of plant biology, 1997. **48**(1): p. 89-108.
111. Pavlov, M.Y. and M. Ehrenberg, *Optimal control of gene expression for fast proteome adaptation to environmental change*. Proceedings of the National Academy of Sciences, 2013. **110**(51): p. 20527-20532.
112. Govan, J.M., et al., *Regulation of transcription through light-activation and light-deactivation of triplex-forming oligonucleotides in mammalian cells*. ACS chemical biology, 2012. **7**(7): p. 1247-1256.
113. Ogasawara, S., *Duration control of protein expression in vivo by light-mediated reversible activation of translation*. ACS chemical biology, 2017. **12**(2): p. 351-356.
114. Shcherbakova, D.M., et al., *Natural photoreceptors as a source of fluorescent proteins, biosensors, and optogenetic tools*. Annual review of biochemistry, 2015. **84**: p. 519-550.
115. Heintz, U. and I. Schlichting, *Blue light-induced LOV domain dimerization enhances the affinity of Aureochrome 1a for its target DNA sequence*. Elife, 2016. **5**: p. e11860.
116. Casal, J.J. and M.J. Yanovsky, *Regulation of gene expression by light*. International Journal of Developmental Biology, 2004. **49**(5-6): p. 501-511.

117. Atkins, P.W. and C. Trapp, *Physical chemistry. Solutions manual for Physical chemistry*. 1978: Oxford university press.
118. Ranjan, A., et al., *Functional analysis of COPI and SPA orthologs from Physcomitrella and rice during photomorphogenesis of transgenic Arabidopsis reveals distinct evolutionary conservation*. BMC plant biology, 2014. **14**(1): p. 178.
119. Wainwright, M., *Tricyclic cationic chromophores as models for new photoantimicrobials*. Journal of the Brazilian Chemical Society, 2015. **26**(12): p. 2390-2404.
120. Mueller, G., W. Waldeck, and K. Braun, *From green to red—To more dead? Autofluorescent proteins as photosensitizers*. Journal of Photochemistry and Photobiology B: Biology, 2010. **98**(1): p. 95-98.
121. Bakhtiari, A.B.S., et al., *An efficient method based on the photothermal effect for the release of molecules from metal nanoparticle surfaces*. Angewandte Chemie International Edition, 2009. **48**(23): p. 4166-4169.
122. Roper, D.K., W. Ahn, and M. Hoepfner, *Microscale heat transfer transduced by surface plasmon resonant gold nanoparticles*. The Journal of Physical Chemistry C, 2007. **111**(9): p. 3636-3641.
123. Rashidi-Huyeh, M. and B. Palpant, *Thermal response of nanocomposite materials under pulsed laser excitation*. Journal of applied physics, 2004. **96**(8): p. 4475-4482.
124. Neupert, J., D. Karcher, and R. Bock, *Design of simple synthetic RNA thermometers for temperature-controlled gene expression in Escherichia coli*. Nucleic acids research, 2008. **36**(19): p. e124-e124.
125. Cruje, C. and B. Chithrani, *Integration of peptides for enhanced uptake of PEGylated gold nanoparticles*. Journal of nanoscience and nanotechnology, 2015. **15**(3): p. 2125-2131.
126. Mathieu-Rivet, E., et al., *Protein N-glycosylation in eukaryotic microalgae and its impact on the production of nuclear expressed biopharmaceuticals*. Frontiers in plant science, 2014. **5**.
127. Vitova, M., et al., *Accumulation of energy reserves in algae: from cell cycles to biotechnological applications*. Biotechnology advances, 2015. **33**(6): p. 1204-1218.

128. Solovchenko, A., *Physiological role of neutral lipid accumulation in eukaryotic microalgae under stresses*. Russian Journal of Plant Physiology, 2012. **59**(2): p. 167-176.
129. Zhu, L., Z. Li, and E. Hiltunen, *Strategies for lipid production improvement in microalgae as a biodiesel feedstock*. BioMed research international, 2016. **2016**.
130. Fukuda, H., A. Kondo, and H. Noda, *Biodiesel fuel production by transesterification of oils*. Journal of bioscience and bioengineering, 2001. **92**(5): p. 405-416.
131. Eibl, J.K., et al., *Bioprospecting for acidophilic lipid-rich green microalgae isolated from abandoned mine site water bodies*. Amb Express, 2014. **4**(1): p. 7.
132. Gunatilake, H., D. Roland-Holst, and G. Sugiyarto, *Energy security for India: Biofuels, energy efficiency and food productivity*. Energy Policy, 2014. **65**: p. 761-767.
133. Zhu, L., et al., *Oil production from pilot-scale microalgae cultivation: an economics evaluation*. Energy Sources, Part B: Economics, Planning, and Policy, 2016. **11**(1): p. 11-17.
134. Yates, C.M., P.C. Calder, and G.E. Rainger, *Pharmacology and therapeutics of omega-3 polyunsaturated fatty acids in chronic inflammatory disease*. Pharmacology & therapeutics, 2014. **141**(3): p. 272-282.
135. Merchant, S.S., et al., *TAG, You're it! Chlamydomonas as a reference organism for understanding algal triacylglycerol accumulation*. Current opinion in biotechnology, 2012. **23**(3): p. 352-363.
136. Goold, H., et al., *Microalgal lipid droplets: composition, diversity, biogenesis and functions*. Plant cell reports, 2015. **34**(4): p. 545-555.
137. Liu, B. and C. Benning, *Lipid metabolism in microalgae distinguishes itself*. Current opinion in biotechnology, 2013. **24**(2): p. 300-309.
138. Blaby, I.K., et al., *The Chlamydomonas genome project: a decade on*. Trends in plant science, 2014. **19**(10): p. 672-680.
139. Li, X., et al., *An indexed, mapped mutant library enables reverse genetics studies of biological processes in Chlamydomonas reinhardtii*. The Plant Cell, 2016: p. TPC2015-00465-LSB.

140. Hu, Q., et al., *Microalgal triacylglycerols as feedstocks for biofuel production: perspectives and advances*. The plant journal, 2008. **54**(4): p. 621-639.
141. Goncalves, E.C., et al., *Metabolic regulation of triacylglycerol accumulation in the green algae: identification of potential targets for engineering to improve oil yield*. Plant biotechnology journal, 2016. **14**(8): p. 1649-1660.
142. Pierre, G., et al., *Prospective treatment in carnitine–acylcarnitine translocase deficiency*. Journal of inherited metabolic disease, 2007. **30**(5): p. 815.
143. Gopalakrishnan, V. and D. Ramamurthy, *Dyeing industry effluent system as lipid production medium of Neochloris sp. for biodiesel feedstock preparation*. BioMed research international, 2014. **2014**.
144. Fan, J., L. Yu, and C. Xu, *A central role for triacylglycerol in membrane lipid breakdown, fatty acid β -oxidation, and plant survival under extended darkness*. Plant physiology, 2017. **174**(3): p. 1517-1530.
145. Liang, M.-H. and J.-G. Jiang, *Advancing oleaginous microorganisms to produce lipid via metabolic engineering technology*. Progress in lipid research, 2013. **52**(4): p. 395-408.
146. Murphy, D.J. and R.M. Leech, *Photosynthesis of Lipids from $^{14}CO_2$ in Spinacia oleracea*. Plant physiology, 1981. **68**(3): p. 762-765.
147. Bates, P.D. and J. Browse, *The significance of different diacylglycerol synthesis pathways on plant oil composition and bioengineering*. Frontiers in plant science, 2012. **3**.
148. Chapman, K.D. and J.B. Ohlrogge, *Compartmentation of triacylglycerol accumulation in plants*. Journal of Biological Chemistry, 2012. **287**(4): p. 2288-2294.
149. Bates, P.D., S. Stymne, and J. Ohlrogge, *Biochemical pathways in seed oil synthesis*. Current opinion in plant biology, 2013. **16**(3): p. 358-364.
150. Xu, C. and J. Shanklin, *Triacylglycerol metabolism, function, and accumulation in plant vegetative tissues*. Annual review of plant biology, 2016. **67**: p. 179-206.
151. Chen, H.-H. and J.-G. Jiang, *Lipid Accumulation Mechanisms in Auto-and Heterotrophic Microalgae*. Journal of agricultural and food chemistry, 2017. **65**(37): p. 8099-8110.

152. Thompson Jr, G.A., *Lipids and membrane function in green algae*. Biochimica et Biophysica Acta (BBA)-Lipids and Lipid Metabolism, 1996. **1302**(1): p. 17-45.
153. Sharma, K.K., H. Schuhmann, and P.M. Schenk, *High lipid induction in microalgae for biodiesel production*. Energies, 2012. **5**(5): p. 1532-1553.
154. Cohen, Z., A. Vonshak, and A. Richmond, *Effect of environmental conditions on fatty acid composition of the red alga Porphyridium cruentum: correlation to growth rate*. Journal of Phycology, 1988. **24**(3): p. 328-332.
155. Bigogno, C., et al., *Lipid and fatty acid composition of the green oleaginous alga Parietochloris incisa, the richest plant source of arachidonic acid*. Phytochemistry, 2002. **60**(5): p. 497-503.
156. Khozin-Goldberg, I., et al., *Nitrogen starvation induces the accumulation of arachidonic acid in the freshwater green alga Parietochloris incisa (Trebuxiophyceae)*. Journal of Phycology, 2002. **38**(5): p. 991-994.
157. Berge, J.-P., et al., *Reassessment of lipid composition of the diatom, Skeletonema costatum*. Phytochemistry, 1995. **39**(5): p. 1017-1021.
158. Eizadora, T.Y., et al., *Triacylglycerol accumulation and profiling in the model diatoms Thalassiosira pseudonana and Phaeodactylum tricornutum (Baccilariophyceae) during starvation*. Journal of Applied Phycology, 2009. **21**(6): p. 669.
159. Khozin-Goldberg, I. and Z. Cohen, *The effect of phosphate starvation on the lipid and fatty acid composition of the fresh water eustigmatophyte Monodus subterraneus*. Phytochemistry, 2006. **67**(7): p. 696-701.
160. Ying, K., W. Zimmerman, and D. Gilmour, *Effects of CO and pH on growth of the microalga Dunaliella salina*. Journal of Microbial and Biochemical Technology, 2014. **6**(3): p. 167-173.
161. Hippler, M., *Chlamydomonas: Biotechnology and Biomedicine*. 2017, Switzerland: Springer International Publishing AG.
162. Giudetti, A., et al., *Nutritional and hormonal regulation of citrate and carnitine/acylcarnitine transporters: Two mitochondrial carriers involved in fatty acid metabolism*. International journal of molecular sciences, 2016. **17**(6): p. 817.
163. *Carnitine-acylcarnitine translocase*. Available from: https://en.wikipedia.org/wiki/Carnitine-acylcarnitine_translocase.

164. Slagt. 2007; Acyl-CoA from the cytosol to the mitochondrial matrix
- J. Available from: https://commons.wikimedia.org/wiki/File:Acyl-CoA_from_cytosol_to_the_mitochondrial_matrix.gif.
165. Amin, S., *Review on biofuel oil and gas production processes from microalgae*. Energy conversion and management, 2009. **50**(7): p. 1834-1840.
166. Hassan, M.A., S. Yacob, and B.A. Ghani, *Utilization of biomass in Malaysia: potential for CDM business*. University Putra Malaysia, Faculty of Biotechnology, 2005.
167. Khan, S.A., et al., *Prospects of biodiesel production from microalgae in India*. Renewable and Sustainable Energy Reviews, 2009. **13**(9): p. 2361-2372.
168. Mata, T.M., A.A. Martins, and N.S. Caetano, *Microalgae for biodiesel production and other applications: a review*. Renewable and sustainable energy reviews, 2010. **14**(1): p. 217-232.
169. Ahmad, A., et al., *Microalgae as a sustainable energy source for biodiesel production: a review*. Renewable and Sustainable Energy Reviews, 2011. **15**(1): p. 584-593.
170. Tarigan, J.B., et al., *Rapid Biodiesel Production From Palm Kernel Through In Situ Transesterification Reaction Using Cao As Catalyst*. International Journal of Applied Chemistry, 2017. **13**(3): p. 631-646.
171. Yasin, M.H.M., et al., *Potentials of palm oil as new feedstock oil for a global alternative fuel: A review*. Renewable and Sustainable Energy Reviews, 2017. **79**: p. 1034-1049.
172. Verma, P., M. Sharma, and G. Dwivedi, *Impact of alcohol on biodiesel production and properties*. Renewable and Sustainable Energy Reviews, 2016. **56**: p. 319-333.
173. Mujeeb, M., A. Vedamurthy, and C. Shivasharana, *Current strategies and prospects of biodiesel production: A review*. Adv Appl Sci Res, 2016. **7**(1): p. 120-133.
174. Naqvi, M. and J. Yan, *First-Generation Biofuels*. 2015: Wiley Online Library.
175. OECD/FAO, *"Biofuels", in OECD-FAO Agricultural Outlook 2016-2025*. 2016, OECD Publishing: paris.

176. EisentrAut, A., *Sustainable Production of Second-Generation Biofuels 2010*: International Energy Agency.
177. Nagle, N. and P. Lemke, *Production of methyl ester fuel from microalgae*. Applied Biochemistry and Biotechnology, 1990. **24**(1): p. 355-361.
178. Sawayama, S., et al., *CO₂ fixation and oil production through microalga*. Energy Conversion and Management, 1995. **36**(6-9): p. 729-731.
179. Miao, X. and Q. Wu, *High yield bio-oil production from fast pyrolysis by metabolic controlling of Chlorella protothecoides*. Journal of biotechnology, 2004. **110**(1): p. 85-93.
180. Rahman, M.M., et al., *Extension of energy crops on surplus agricultural lands: A potentially viable option in developing countries while fossil fuel reserves are diminishing*. Renewable and Sustainable Energy Reviews, 2014. **29**: p. 108-119.
181. Meng, X., et al., *Biodiesel production from oleaginous microorganisms*. Renewable energy, 2009. **34**(1): p. 1-5.
182. Radakovits, R., et al., *Genetic engineering of algae for enhanced biofuel production*. Eukaryotic cell, 2010. **9**(4): p. 486-501.
183. Courchesne, N.M.D., et al., *Enhancement of lipid production using biochemical, genetic and transcription factor engineering approaches*. Journal of biotechnology, 2009. **141**(1-2): p. 31-41.
184. Li, Y., et al., *Effects of nitrogen sources on cell growth and lipid accumulation of green alga Nannochloris oleoabundans*. Applied microbiology and biotechnology, 2008. **81**(4): p. 629-636.
185. Takagi, M. and T. Yoshida, *Effect of salt concentration on intracellular accumulation of lipids and triacylglyceride in marine microalgae Dunaliella cells*. Journal of bioscience and bioengineering, 2006. **101**(3): p. 223-226.
186. Converti, A., et al., *Effect of temperature and nitrogen concentration on the growth and lipid content of Nannochloropsis oculata and Chlorella vulgaris for biodiesel production*. Chemical Engineering and Processing: Process Intensification, 2009. **48**(6): p. 1146-1151.
187. Cordero, B.F., et al., *Enhancement of lutein production in Chlorella sorokiniana (Chlorophyta) by improvement of culture conditions and random mutagenesis*. Marine drugs, 2011. **9**(9): p. 1607-1624.

188. de-Bashan, L.E., et al., *Chlorella sorokiniana* UTEX 2805, a heat and intense, sunlight-tolerant microalga with potential for removing ammonium from wastewater. *Bioresource Technology*, 2008. **99**(11): p. 4980-4989.
189. Chaisutyakorn, P., J. Praiboon, and C. Kaewsuralikhit, *The effect of temperature on growth and lipid and fatty acid composition on marine microalgae used for biodiesel production*. *Journal of Applied Phycology*, 2018. **30**(1): p. 37-45.
190. Yodsuwan, N., S. Sawayama, and S. Sirisansaneeyakul, *Effect of nitrogen concentration on growth, lipid production and fatty acid profiles of the marine diatom Phaeodactylum tricorutum*. *Agriculture and Natural Resources*, 2017. **51**(3): p. 190-197.
191. Dunahay, T.G., E.E. Jarvis, and P.G. Roessler, *Genetic transformation of the diatoms Cyclotella cryptica and Navicula saprophila*. *Journal of Phycology*, 1995. **31**(6): p. 1004-1012.
192. Sheehan, J., et al., *Look back at the US department of energy's aquatic species program: biodiesel from algae; close-out report*. 1998, National Renewable Energy Lab., Golden, CO.(US).
193. Li, Y., et al., *Chlamydomonas starchless mutant defective in ADP-glucose pyrophosphorylase hyper-accumulates triacylglycerol*. *Metabolic engineering*, 2010. **12**(4): p. 387-391.
194. Yu, W.-L., et al., *Modifications of the metabolic pathways of lipid and triacylglycerol production in microalgae*. *Microbial cell factories*, 2011. **10**(1): p. 91.
195. Trentacoste, E.M., et al., *Metabolic engineering of lipid catabolism increases microalgal lipid accumulation without compromising growth*. *Proceedings of the National Academy of Sciences*, 2013. **110**(49): p. 19748-19753.
196. Moellering, E.R. and C. Benning, *RNA interference silencing of a major lipid droplet protein affects lipid droplet size in Chlamydomonas reinhardtii*. *Eukaryotic cell*, 2010. **9**(1): p. 97-106.
197. Deng, X., J. Cai, and X. Fei, *Effect of the expression and knockdown of citrate synthase gene on carbon flux during triacylglycerol biosynthesis by green algae Chlamydomonas reinhardtii*. *BMC biochemistry*, 2013. **14**(1): p. 38.
198. Kobayashi, Y. and D. Weigel, *Move on up, it's time for change—mobile signals controlling photoperiod-dependent flowering*. *Genes & development*, 2007. **21**(19): p. 2371-2384.

199. Deng, X., et al., *A photoperiod-regulating gene CONSTANS is correlated to lipid biosynthesis in Chlamydomonas reinhardtii*. BioMed research international, 2015. **2015**.
200. Lytton-Jean, A.K., R. Langer, and D.G. Anderson, *Five years of siRNA delivery: spotlight on gold nanoparticles*. Small, 2011. **7**(14): p. 1932-1937.
201. Seferos, D.S., et al., *Polyvalent DNA nanoparticle conjugates stabilize nucleic acids*. Nano letters, 2008. **9**(1): p. 308-311.
202. Lee, S.E., et al., *Remote optical switch for localized and selective control of gene interference*. Nano letters, 2009. **9**(2): p. 562-570.
203. Huschka, R., et al., *Light-induced release of DNA from gold nanoparticles: nanoshells and nanorods*. Journal of the American Chemical Society, 2011. **133**(31): p. 12247-12255.
204. Huschka, R., et al., *Gene silencing by gold nanoshell-mediated delivery and laser-triggered release of antisense oligonucleotide and siRNA*. ACS nano, 2012. **6**(9): p. 7681-7691.
205. Vinhas, R., A.R. Fernandes, and P.V. Baptista, *Gold Nanoparticles for BCR-ABL1 gene silencing: Improving tyrosine kinase inhibitor efficacy in chronic myeloid leukemia*. Molecular Therapy-Nucleic Acids, 2017. **7**: p. 408-416.
206. Khlebtsov, B. and N. Khlebtsov, *On the measurement of gold nanoparticle sizes by the dynamic light scattering method*. Colloid Journal, 2011. **73**(1): p. 118-127.
207. Zhang, X.-F., et al., *Silver nanoparticles: synthesis, characterization, properties, applications, and therapeutic approaches*. International journal of molecular sciences, 2016. **17**(9): p. 1534.
208. Farooqui, M., et al., *Use of complementary and alternative medicines among Malaysian cancer patients: A descriptive study*. Journal of traditional and complementary medicine, 2016. **6**(4): p. 321-326.
209. Shaner, N.C., et al., *Improved monomeric red, orange and yellow fluorescent proteins derived from Discosoma sp. red fluorescent protein*. Nature biotechnology, 2004. **22**(12): p. 1567.
210. Tu, Q., et al., *Room temperature electrocompetent bacterial cells improve DNA transformation and recombineering efficiency*. Scientific reports, 2016. **6**: p. 24648.

211. Kumar, C.S., *UV-VIS and Photoluminescence Spectroscopy for Nanomaterials Characterization*. 2013: Springer.
212. Andersen, R.A., *Algal culturing techniques*. 2005: Elsevier.
213. Gorman, D.S. and R. Levine, *Cytochrome f and plastocyanin: their sequence in the photosynthetic electron transport chain of Chlamydomonas reinhardi*. Proceedings of the National Academy of Sciences, 1965. **54**(6): p. 1665-1669.
214. Harris, E., *Culture and storage methods*. The Chlamydomonas Sourcebook. A Comprehensive Guide to Biology and Laboratory Use, 1989: p. 25-63.
215. Sueoka, N., *Mitotic replication of deoxyribonucleic acid in Chlamydomonas reinhardi*. Proceedings of the National Academy of Sciences, 1960. **46**(1): p. 83-91.
216. Yamano, T., H. Iguchi, and H. Fukuzawa, *Rapid transformation of Chlamydomonas reinhardtii without cell-wall removal*. Journal of bioscience and bioengineering, 2013. **115**(6): p. 691-694.
217. Walker, T.L., et al., *Towards the development of a nuclear transformation system for Dunaliella tertiolecta*. Journal of applied phycology, 2005. **17**(4): p. 363-368.
218. Kilian, O., et al., *High-efficiency homologous recombination in the oil-producing alga Nannochloropsis sp.* Proceedings of the National Academy of Sciences, 2011. **108**(52): p. 21265-21269.
219. Boynton, J.E., et al., *Chloroplast transformation in Chlamydomonas with high velocity microprojectiles*. Science, 1988. **240**(4858): p. 1534-1538.
220. Jin, E., J.E. Polle, and A. Melis, *Involvement of zeaxanthin and of the Cbr protein in the repair of photosystem II from photoinhibition in the green alga Dunaliella salina*. Biochimica et Biophysica Acta (BBA)-Bioenergetics, 2001. **1506**(3): p. 244-259.
221. Livak, K.J. and T.D. Schmittgen, *Analysis of relative gene expression data using real-time quantitative PCR and the 2⁻ ΔΔCT method*. methods, 2001. **25**(4): p. 402-408.
222. Mulvaney, P., *Surface plasmon spectroscopy of nanosized metal particles*. Langmuir, 1996. **12**(3): p. 788-800.

223. Zuber, A., et al., *Detection of gold nanoparticles with different sizes using absorption and fluorescence based method*. Sensors and Actuators B: Chemical, 2016. **227**: p. 117-127.
224. Alba-Molina, D., et al., *Ion-Mediated Aggregation of Gold Nanoparticles for Light-Induced Heating*. Applied Sciences, 2017. **7**(9): p. 916.
225. Dasari, T.S., Y. Zhang, and H. Yu, *Antibacterial activity and cytotoxicity of gold (I) and (III) ions and gold nanoparticles*. Biochemistry & pharmacology: open access, 2015. **4**(6).
226. Raju, D., U.J. Mehta, and A. Ahmad, *Phytosynthesis of intracellular and extracellular gold nanoparticles by living peanut plant (Arachis hypogaea L.)*. Biotechnology and applied biochemistry, 2012. **59**(6): p. 471-478.
227. Shittu, K., et al., *Application of gold nanoparticles for improved drug efficiency*. Advances in Natural Sciences: Nanoscience and Nanotechnology, 2017. **8**(3): p. 035014.
228. Shabestarian, H., et al., *Green synthesis of gold nanoparticles using Sumac aqueous extract and their antioxidant activity*. Materials Research, 2017. **20**(1): p. 264-270.
229. Govorov, A.O., et al., *Gold nanoparticle ensembles as heaters and actuators: melting and collective plasmon resonances*. Nanoscale Research Letters, 2006. **1**(1): p. 84.
230. Naccache, R., et al., *Terahertz thermometry: Combining hyperspectral imaging and temperature mapping at terahertz frequencies*. Laser & Photonics Reviews, 2017. **11**(5): p. 1600342.
231. Kuzyk, A., et al., *Reconfigurable 3D plasmonic metamolecules*. Nature materials, 2014. **13**(9): p. 862.
232. Johnson, P.B. and R.-W. Christy, *Optical constants of the noble metals*. Physical review B, 1972. **6**(12): p. 4370.
233. Morales-Avila, E., et al., *Antibacterial efficacy of gold and silver nanoparticles functionalized with the ubiquicidin (29–41) antimicrobial peptide*. Journal of Nanomaterials, 2017. **2017**.
234. Poon, L., et al., *Photothermal release of single-stranded DNA from the surface of gold nanoparticles through controlled denaturing and $au-s$ bond breaking*. Acs Nano, 2010. **4**(11): p. 6395-6403.

235. Dean, N.M. and C.F. Bennett, *Antisense oligonucleotide-based therapeutics for cancer*. *Oncogene*, 2003. **22**(56): p. 9087.
236. Marcusson, E.G., et al., *Phosphorothioate oligodeoxyribonucleotides dissociate from cationic lipids before entering the nucleus*. *Nucleic acids research*, 1998. **26**(8): p. 2016-2023.
237. Reichelt, K., et al., *Phytochemical characterization of South African bush tea (*Athrixia phylicoides* DC.)*. *South African journal of botany*, 2012. **83**: p. 1-8.
238. Ji, J., Z. Long, and D. Lin, *Toxicity of oxide nanoparticles to the green algae *Chlorella* sp.* *Chemical Engineering Journal*, 2011. **170**(2-3): p. 525-530.
239. Aruoja, V., et al., *Toxicity of nanoparticles of CuO, ZnO and TiO₂ to microalgae *Pseudokirchneriella subcapitata**. *Science of the total environment*, 2009. **407**(4): p. 1461-1468.
240. Franklin, N.M., et al., *Comparative toxicity of nanoparticulate ZnO, bulk ZnO, and ZnCl₂ to a freshwater microalga (*Pseudokirchneriella subcapitata*): the importance of particle solubility*. *Environmental science & technology*, 2007. **41**(24): p. 8484-8490.
241. Alishah, H., et al., *Extract-mediated synthesis of Ag@ AgCl nanoparticles using *Conium maculatum* seeds: characterization, antibacterial activity and cytotoxicity effect against MCF-7 cell line*. *RSC Advances*, 2016. **6**(77): p. 73197-73202.
242. Alishah, H., et al., *A Green Approach for the Synthesis of Silver Nanoparticles Using Root Extract of *Chelidonium majus*: Characterization and Antibacterial Evaluation*. *Journal of Cluster Science*: p. 1-9.

AUTOBIOGRAPHICAL SUMMARY

MC Hossein Alishah Aratboni

Candidate for the degree of

Doctorate of Science with orientation of **Applied Microbiology**

Thesis: Optical Control of Gene Expression in Biological Systems Using Gold Nanoparticles: Photothermal Gene Expression in *Escherichia coli* and Gene Silencing in *Chlamydomonas reinhardtii*

Age: 29 years old

Field of study: Development of therapeutic agents

Biography:

Personal Data: Born in Neka, Mazandaran, Iran, on September 19, 1990, son of Ebrahim Alishah Aratboni and Mohtaram Vadoudi.

Education: Gorgan University of Agricultural Sciences and Natural Resources / B.Sc. agriculture engineering – plant breeding / 2013. University of Shahid Bahonar / M.Sc. agriculture engineering – biotechnology / 2016